UNCOVERING THE PROTECTIVE ROLE OF *POLG*^{D257A}, A MITOCHONDRIAL DNA MUTATOR, ON DIABETES AND OBESITY

Raymond George Fox

A dissertation submitted to the faculty of the Curriculum in Genetics and Molecular Biology at the University of North Carolina at Chapel Hill in partial fulfillment of the requirements for the degree of Doctor of Philosophy

Chapel Hill
2011

Approved by:

Nobuyo Maeda, PhD

Kathleen Caron, PhD

Karen Mohlke, PhD

Scott Magness, PhD

William B. Coleman, PhD

Mark W. Majesky, PhD

ABSTRACT

Raymond George Fox: Uncovering the Protective Role of *Polg*^{D257A}, a Mitochondrial DNA Mutator, on Diabetes and Obesity
(Under the direction of Nobuyo Maeda, PhD)

Mitochondria are highly conserved organelles, found in most cells throughout the body, and perform many essential biological processes. Mitochondria are responsible for the production of energy in the form of ATP that is required to maintain normal function in eukaryotic cells. While this is beneficial to the cell, mitochondria have the unique role in initiating cell death. It is not surprising that mitochondrial dysfunction is the hallmark of many metabolic disorders such as maternally inherited diabetes and deafness. Some evidence suggests that mitochondrial dysfunction via mitochondrial DNA damage in the form of DNA deletions and mutations can contribute to complications associated with diabetes, yet a causal role of mitochondrial DNA mutations in diabetic complications has not been answered. The PolgD257A mutant mouse disrupts the proofreading domain of DNA polymerase gamma resulting in the random accumulation of mitochondrial DNA mutations. The research presented in this dissertation aims to utilize the PolgD257A mutant mouse as a genetic tool to further investigate the role that accumulating mitochondrial DNA mutations have in diabetes, obesity, and diabetic complications.

I demonstrate that accumulating mitochondrial DNA mutations in "Akita" diabetic mice improves the diabetic phenotype of the male mice. Within this study, I determined that mitochondrial dysfunction in the testis reduces appetite thereby improving diabetes, underlining the importance of hyperphagia in the diabetic Akita mouse. Over the course of this study, I uncovered a phenotype of the small intestine that was not described previously. In a separate study, I characterized the small intestine phenotype demonstrating that the PolgD257A mutation disrupts the cell cycle of the rapidly dividing cells in the small intestine leading to an increase in cell death. While the small intestine phenotype does not seem to cause an observable phenotype in the PolgD257A mice, the final study investigated the functional aspect of the small intestine by challenging the mice with a high fat, high carbohydrate diet. The diet challenged mice were protected against obesity suggesting a role for mitochondria in normal lipid absorption. Together, these studies have elucidated the unexpected role of mitochondrial DNA mutations in reversing diabetes and preventing obesity.

ACKNOWLEDGMENTS

I would like to thank:
Dr. Nobuyo Maeda (advisor) and Dr. Oliver Smithies
Dr. Randy Thresher

The Smithies-Maeda Lab, past and present members:
Kumar Pandya, Lance Johnson, Avani Pendse, Marcus McNair, Feng Li, Heather Doherty, Hirofumi Tomita, Masao Kakoki, José Arbones-Mainar, Mike Altenburg, Jen Wilder, Sylvia Hiller, Hyung-Suk Kim, Shin-Ja Kim, Svetlana Zhilicheva, Ron Xu, Xianwen Yi, Sabrina Baxter, Ruri Grant, John Hagaman, Jenny Holt, Sarah Karkanawi, Melissa Knudson, Taylor Nipp, and Yukako Uchiyama

I would like to thank the Magness lab and Caron lab for their contributions to this work.

My Committee Members
Kathleen Caron
Karen Mohlke
Scott Magness
Bill Coleman
Mark Majesky

My Parents, Ray and Fannie Fox
My in-laws, Robert and Kathy Byrnes

My Wife, Jessica
For all of her love, support and advice.

I dedicate this dissertation to my kids:
Jack and Riley

TABLE OF CONTENTS

LIST OF TABLES

LIST OF FIGURES

LIST OF ABBREVIATIONS

3-HB	3-hydroxybutyrate
ATP	Adenosine triphosphate
CoxIII	Cytochrome c oxidase subunit 3
Cytb	Cytochrome b
Dlp1	Dynamin-like protein 1
DNA	Deoxyribonucleic acid
dsDNA	Double strained deoxyribonucleic acid
EdU	5-ethynyl-2´-deoxyuridine
ELISA	Enzyme-linked immunosorbent assay
EM	Electron microscopy
Fabp1	Fatty acid binding protein 1
Fabp2	Fatty acid binding protein 2
FCCP	Carbonylcyanide p-trifluoromethoxyphenylhydrazone
gDNA	Genomic deoxyribonucleic acid
GF	Perigonadal fat
GI	Gastrointestinal
Glut2	Glucose transporter - 2
GTT	Glucose tolerance test
H&E	Hematoxylin and eosin
HFD	High fat diet
hFisp1	Human mitochondrial fission protein 1
Hpt1	Cadherin 17

IF	Inguinal fat
Ins2	Insulin 2
ITT	Insulin tolerance test
LHON	Lieber's Hereditary Optic Neuropathy
Lyve-1	Lymphatic vessel endothelial hyaluronan receptor
Mcm2	Minichromosome maintenance complex component 2
Mct1	Monocarboxylate transporter 1
MELAS	Mitochondrial encephalomyopathy, lactic acidosis, and stroke-like episodes
MERRF	Myoclonic epilepsy with ragged red fibers
Mfn1	Mitofusin 1
mRNA	Messenger ribonucleic acid
mtDNA	Mitochondria deoxyribonucleic acid
mtSNP	Mitochondrial single nucleotide polymorphism
Nadc1	Sodium-dicarboxylate transporter
Nbc3	Sodium bicarbonate cotransporter 3
ND	Normal diet
ND1	mitochondrial encoded NADH dehydrogenase 1
ND3	mitochondrial encoded NADH dehydrogenase 3
ND4	mitochondrial encoded NADH dehydrogenase 4
ND5	mitochondrial encoded NADH dehydrogenase 5
ND6	mitochondrial encoded NADH dehydrogenase 6
NIDDK	National Institute of Diabetes and Digestive and Kidney Diseases
Nkcc2	Na-K-Cl transporter 2

Npy	Neuropeptide Y
NS	Non-significant
OCR	Oxygen consumption rate
Octn2	Organic cation/carnitine transporter 2
O_H	Origin of heavy strand
O_L	Origin of light strand
Opa1	Optic atrophy type 1
PA	(Polg-Akita) $Polg^{D257A/D257A};Ins2^{C96Y/+}$
PAS	Periodic acid schiff
PBS	Phosphate buffered saline
PCR	Polymerase chain reaction
PEO	Progressive External Ophthalmoplegia
Pept1	Peptide transporter 1
PFA	Paraformaldehyde
pH3	Phospho-Histone H3
Pol γ α	Polymerase gamma, α subunit
Pol γ β	Polymerase gamma, β subunit
Polg	Polymerase gamma
Pomc	Proopiomelanocortin
PP	(Polg) $Polg^{D257A/D257A}$
RER	Respiratory exchange ratio
RNA	Ribonucleic acid
ROS	Reactive oxygen species

RT-PCR	Real time polymerase chain reaction
SANDO	Sensory Ataxic Neuropathy, Dysarthria, and Ophthalmoparesis
SEM	Standard error mean
Sfxn1	Sideroflexin 1
Sglt	Sodium-dependent glucose cotransporter 1
SSB	Single standed binding
Svct1	Sodium-dependent vitamin C transporter 1
TA	Transit amplifying
TCA	Tricarboxylic acid cycle or the Krebs cycle
Tfam	Transcription factor a, mitochondrial
TG	Triglyceride
tRNA	Transfer ribonucleic acid
TUNEL	Terminal deoxynucleotidyl transferase dUTP nick end labeling
W	(WT) *Wild type*
WA	(Akita) $Ins2^{C96Y/+}$

Chapter 1

INTRODUCTION

1.1 Mitochondria

The origin of mitochondria in eukaryotic cells has been a controversial topic since the early 20th century. Multiple theories have been proposed. The discovery of small circular DNA of mitochondria in animal tissues in the 1960's by Rabinowitz et al provided some evidence to the theory that mitochondria originated from a bacterial source (1). However, it was not until the 1980's that Dr. Lynn Margulis' theory of endosymbiosis was accepted as the most plausible origin of mitochondria (2). The endosymbiosis theory states that mitochondria originate from an ancient bacterial species being engulfed, but not lysed, by an early eukaryotic cell forming a mutually beneficial symbiotic relationship (3). During evolution, eukaryotic cells began to rely on mitochondria for efficient production of ATP (4).

The human body is a prime example of utilization of this symbiotic relationship. There are many cells in the human body that require high energy production, including neurons, hair cells of the inner ears, heart and skeletal myocytes, pancreatic beta cells, as well as gut and kidney epithelial cells; and all of these cell types are highly packed with mitochondria (5-9). Mitochondria provide the highly specialized functions of energy production, cell death/apoptosis signaling, and regulation of cell cycle (10). The highly specialized efficient production of ATP has earned mitochondria the nickname "powerhouse of the cell." The number of mitochondria per cell in the human body varies from tissue to tissue and is dependent on the level of metabolic activity of the cell. Wiesner et al estimated by PCR that there are on average approximately 1-3 copies of mitochondrial DNA (mtDNA) per rat mitochondria, and this varies in number depending on the tissue (11).

1.2 Mitochondrial DNA Mutations and Aging

Elucidating the mechanism of aging has become an important issue for the medical sciences. As people live longer, the cost to combat aging-related disease has become a burden for society. It has become apparent that mitochondria play an influential role in the aging process (12-22). This is not surprising since mitochondria are essential for maintaining the metabolic activity of the cells throughout the body, and that any metabolic imbalance would alter cellular function within a particular tissue. The mitochondrial theory of aging is based on the idea that reactive oxygen species (ROS) damage mitochondrial DNA (23-25). With age, an accumulation of DNA damage leads to irreversible dysfunction of the mitochondrion and an eventual aging phenotype.

Epidemiological studies comparing young and old individuals have described a significant increase in mitochondrial DNA mutations in older individuals (26). Comparison of DNA sequence of mitochondria from young and old mice showed that aged mice have significantly higher levels of mtDNA mutations than younger mice (27). Despite the evidence for accumulating mitochondrial DNA mutations in aging, however, debate has persisted related to the causal role of mitochondrial mutations in the aging process: does aging cause increased mtDNA mutations or are accumulation of mtDNA mutations sufficient for aging? A recent mouse model of aging suggests that mitochondrial DNA mutations are the driving force behind the aging process (18, 21).

1.3 Mitochondria in Disease

Several progressive age-related diseases have been directly linked to point mutations found throughout the mitochondrial genome. Mitochondrial disorders affect many organ systems through out the body including the brain, eyes, pancreas, skeletal muscles,

gastrointestinal system, and heart. Surprisingly, a single base change in the mitochondrial genome is sufficient to cause a mitochondrial disease. Tables 1.1 and 1.2 summarize the point mutations found to date in mtDNA and the disorder linked to the change in either a mitochondrial gene or a mitochondrial tRNA. The vast majority of point mutations found involve mutations in tRNAs.

Table 1.1: Disorders with mitochondrial DNA mutations in mitochondrial genes

Mutation	Gene	Clinical phenotype	References
A1555G	12s rRNA	deafness, aminoglycoside ototoxicity	Prezant 1993 (28)
T8993C	ATPase 6	Leigh Disease	de Vries 1993 (29)
T8993G	ATPase 6	Leigh Disease	Tatuch 1992 (30)
T9185C	ATPase 6	Leigh Disease	Moslemi 2005 (31)
T9191C	ATPase 6	Leigh Disease	Moslemi 2005 (31)
T8993G	ATPase 6	Neuropathy, ataxia, retinitis pigmentosa	Holt 1990 (32)
T9957C	COXIII	MELAS	Manfredi 1995 (33)
G13513A	ND5	MELAS	Santorelli 1997 (34)
G15059A	CYTB	fatigue, muscle weakness, exercise intol.	Andreu 1999 (35)
G11832A	ND4	Exercise intolerance	Andreu 1999 (36)
G3460A	ND1	LHON	Huoponen 1991 (37)
T4160C	ND1	LHON	Howell 1991
A4136G	ND1	LHON	Howell 1991 (38)
A11696G	ND4	LHON	de Vries 1996 (39)
G11778A	ND4	LHON	Wallace 1988 (40)
G14459A	ND6	LHON	Jun 1994 (41)
T14484C	ND6	LHON	Johns 1992 (42)
T10191C	ND3	epilepsy, stroke-like episodes, optic atrophy	Taylor 2001 (43)
T10158C	ND3	infantile encephalopathy	McFarland 2004 (44)

(LHON – Lieber's Hereditary Optic Neuropathy, MELAS - *Mitochondrial Encephalomyopathy, Lactic Acidosis, and Stroke*-like episodes)

Table 1.2: Disorders with mitochondrial DNA mutations in tRNAs

Mutation	tRNA	Clinical phenotype	References
A4336G	tRNA-Gln	Alzheimers/Parkinsons	Egensperger 1997 (45)
A4300G	tRNA-Ile	Cardiomyopathy	Casali 1995 (46)
C3303T	tRNA-Leu	Cardiomyopathy	Silvestri 1994 (47)
A3260G	tRNA-Leu	Cardiomyopathy, myopathy	Zeviani 1991 (48)
A4269G	tRNA-Ile	Fatal cardiomyopathy	Taniike 1992 (49)
A3243G	tRNA-Leu	diabetes and deafness	van den Ouweland 1992 (50)
C4320T	tRNA-Ile	Encephalomyopathy	Santorelli 1995 (51)
T14709C	tRNA-Glu	Encephalomyopathy	Hanna 1995 (52)
G12315A	tRNA-Leu	Encephalomyopathy	Fu 1996 (53)
G15915A	tRNA-Thr	Encephalomyopathy	Nishino 1996 (54)
G8313A	tRNA-Lys	encephaloneuropathy, GI	Verma 1997 (55)
A5814G	tRNA-Cys	Encephalopathy	Manfredi 1996 (56)
G5549A	tRNA-Trp	Encephalopathy	Nelson 1995 (57)
G8363A	tRNA-Lys	Encephalopathy, hearing loss, cardiomyopathy	Santorelli 1996 (58)
G8363A	tRNA-Lys	Neuropathy	Pineda 2004 (59)
A15923/4G	tRNA-Thr	Fatal, infantile Respiratory defect	Yoon 1991 (60)
T7511C	tRNA-Ser	hearing loss	Sue 1999 (61)
T7445C	tRNA-Ser	hearing loss	Reid 1994 (62)
T9997C	tRNA-Gly	hypertrophic Cardiomyopathy	Merante 1994 (63)
A4295G	tRNA-Ile	hypertrophic Cardiomyopathy	Merante 1996 (64)
T7512C	tRNA-Ser	MERRF/MELAS	Nakamura 1995 (65)
A8344G	tRNA-Lys	Myoclonic epilepsy, myopathy	Shoffner 1990 (66)
T8356C	tRNA-Lys	Myoclonic epilepsy, myopathy	Silvestri 1992 (67)
A12320G	tRNA-Leu	Myopathy	Weber 1997 (68)
A3288G	tRNA-Leu	Myopathy	Hadjigeorgiou 1999 (69)
A3302G	tRNA-Leu	Myopathy	Bindoff 1993 (70)
T3250C	tRNA-Leu	Myopathy	Goto 1992 (71)
G15990A	tRNA-Pro	Myopathy	Moraes 1993 (72)
T14709C	tRNA-Glu	myopathy, weakness, diabetes	Hao 1995 (73)

A3243G	tRNA-Leu	MELAS	Goto 1990 (74)
A3252G	tRNA-Leu	MELAS	Morten 1993 (75)
T3271C	tRNA-Leu	MELAS	Goto 1991 (76)
T3291C	tRNA-Leu	MELAS	Goto 1994 (77)
T5537l	tRNA-Trp	MELAS	Santorelli 1997 (78)
G1642A	tRNA-Val	MELAS	Taylor 1996 (79)
G5703A	tRNA-Asn	PEO	Moraes 1993 (80)
T4285C	tRNA-Ile	PEO	Silvestri 1996 (81)
C3256T	tRNA-Leu	PEO	Moraes 1993 (80)
A10044G	tRNA-Gly	Unexpected Death	Santorelli 1996 (82)

(PEO – Progressive External Ophthalmoplegia, MELAS - *Mitochondrial Encephalomyopathy, Lactic Acidosis, and Stroke*-like episodes, MERRF - *Myoclonic Epilepsy with Ragged Red Fibers*)

Diabetes and Obesity

Diabetes mellitus is becoming increasingly common worldwide. Type 1 diabetes accounts for 5 to 10 percent of all cases of diabetes in the US (83). Type 1 diabetes is characterized by the inability of the pancreas to produce sufficient insulin to effectively lower blood glucose levels. In humans, type 1 diabetes is classified as a chronic autoimmune disorder that destroys the beta cell of the pancreatic islets (84, 85). The exact trigger of the autoimmune response still remains a mystery (85). However, it has been reported that auto reactive T-cell destruction of beta cells is a contributing event that leads to autoimmune diabetes in humans (86). In support of this mechanism, the activated T-cells lead to beta cell apoptosis followed by progression to diabetes in non-obese diabetic (NOD) mice that have a mutation in (87-90).

Obesity and type 2 diabetes is becoming increasingly common worldwide. In the US, type 2 diabetes accounts for 90 to 95 % of all cases of diabetes with a growing portion of the diabetic cases occurring in young individuals. Type 2 diabetes is characterized by the insulin resistance of peripheral tissues leading to prolonged elevation of insulin levels. There is a large body of data demonstrating links between mitochondrial dysfunction, insulin resistance, and type 2 diabetes (91).

Mitochondrial Dysfunction and Diabetes

A subset of diabetic patients is classified as having maternally inherited diabetes and deafness (MIDD). MIDD has been traced to a point mutation in the mitochondrial DNA producing A3243G in tRNA-Leu (50, 92). Although, only one instance of a maternally inherited point mutation that leads to diabetes and deafness has been discovered so far, there is a potential for greater number of point mutations that lead to diabetes and obesity since new mutations are being added to a growing database of mitochondrial diseases. Whether defects

caused by mtDNA mutations are sufficient to induce diabetes remains unknown. However, since mitochondria are key to energy metabolism, one could speculate that mtDNA mutations would lead to diabetes. Mitochondrial dysfunction caused by mutations in mitochondrial DNA can directly influence the development of type I diabetes through effects on the production of insulin (92). It remains unclear whether the mitochondrial problems act causally with respect to diabetes or are consequences of the condition. A recent study has shown that adipocyte dysfunction was caused by a reduction in the number of mitochondria in adipocytes leading to the development of type 2 diabetes (93). However, this study did not explore the cause of the reduction in mitochondria: is it related to mitochondrial dysfunction? Further links involving mitochondrial related problems with adipocytes leading to the development of obesity and type 2 diabetes have been described with emphasis on adipocyte dysfunction, metabolic overload, and inflammatory damage to adipocytes (94). It has been suggested that mitochondrial dysfunction is a contributing factor in the insulin resistance of peripheral tissues, the secretion of insulin from the beta cells, energy expenditure, and removal of ROS all of which contribute to type 2 diabetes (95-98). Since, insulin secretion from the beta cells requires ATP, it is not surprising that mitochondrial dysfunction would lead to impaired release of insulin in response to glucose. Thus, the causal role of mitochondrial DNA mutations in diabetes and obesity remains an important question.

Diabetic Complications

Prolonged diabetes can damage the cardiovascular system, kidney, retina, peripheral and central nervous system, and muscles leading to serious complications that increase the risk of morbidity and mortality. This dissertation focuses on one complication, diabetic nephropathy. Diabetic nephropathy is the major cause of end stage renal disease in the United

States, but not all diabetic patients develop nephropathy (83). This suggests underlying genetic factors may contribute towards nephropathy in select individuals. Mouse models are ideal in studying the pathophysiology of diseases such as nephropathy. However, mouse models have their limitations in the study of human disease because they often do not recapitulate the disease. For instance, C57BL/6 mice are relatively resistant to nephropathy while other models do not exhibit all the characteristics of human renal disease (99, 100).

Previous work in our lab suggests a link between mitochondrial DNA mutations and diabetic nephropathy. Interestingly, removal of the bradykinin B2 receptor in diabetic "Akita" mice enhanced nephropathy (101). In addition, a premature aging phenotype was described in mice with the diabetic Akita mutation and the removal of B2-receptor (102). These mice also had increased mtDNA mutations, mtDNA deletions, and many symptoms of aging (hair loss, kyphosis, and osteoporosis). However, neither study addressed whether mitochondrial DNA mutations contribute directly to the diabetic nephropathy or if the mtDNA mutations are simply a consequence of the disease. This prompted an evaluation of the contribution of mtDNA mutations in the development of diabetic nephropathy.

1.4 Mitochondrial Replication

Mitochondria contain their own circular DNA that is approximately 16.3 kB in length in mice (103). During cell division, mother cells must replicate mitochondria in order to provide daughter cells with enough mitochondria to grow, function, and survive. The duplication of mitochondria requires the synthesis of mtDNA followed by mitochondrial division via fission. Mitochondrial fission is the process by which mitochondria divide into two identical organelles (104). Mitochondrial fission is regulated through an interaction between *hFisp1*, a mitochondrial protein, and *DLP1*, Dynamin-like protein (105-107). Mitochondria

also undergo fusion in order to maintain the numbers of functional mitochondria in the cell. Mitochondrial fusion machinery consists of two GTPases, *Mtn1* and *OPA1*, which when combined cause a linkage between mitochondria and results in the fusion event (108). The balance of mitochondrial fusion and fission is essential in the maintenance of functional mitochondria and normal cellular function. Any imbalance in fusion and fission results in loss of function, fragmentation of mitochondria, and apoptosis (109, 110). Prior to mitochondrial fission, mtDNA must be replicated in order to provide the newly generated mitochondrion the genetic information required to produce the enzymes associated with the electron transport chain. Mitochondria DNA replication occurs by asymmetric strand displacement replication (111-114). Briefly, synthesis of mtDNA is initiated at the origin of heavy strand (O_H) by mtDNA polymerase gamma (*Polg*). The O_H strand is replicated displacing the light strand (O_L) allowing single stranded binding protein (SSB) to bind to the O_L strand until the replication of O_H has proceeded past O_L at which point *Polg* begins replicating the light strand.

1.5 Mitochondrial DNA Polymerase gamma

Mitochondrial DNA polymerase gamma (*Polg*), a nuclear encoded gene, is solely responsible for replication and proofreading of mitochondrial DNA. Mouse *Polg* and human *POLG* genes, located on chromosome 7 and 15, respectively, consist of 23 exons, and are well conserved (115). The POLG protein has three exonuclease domains that contribute to the fidelity of the polymerase (116). Human polymerase γ contains a catalytic core (pol γ-α), which consists of the polymerase and exonuclease domains, and an accessory subunit (pol γ-β), which is a dimer and stimulates DNA binding and holoenzyme processing (Fig. 1.1) (117). Figure 1.2 illustrates a schematic of the gene and protein structure of Human *POLG*. Figure 1.2 also illustrates the known polymorphisms found in POLG and their association with disease

(118). In humans, there have been approximately 150 mutations consisting of both mtSNPs and point mutations (associated with disease) described in POLG (118). Point mutations in POLG cause an increase in mtDNA deletions (119). Recently a new body of work has underlined the importance of point mutations in POLG that directly lead to various neurological diseases in human patients. For example, a point mutation G451E in the linker region of POLG directly causes progressive external ophthalmoplegia by disruption of mitochondria maintenance (120, 121). Two point mutations, A467T and R627W, (found in the linker region) in POLG lead to Sensory Ataxic Neuropathy, Dysarthria and Ophthalmoparesis (SANDO) (121). Two recent reports described the W748S mutation, also in the linker region of POLG, as a cause of autosomal recessive neurodegenerative disorders (122, 123). Furthermore, mutations Y955C and R953C, located in the polymerase domain, and mutation N468D located in the linker region of POLG, have been found to co-segregate with Parkinsonism (124). *Polg* in mice is essential for life since removal of the gene leads to embryonic developmental arrest at E7.5-E8.5 (125). In *Saccharomyces cerevisiae,* ablating the exonuclease domain activity leads to an approximately 500 to 1500-fold increase in mitochondrial DNA mutations (126, 127). In summary, *POLG* is essential for life, provides both replication and proofreading of mtDNA, and point mutations in the gene have a wide-ranging impact on the human population in neurological and muscle disorders.

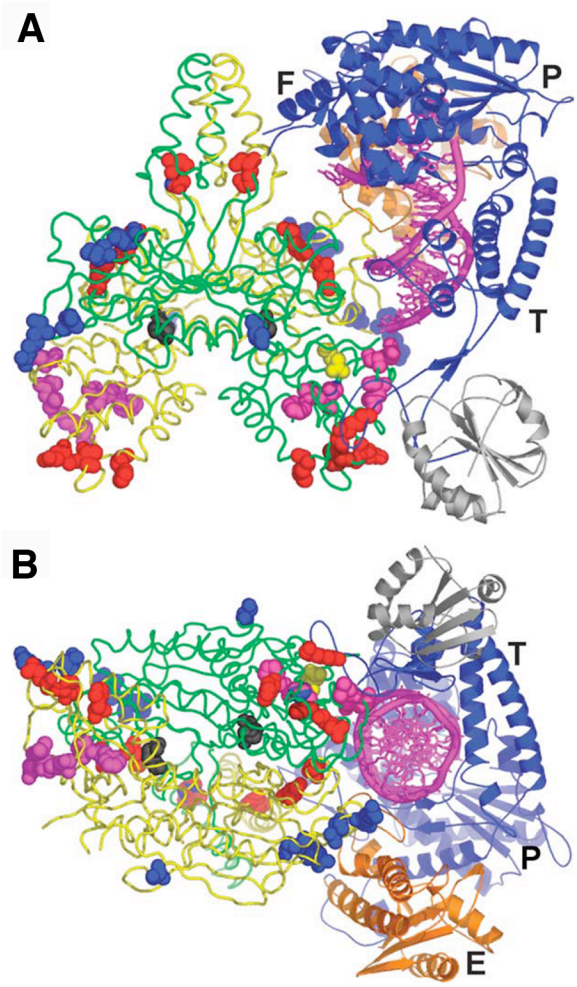

Figure 1.1: Structural model of human pol γ

A) Accessory Pol γ-β subunits (green and yellow) interacting with the catalytic Pol γ-α core (blue and orange ribbons), and binding to dsDNA (magenta). F – finger, P – palm, and T – thumb domains of polymerase.

(B) Alternate view of the Pol γ complex with clear view of E - exonuclease domain of polymerase.

Note: Thioredoxin (gray) from T7 DNA polymerase is not found in Pol γ.

"Reprinted from Journal of Molecular Biology, 358, Fan L, et al., A Novel Processive Mechanism for DNA Synthesis Revealed by Structure, Modeling and Mutagenesis of the Accessory Subunit of Human Mitochondrial DNA Polymerase, 1229-1243, Copyright (2006), with permission from Elsevier."

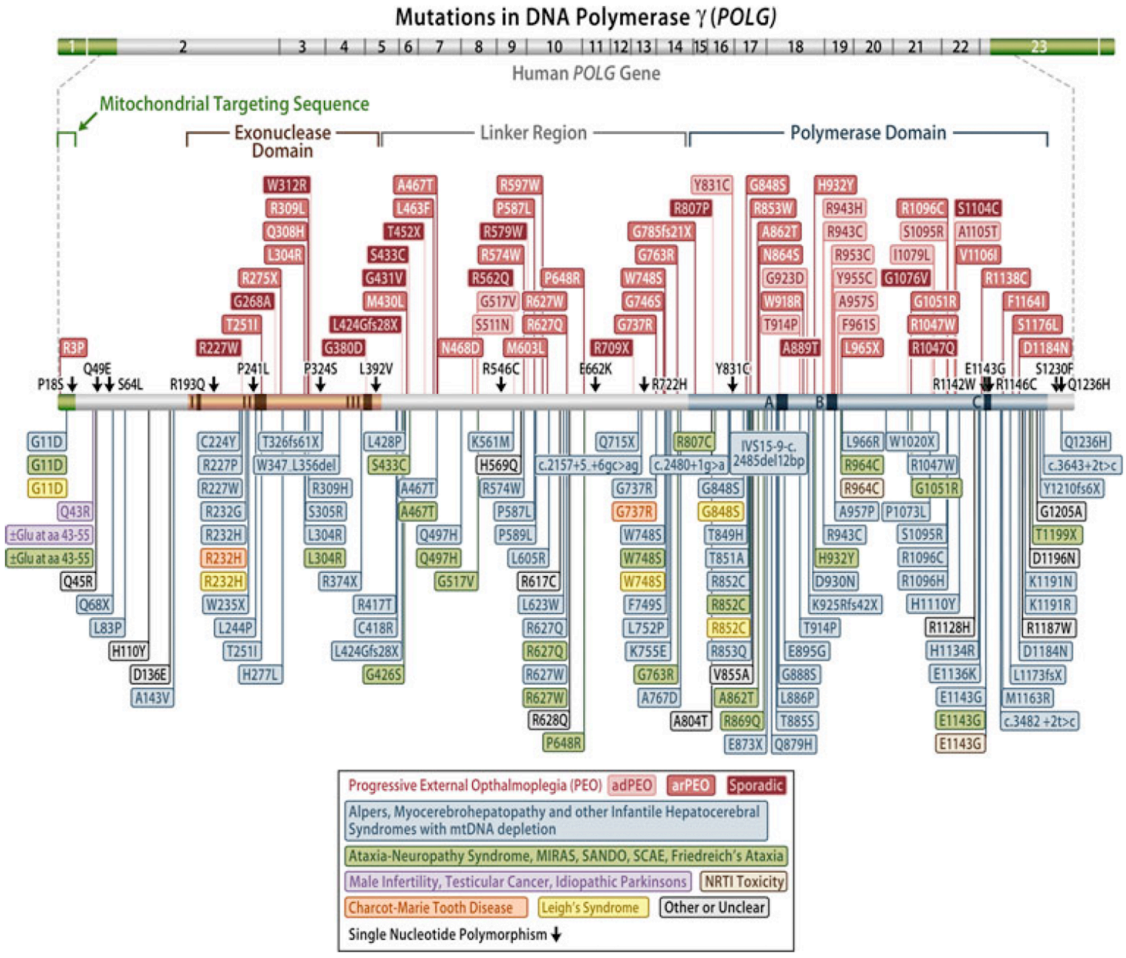

Figure 1.2: Illustration of Human polymerase γ (POLG) and point mutations associated with disease. POLG gene (top) consists of 23 exons. The POLG protein (bottom) structure is highlighted by a mitochondrial targeting sequence, exonuclease domain, linker region, and polymerase domain. Boxes represent amino acid changes causes by point mutations within the mitochondrial genome and the disease associated with the mutation. "With kind permission from Springer Science+Business Media: Cellular and Molecular Life Sciences, Mitochondrial DNA replication and disease: insights from DNA polymerase γ mutations, (2011) 68:219-233, Stumpf, JD and Copeland, WC, Figure 3, © Springer Basel AG (outside the USA) 2010."

1.6 Mitochondrial DNA Mutator Mice (Polg-D257A)

The creation of mitochondrial DNA mutator mice, which displays many of the phenotypes of aging as well as a reduced lifespan, have helped to shed light on the causal role of mitochondrial mutations in aging. A mutation from aspartic acid to alanine at amino acid position D230A in POLG has been reported to cause an ablation of the proofreading domain of the polymerase without affecting the replication efficiency of the polymerase resulting in a premature aging phenotype (126, 127). Aspartate residues are important for the catalytic function of exonuclease activity of POLG and are evolutionarily conserved (127). Two independent groups introduced the POLG-D257A mutation in mice. Homozygous mutants have an acceleration of mitochondrial DNA mutations over the lifespan of the mouse (18, 21). As seen in Figure 1.3, the mutation decreases lifespan to 13 months in *Polg* mice homozygous for D257A mutation compared to 30 months in wild type mice. Physical signs of premature aging include hair loss, kyphosis, and decreased bone density. The major tissues affected by this mutation are the highly proliferating tissues of the bone marrow, skin, testis, and small intestine (18, 21). Chen et al recently reported that the $Polg^{D257A/D257A}$ mice die prematurely due to a severe fatal anemia caused by mitochondrial dysfunction (128). The amount of mtDNA mutations accumulated in 13-month old $Polg^{D257A/D257A}$ mice has been estimated as high as $1x10^{-3}$ mutations/bp in most tissues compared to $<5x10^{-4}$ mutations/bp in wild type mice (18, 21, 129, 130). Since Polg is a processing enzyme mitochondrial DNA mutations are increased in the heterozygous Polg-D257A mice compared to wild type mice (18, 21). However, heterozygotes have a natural lifespan and show no aging-associated phenotype. The authors suggested the premature aging phenotypes is not because of nucleotide substitutions in mitochondrial DNA but because of deletions in mtDNA which is

increased by 90 fold in homozygotes compared to heterozygotes (18, 21). It is noted that the *Polg*$^{D257A/D257A}$ mice display many of the age-related phenotypes seen in human aging (129). Nevertheless, the *Polg*$^{D257A/D257A}$ mice provide a genetic means to artificially induce global increases in mitochondrial DNA mutations, and this tool will provide us with a means to study the effects of mitochondrial DNA mutations on pathophysiology of age-related diseases such as diabetes and obesity.

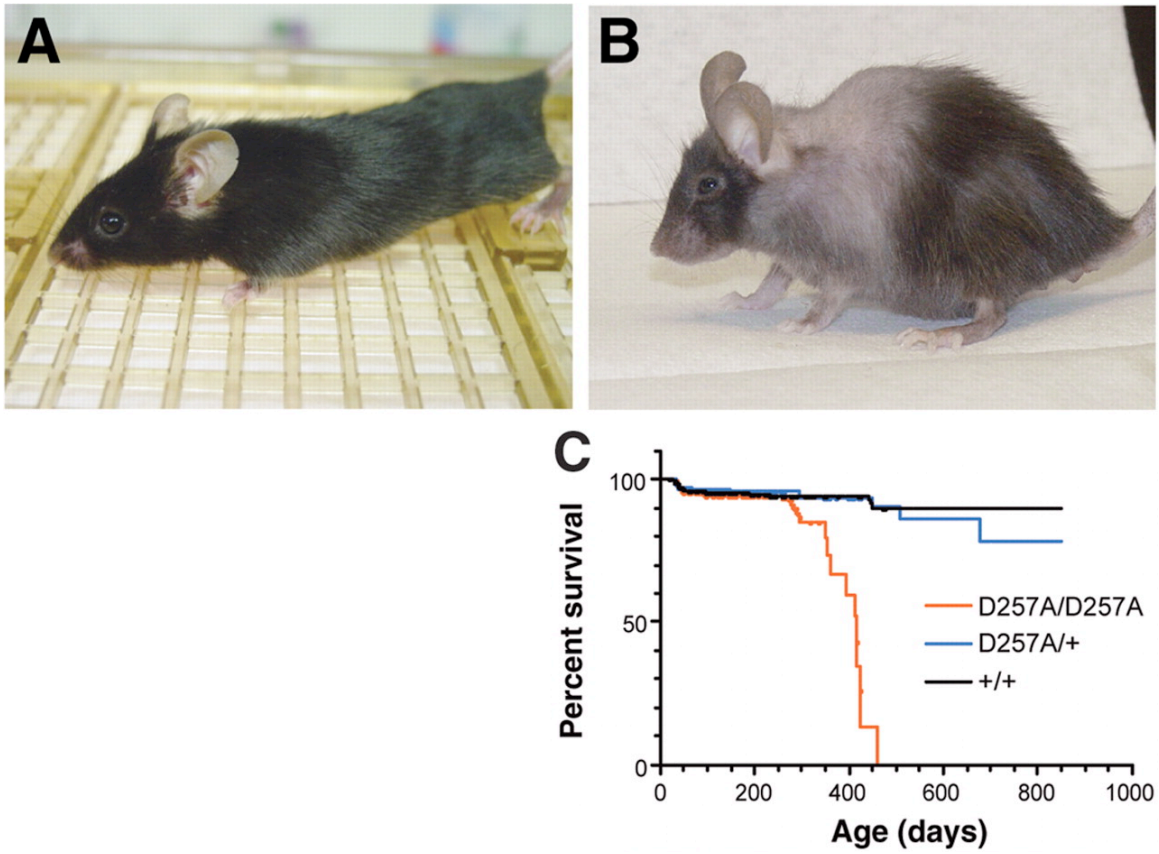

Figure 1.3: Premature aging phenotype induced by the Polg-D257A mutation. (A) Wild type and (B) the accelerated aging phenotype of *Polg*$^{D257A/D257A}$ mice are shown at ~ 13 months of age, with Polg mice displaying hair loss and kyphosis that is commonly associated with aging in humans. (C) Reduced survival of Polg homozygous (D257A/D257A) compared to Polg heterozygous (D257A/+) and wild type (+/+) mice. From Kujoth GC, *et al.* (2005) Mitochondrial DNA mutations, oxidative stress, and apoptosis in mammalian aging. *Science (New York, N.Y.)* 309(5733):481-484. Reprinted with permission from AAAS.

1.7 Mouse Models Used for these Studies

Polg$^{D257A/D257A}$ Mice, a Mitochondrial DNA Mutator Mouse

For induction of mitochondrial DNA mutations, I employed the use of a mutation in Polymerase gamma (D257A) that ablates the proofreading activity without affecting the replication activity of the enzyme. As described earlier in section 1.6, the *Polg*$^{D257A/D257A}$ mouse develops a premature aging phenotype with hair loss, graying of the hair, and kyphosis (18, 21). Furthermore, the Polg mutant mice have increased cell apoptosis and no changes to ROS (18, 21). The median lifespan of this model is 13 months of age, and the extent of the lifespan is determined by the severity of a fatal anemia that these mice are prone to developing (128). There is a general increase in mitochondrial DNA mutations in all tissues especially tissues which are actively proliferating (small intestine, skin, testis, and bone marrow) or metabolically active (liver). While there have been no reports of diabetes or obesity in the Polg-D257A mouse model, therefore it is suitable to test whether increased mtDNA mutations would accelerate diabetes related complications.

Akita (*Ins2*$^{C96Y/+}$) Mice, a Mouse Model of Type 1 Diabetes

While there are several models available for the study of type 1 diabetes (131), I chose a well-studied genetic model of type 1 diabetes caused by a depletion of insulin due to a spontaneous mutation in the Insulin 2 gene of the mouse (132, 133). This model, termed Akita, is a well-established and frequently used model for type 1 diabetes. The Akita mouse has an amino acid change at position 96 from cytosine to tyrosine that disrupts the disulfide bond that keeps Insulin 2 properly folded. Accumulation of the mis-folded pro-insulin in the pancreatic beta cell induces endoplasmic reticulum stress, and eventually causes beta cell apoptosis (134).

Homozygous males with the Akita mutation die at about 8 weeks of age due extremely severe diabetes. The Akita mutation is an autosomal dominant mutation where heterozygous males are severely hyperglycemic and are used as a model for type 1 diabetes (Akita mouse). Hyperglycemia is pronounced in male mice where plasma glucose levels may reach as high as 500 mg/dL, while glucose levels in female mice only reach about 280 mg/dL. In addition to increased plasma glucose levels, Akita mice exhibited several other diabetic symptoms including increased water consumption, increased appetite, increased urination, and decreased body weights. These symptoms are typically seen in diabetic patients prior to treatment with insulin. Due to the severe hyperglycemia, the untreated Akita male mice have a reduced lifespan to about 13 months of age. It is important to note that despite the severe hyperglycemia the Akita male mouse does not develop overt diabetic complications such as nephropathy suggesting that there is an underlying genetic factor required to induce diabetic complications. This model was used to induce diabetes in the presence of the Polg-D257A mutation for the first part of my dissertation.

Mouse Models of Obesity and Type 2 Diabetes

For induction of obesity and type 2 diabetes, I chose to use a well-established dietary model. Induction of obesity and type 2 diabetes occurs through a dietary regime high in carbohydrates and fat (135). The animals are fed *ad libitum* for 12-14 weeks that results in a diabetic and obesity phenotype characterized by hyperinsulinemia, hyperglycemia, and significant gain in weight due to the storage of fat in the subcutaneous and inguinal fat depots (136). The diet induced obesity leads to a sustained increase in circulating insulin that over time will develop the insulin resistance phenotype. Similar to Akita mice, the mice do not develop diabetic complications. This model was utilized in the second part of my dissertation.

1.8 Overall Goals and Hypotheses

The overall goals of this dissertation project were to determine the effects of artificially increasing mitochondrial DNA mutations on the metabolic diseases of diabetes and obesity. To do so, I utilized genetically engineered models of diabetes along with the PolgD257A mouse model for inducing an accumulation of mitochondrial DNA mutations. The work presented in **Chapter 2** explores the role of increasing mitochondrial DNA mutations on both diabetes and diabetic complications. The expectation being that increasing mitochondrial DNA mutations would accelerate diabetes and diabetes-related complications. Surprisingly, the diabetic phenotype of the double mutant mice becomes less severe as they age. **Chapter 3** characterizes the effect of the PolgD257A mutation on the small intestine. These experiments demonstrate the effects of the PolgD257A mutation on the cell cycle in the small intestine transit amplifying cells. **Chapter 4** builds on this by uncovering the functional aspect of the cell cycle changes in the small intestine of PolgD257A mice. Again surprisingly, the PolgD257A mice fed a normal diet do not experience any outward phenotype, however after given a diet high in carbohydrates and fat the PolgD257A mice do not become obese and they are protected against high-fat diet induced metabolic dysfunction.

REFERENCES

1. Rabinowitz M, Sinclair J, DeSalle L, Haselkorn R, & Swift HH (1965) Isolation of deoxyribonucleic acid from mitochondria of chick embryo heart and liver. *Proc Natl Acad Sci U S A* 53(5):1126-1133.

2. Martin W, Hoffmeister M, Rotte C, & Henze K (2001) An overview of endosymbiotic models for the origins of eukaryotes, their ATP-producing organelles (mitochondria and hydrogenosomes), and their heterotrophic lifestyle. *Biol Chem* 382(11):1521-1539.

3. Sagan L (1967) On the origin of mitosing cells. *J Theor Biol* 14(3):255-274.

4. Dyall SD, Brown MT, & Johnson PJ (2004) Ancient invasions: from endosymbionts to organelles. *Science* 304(5668):253-257.

5. Simmons RA, Suponitsky-Kroyter I, & Selak MA (2005) Progressive accumulation of mitochondrial DNA mutations and decline in mitochondrial function lead to beta-cell failure. *J Biol Chem* 280(31):28785-28791.

6. Someya S*, et al.* (2008) The role of mtDNA mutations in the pathogenesis of age-related hearing loss in mice carrying a mutator DNA polymerase gamma. *Neurobiol Aging* 29(7):1080-1092.

7. Trifunovic A & Larsson NG (2008) Mitochondrial dysfunction as a cause of ageing. *J Intern Med* 263(2):167-178.

8. Wang J, Markesbery WR, & Lovell MA (2006) Increased oxidative damage in nuclear and mitochondrial DNA in mild cognitive impairment. *J Neurochem* 96(3):825-832.

9. Zhang D*, et al.* (2003) Mitochondrial DNA mutations activate the mitochondrial apoptotic pathway and cause dilated cardiomyopathy. *Cardiovasc Res* 57(1):147-157.

10. McBride HM, Neuspiel M, & Wasiak S (2006) Mitochondria: more than just a powerhouse. *Curr Biol* 16(14):R551-560.

11. Wiesner RJ, Ruegg JC, & Morano I (1992) Counting target molecules by exponential polymerase chain reaction: copy number of mitochondrial DNA in rat tissues. *Biochem Biophys Res Commun* 183(2):553-559.

12. Kujoth GC, Bradshaw PC, Haroon S, & Prolla TA (2007) The role of mitochondrial DNA mutations in mammalian aging. *PLoS Genet* 3(2):e24.

13. Kujoth GC & Prolla TA (2008) Evolving insight into the role of mitochondrial DNA mutations in aging. *Exp Gerontol* 43(1):20-23.

14. Lenaz G, Baracca A, Fato R, Genova ML, & Solaini G (2006) New insights into structure and function of mitochondria and their role in aging and disease. *Antioxid Redox Signal* 8(3-4):417-437.

15. Chomyn A & Attardi G (2003) MtDNA mutations in aging and apoptosis. *Biochem Biophys Res Commun* 304(3):519-529.

16. Dubec SJ, Aurora R, & Zassenhaus HP (2008) Mitochondrial DNA mutations may contribute to aging via cell death caused by peptides that induce cytochrome c release. *Rejuvenation Res* 11(3):611-619.

17. Krishnan KJ, Greaves LC, Reeve AK, & Turnbull DM (2007) Mitochondrial DNA mutations and aging. *Ann N Y Acad Sci* 1100:227-240.

18. Kujoth GC*, et al.* (2005) Mitochondrial DNA mutations, oxidative stress, and apoptosis in mammalian aging. *Science* 309(5733):481-484.

19. Kujoth GC, Leeuwenburgh C, & Prolla TA (2006) Mitochondrial DNA mutations and apoptosis in mammalian aging. *Cancer Res* 66(15):7386-7389.

20. Larsson NG (2010) Somatic mitochondrial DNA mutations in mammalian aging. *Annu Rev Biochem* 79:683-706.

21. Trifunovic A*, et al.* (2004) Premature ageing in mice expressing defective mitochondrial DNA polymerase. *Nature* 429(6990):417-423.

22. Wallace DC (2010) Mitochondrial DNA mutations in disease and aging. *Environ Mol Mutagen* 51(5):440-450.

23. Cheng KC, Cahill DS, Kasai H, Nishimura S, & Loeb LA (1992) 8-Hydroxyguanine, an abundant form of oxidative DNA damage, causes G----T and A----C substitutions. *J Biol Chem* 267(1):166-172.

24. Fraga CG, Shigenaga MK, Park JW, Degan P, & Ames BN (1990) Oxidative damage to DNA during aging: 8-hydroxy-2'-deoxyguanosine in rat organ DNA and urine. *Proc Natl Acad Sci U S A* 87(12):4533-4537.

25. Kino K & Sugiyama H (2001) Possible cause of G-C-->C-G transversion mutation by guanine oxidation product, imidazolone. *Chem Biol* 8(4):369-378.

26. Michikawa Y, Mazzucchelli F, Bresolin N, Scarlato G, & Attardi G (1999) Aging-dependent large accumulation of point mutations in the human mtDNA control region for replication. *Science* 286(5440):774-779.

27. Khaidakov M, Heflich RH, Manjanatha MG, Myers MB, & Aidoo A (2003) Accumulation of point mutations in mitochondrial DNA of aging mice. *Mutat Res* 526(1-2):1-7.

28. Prezant TR*, et al.* (1993) Mitochondrial ribosomal RNA mutation associated with both antibiotic-induced and non-syndromic deafness. *Nat Genet* 4(3):289-294.

29. de Vries DD, van Engelen BG, Gabreels FJ, Ruitenbeek W, & van Oost BA (1993) A second missense mutation in the mitochondrial ATPase 6 gene in Leigh's syndrome. *Ann Neurol* 34(3):410-412.

30. Tatuch Y*, et al.* (1992) Heteroplasmic mtDNA mutation (T----G) at 8993 can cause Leigh disease when the percentage of abnormal mtDNA is high. *Am J Hum Genet* 50(4):852-858.

31. Moslemi AR, Darin N, Tulinius M, Oldfors A, & Holme E (2005) Two new mutations in the MTATP6 gene associated with Leigh syndrome. *Neuropediatrics* 36(5):314-318.

32. Holt IJ, Harding AE, Petty RK, & Morgan-Hughes JA (1990) A new mitochondrial disease associated with mitochondrial DNA heteroplasmy. *Am J Hum Genet* 46(3):428-433.

33. Manfredi G*, et al.* (1995) A new mutation associated with MELAS is located in a mitochondrial DNA polypeptide-coding gene. *Neuromuscul Disord* 5(5):391-398.

34. Santorelli FM*, et al.* (1997) Identification of a novel mutation in the mtDNA ND5 gene associated with MELAS. *Biochem Biophys Res Commun* 238(2):326-328.

35. Andreu AL*, et al.* (1999) A nonsense mutation (G15059A) in the cytochrome b gene in a patient with exercise intolerance and myoglobinuria. *Ann Neurol* 45(1):127-130.

36. Andreu AL*, et al.* (1999) Exercise intolerance due to a nonsense mutation in the mtDNA ND4 gene. *Ann Neurol* 45(6):820-823.

37. Huoponen K, Vilkki J, Aula P, Nikoskelainen EK, & Savontaus ML (1991) A new mtDNA mutation associated with Leber hereditary optic neuroretinopathy. *Am J Hum Genet* 48(6):1147-1153.

38. Howell N, Kubacka I, Xu M, & McCullough DA (1991) Leber hereditary optic neuropathy: involvement of the mitochondrial ND1 gene and evidence for an intragenic suppressor mutation. *Am J Hum Genet* 48(5):935-942.

39. De Vries DD*, et al.* (1996) Genetic and biochemical impairment of mitochondrial complex I activity in a family with Leber hereditary optic neuropathy and hereditary spastic dystonia. *Am J Hum Genet* 58(4):703-711.

40. Wallace DC*, et al.* (1988) Mitochondrial DNA mutation associated with Leber's hereditary optic neuropathy. *Science* 242(4884):1427-1430.

41. Jun AS, Brown MD, & Wallace DC (1994) A mitochondrial DNA mutation at nucleotide pair 14459 of the NADH dehydrogenase subunit 6 gene associated with maternally inherited Leber hereditary optic neuropathy and dystonia. *Proc Natl Acad Sci U S A* 91(13):6206-6210.

42. Johns DR, Neufeld MJ, & Park RD (1992) An ND-6 mitochondrial DNA mutation associated with Leber hereditary optic neuropathy. *Biochem Biophys Res Commun* 187(3):1551-1557.

43. Taylor RW, Singh-Kler R, Hayes CM, Smith PE, & Turnbull DM (2001) Progressive mitochondrial disease resulting from a novel missense mutation in the mitochondrial DNA ND3 gene. *Ann Neurol* 50(1):104-107.

44. McFarland R*, et al.* (2004) De novo mutations in the mitochondrial ND3 gene as a cause of infantile mitochondrial encephalopathy and complex I deficiency. *Ann Neurol* 55(1):58-64.

45. Egensperger R, Kosel S, Schnopp NM, Mehraein P, & Graeber MB (1997) Association of the mitochondrial tRNA(A4336G) mutation with Alzheimer's and Parkinson's diseases. *Neuropathol Appl Neurobiol* 23(4):315-321.

46. Casali C, *et al.* (1995) A novel mtDNA point mutation in maternally inherited cardiomyopathy. *Biochem Biophys Res Commun* 213(2):588-593.

47. Silvestri G, *et al.* (1994) A new mtDNA mutation in the tRNA(Leu(UUR)) gene associated with maternally inherited cardiomyopathy. *Hum Mutat* 3(1):37-43.

48. Zeviani M, *et al.* (1991) Maternally inherited myopathy and cardiomyopathy: association with mutation in mitochondrial DNA tRNA(Leu)(UUR). *Lancet* 338(8760):143-147.

49. Taniike M, *et al.* (1992) Mitochondrial tRNA(Ile) mutation in fatal cardiomyopathy. *Biochem Biophys Res Commun* 186(1):47-53.

50. van den Ouweland JM, *et al.* (1992) Mutation in mitochondrial tRNA(Leu)(UUR) gene in a large pedigree with maternally transmitted type II diabetes mellitus and deafness. *Nat Genet* 1(5):368-371.

51. Santorelli FM, *et al.* (1995) A novel mitochondrial DNA point mutation associated with mitochondrial encephalocardiomyopathy. *Biochem Biophys Res Commun* 216(3):835-840.

52. Hanna MG, *et al.* (1995) Congenital encephalomyopathy and adult-onset myopathy and diabetes mellitus: different phenotypic associations of a new heteroplasmic mtDNA tRNA glutamic acid mutation. *Am J Hum Genet* 56(5):1026-1033.

53. Fu K, *et al.* (1996) A novel heteroplasmic tRNAleu(CUN) mtDNA point mutation in a sporadic patient with mitochondrial encephalomyopathy segregates rapidly in skeletal muscle and suggests an approach to therapy. *Hum Mol Genet* 5(11):1835-1840.

54. Nishino I, *et al.* (1996) A novel mutation in the mitochondrial tRNA(Thr) gene associated with a mitochondrial encephalomyopathy. *Biochem Biophys Res Commun* 225(1):180-185.

55. Verma A, *et al.* (1997) A novel mitochondrial G8313A mutation associated with prominent initial gastrointestinal symptoms and progressive encephaloneuropathy. *Pediatr Res* 42(4):448-454.

56. Manfredi G, *et al.* (1996) Identification of a mutation in the mitochondrial tRNA(Cys) gene associated with mitochondrial encephalopathy. *Hum Mutat* 7(2):158-163.

57. Nelson I, *et al.* (1995) A new mitochondrial DNA mutation associated with progressive dementia and chorea: a clinical, pathological, and molecular genetic study. *Ann Neurol* 37(3):400-403.

58. Santorelli FM, *et al.* (1996) Maternally inherited cardiomyopathy and hearing loss associated with a novel mutation in the mitochondrial tRNA(Lys) gene (G8363A). *Am J Hum Genet* 58(5):933-939.

59. Pineda M, *et al.* (2004) Peripheral neuropathy with ataxia in childhood as a result of the G8363A mutation in mitochondrial DNA. *Pediatr Res* 56(1):55-59.

60. Yoon KL, Aprille JR, & Ernst SG (1991) Mitochondrial tRNA(thr) mutation in fatal infantile respiratory enzyme deficiency. *Biochem Biophys Res Commun* 176(3):1112-1115.

61. Sue CM, *et al.* (1999) Maternally inherited hearing loss in a large kindred with a novel T7511C mutation in the mitochondrial DNA tRNA(Ser(UCN)) gene. *Neurology* 52(9):1905-1908.

62. Reid FM, Vernham GA, & Jacobs HT (1994) A novel mitochondrial point mutation in a maternal pedigree with sensorineural deafness. *Hum Mutat* 3(3):243-247.

63. Merante F, Tein I, Benson L, & Robinson BH (1994) Maternally inherited hypertrophic cardiomyopathy due to a novel T-to-C transition at nucleotide 9997 in the mitochondrial tRNA(glycine) gene. *Am J Hum Genet* 55(3):437-446.

64. Merante F, Myint T, Tein I, Benson L, & Robinson BH (1996) An additional mitochondrial tRNA(Ile) point mutation (A-to-G at nucleotide 4295) causing hypertrophic cardiomyopathy. *Hum Mutat* 8(3):216-222.

65. Nakamura M, *et al.* (1995) A novel point mutation in the mitochondrial tRNA(Ser(UCN)) gene detected in a family with MERRF/MELAS overlap syndrome. *Biochem Biophys Res Commun* 214(1):86-93.

66. Shoffner JM, *et al.* (1990) Myoclonic epilepsy and ragged-red fiber disease (MERRF) is associated with a mitochondrial DNA tRNA(Lys) mutation. *Cell* 61(6):931-937.

67. Silvestri G, Moraes CT, Shanske S, Oh SJ, & DiMauro S (1992) A new mtDNA mutation in the tRNA(Lys) gene associated with myoclonic epilepsy and ragged-red fibers (MERRF). *Am J Hum Genet* 51(6):1213-1217.

68. Weber K, *et al.* (1997) A new mtDNA mutation showing accumulation with time and restriction to skeletal muscle. *Am J Hum Genet* 60(2):373-380.

69. Hadjigeorgiou GM, *et al.* (1999) A new mitochondrial DNA mutation (A3288G) in the tRNA(Leu(UUR)) gene associated with familial myopathy. *J Neurol Sci* 164(2):153-157.

70. Bindoff LA, *et al.* (1993) Abnormal RNA processing associated with a novel tRNA mutation in mitochondrial DNA. A potential disease mechanism. *J Biol Chem* 268(26):19559-19564.

71. Goto Y, Tojo M, Tohyama J, Horai S, & Nonaka I (1992) A novel point mutation in the mitochondrial tRNA(Leu)(UUR) gene in a family with mitochondrial myopathy. *Ann Neurol* 31(6):672-675.

72. Moraes CT, *et al.* (1993) A mitochondrial tRNA anticodon swap associated with a muscle disease. *Nat Genet* 4(3):284-288.

73. Hao H, Bonilla E, Manfredi G, DiMauro S, & Moraes CT (1995) Segregation patterns of a novel mutation in the mitochondrial tRNA glutamic acid gene associated with myopathy and diabetes mellitus. *Am J Hum Genet* 56(5):1017-1025.

74. Goto Y, Nonaka I, & Horai S (1990) A mutation in the tRNA(Leu)(UUR) gene associated with the MELAS subgroup of mitochondrial encephalomyopathies. *Nature* 348(6302):651-653.

75. Morten KJ, *et al.* (1993) A new point mutation associated with mitochondrial encephalomyopathy. *Hum Mol Genet* 2(12):2081-2087.

76. Goto Y, Nonaka I, & Horai S (1991) A new mtDNA mutation associated with mitochondrial myopathy, encephalopathy, lactic acidosis and stroke-like episodes (MELAS). *Biochim Biophys Acta* 1097(3):238-240.

77. Goto Y, Tsugane K, Tanabe Y, Nonaka I, & Horai S (1994) A new point mutation at nucleotide pair 3291 of the mitochondrial tRNA(Leu(UUR)) gene in a patient with mitochondrial myopathy, encephalopathy, lactic acidosis, and stroke-like episodes (MELAS). *Biochem Biophys Res Commun* 202(3):1624-1630.

78. Santorelli FM*, et al.* (1997) Maternally inherited encephalopathy associated with a single-base insertion in the mitochondrial tRNATrp gene. *Ann Neurol* 42(2):256-260.

79. Taylor RW*, et al.* (1996) MELAS associated with a mutation in the valine transfer RNA gene of mitochondrial DNA. *Ann Neurol* 40(3):459-462.

80. Moraes CT*, et al.* (1993) Two novel pathogenic mitochondrial DNA mutations affecting organelle number and protein synthesis. Is the tRNA(Leu(UUR)) gene an etiologic hot spot? *J Clin Invest* 92(6):2906-2915.

81. Silvestri G*, et al.* (1996) A novel mitochondrial DNA point mutation in the tRNA(Ile) gene is associated with progressive external ophtalmoplegia. *Biochem Biophys Res Commun* 220(3):623-627.

82. Santorelli FM, Schlessel JS, Slonim AE, & DiMauro S (1996) Novel mutation in the mitochondrial DNA tRNA glycine gene associated with sudden unexpected death. *Pediatr Neurol* 15(2):145-149.

83. Anonymous (2003) USRDS: the United States Renal Data System. *Am J Kidney Dis* 42(6 Suppl 5):1-230.

84. Eisenbarth GS (1986) Type I diabetes mellitus. A chronic autoimmune disease. *N Engl J Med* 314(21):1360-1368.

85. Notkins AL & Lernmark A (2001) Autoimmune type 1 diabetes: resolved and unresolved issues. *J Clin Invest* 108(9):1247-1252.

86. Katz JD, Benoist C, & Mathis D (1995) T helper cell subsets in insulin-dependent diabetes. *Science* 268(5214):1185-1188.

87. Kurrer MO, Pakala SV, Hanson HL, & Katz JD (1997) Beta cell apoptosis in T cell-mediated autoimmune diabetes. *Proc Natl Acad Sci U S A* 94(1):213-218.

88. Augstein P*, et al.* (1998) Beta-cell apoptosis in an accelerated model of autoimmune diabetes. *Mol Med* 4(8):495-501.

89. Kim YH*, et al.* (1999) Apoptosis of pancreatic beta-cells detected in accelerated diabetes of NOD mice: no role of Fas-Fas ligand interaction in autoimmune diabetes. *Eur J Immunol* 29(2):455-465.

90. Yoon JW, Jun HS, & Santamaria P (1998) Cellular and molecular mechanisms for the initiation and progression of beta cell destruction resulting from the collaboration between macrophages and T cells. *Autoimmunity* 27(2):109-122.

91. Patti ME & Corvera S (2010) The Role of Mitochondria in the Pathogenesis of Type 2 Diabetes. *Endocr Rev* .

92. de Andrade PB*, et al.* (2006) Diabetes-associated mitochondrial DNA mutation A3243G impairs cellular metabolic pathways necessary for beta cell function. *Diabetologia* 49(8):1816-1826.

93. Choo HJ*, et al.* (2006) Mitochondria are impaired in the adipocytes of type 2 diabetic mice. *Diabetologia* 49(4):784-791.

94. Guilherme A, Virbasius JV, Puri V, & Czech MP (2008) Adipocyte dysfunctions linking obesity to insulin resistance and type 2 diabetes. *Nat Rev Mol Cell Biol* 9(5):367-377.

95. Bournat JC & Brown CW (2010) Mitochondrial dysfunction in obesity. *Curr Opin Endocrinol Diabetes Obes* 17(5):446-452.

96. Hojlund K, Mogensen M, Sahlin K, & Beck-Nielsen H (2008) Mitochondrial dysfunction in type 2 diabetes and obesity. *Endocrinol Metab Clin North Am* 37(3):713-731, x.

97. Lowell BB & Shulman GI (2005) Mitochondrial dysfunction and type 2 diabetes. *Science* 307(5708):384-387.

98. Sivitz WI & Yorek MA (2010) Mitochondrial dysfunction in diabetes: from molecular mechanisms to functional significance and therapeutic opportunities. *Antioxid Redox Signal* 12(4):537-577.

99. Qi Z*, et al.* (2005) Characterization of susceptibility of inbred mouse strains to diabetic nephropathy. *Diabetes* 54(9):2628-2637.

100. Breyer MD*, et al.* (2005) Mouse models of diabetic nephropathy. *J Am Soc Nephrol* 16(1):27-45.

101. Kakoki M, Takahashi N, Jennette JC, & Smithies O (2004) Diabetic nephropathy is markedly enhanced in mice lacking the bradykinin B2 receptor. *Proc Natl Acad Sci U S A* 101(36):13302-13305.

102. Kakoki M*, et al.* (2006) Senescence-associated phenotypes in Akita diabetic mice are enhanced by absence of bradykinin B2 receptors. *J Clin Invest* 116(5):1302-1309.

103. Bayona-Bafaluy MP*, et al.* (2003) Revisiting the mouse mitochondrial DNA sequence. *Nucleic Acids Res* 31(18):5349-5355.

104. Yaffe MP (1999) The machinery of mitochondrial inheritance and behavior. *Science* 283(5407):1493-1497.

105. Smirnova E, Griparic L, Shurland DL, & van der Bliek AM (2001) Dynamin-related protein Drp1 is required for mitochondrial division in mammalian cells. *Mol Biol Cell* 12(8):2245-2256.

106. James DI, Parone PA, Mattenberger Y, & Martinou JC (2003) hFis1, a novel component of the mammalian mitochondrial fission machinery. *J Biol Chem* 278(38):36373-36379.

107. Yoon Y, Krueger EW, Oswald BJ, & McNiven MA (2003) The mitochondrial protein hFis1 regulates mitochondrial fission in mammalian cells through an interaction with the dynamin-like protein DLP1. *Mol Cell Biol* 23(15):5409-5420.

108. Chan DC (2006) Mitochondrial fusion and fission in mammals. *Annu Rev Cell Dev Biol* 22:79-99.

109. Bossy-Wetzel E, Barsoum MJ, Godzik A, Schwarzenbacher R, & Lipton SA (2003) Mitochondrial fission in apoptosis, neurodegeneration and aging. *Curr Opin Cell Biol* 15(6):706-716.

110. Yu T, Fox RJ, Burwell LS, & Yoon Y (2005) Regulation of mitochondrial fission and apoptosis by the mitochondrial outer membrane protein hFis1. *J Cell Sci* 118(Pt 18):4141-4151.

111. Piko L & Matsumoto L (1977) Complex forms and replicative intermediates of mitochondrial DNA in tissues from adult and senescent mice. *Nucleic Acids Res* 4(5):1301-1314.

112. Rajamanickam C*, et al.* (1979) Changes in mitochondrial DNA in cardiac hypertrophy in the rat. *Circ Res* 45(4):505-515.

113. Piko L, Bulpitt KJ, & Meyer R (1984) Structural and replicative forms of mitochondrial DNA in tissues from adult and senescent BALB/c mice and Fischer 344 rats. *Mech Ageing Dev* 26(1):113-131.

114. Brown TA, Cecconi C, Tkachuk AN, Bustamante C, & Clayton DA (2005) Replication of mitochondrial DNA occurs by strand displacement with alternative light-strand origins, not via a strand-coupled mechanism. *Genes Dev* 19(20):2466-2476.

115. Mott JL, Denniger G, Zullo SJ, & Zassenhaus HP (2000) Genomic structure of murine mitochondrial DNA polymerase-gamma. *DNA Cell Biol* 19(10):601-605.

116. Kaguni LS (2004) DNA polymerase gamma, the mitochondrial replicase. *Annu Rev Biochem* 73:293-320.

117. Fan L*, et al.* (2006) A novel processive mechanism for DNA synthesis revealed by structure, modeling and mutagenesis of the accessory subunit of human mitochondrial DNA polymerase. *J Mol Biol* 358(5):1229-1243.

118. Stumpf JD & Copeland WC (2011) Mitochondrial DNA replication and disease: insights from DNA polymerase gamma mutations. *Cell Mol Life Sci* 68(2):219-233.

119. Di Fonzo A*, et al.* (2003) POLG mutations in sporadic mitochondrial disorders with multiple mtDNA deletions. *Hum Mutat* 22(6):498-499.

120. Longley MJ, *et al.* (2006) Mutant POLG2 disrupts DNA polymerase gamma subunits and causes progressive external ophthalmoplegia. *Am J Hum Genet* 78(6):1026-1034.

121. Van Goethem G, *et al.* (2003) Recessive POLG mutations presenting with sensory and ataxic neuropathy in compound heterozygote patients with progressive external ophthalmoplegia. *Neuromuscul Disord* 13(2):133-142.

122. Hakonen AH, *et al.* (2005) Mitochondrial DNA polymerase W748S mutation: a common cause of autosomal recessive ataxia with ancient European origin. *Am J Hum Genet* 77(3):430-441.

123. Van Goethem G, *et al.* (2004) POLG mutations in neurodegenerative disorders with ataxia but no muscle involvement. *Neurology* 63(7):1251-1257.

124. Luoma P, *et al.* (2004) Parkinsonism, premature menopause, and mitochondrial DNA polymerase gamma mutations: clinical and molecular genetic study. *Lancet* 364(9437):875-882.

125. Hance N, Ekstrand MI, & Trifunovic A (2005) Mitochondrial DNA polymerase gamma is essential for mammalian embryogenesis. *Hum Mol Genet* 14(13):1775-1783.

126. Foury F & Vanderstraeten S (1992) Yeast mitochondrial DNA mutators with deficient proofreading exonucleolytic activity. *EMBO J* 11(7):2717-2726.

127. Vanderstraeten S, Van den Brule S, Hu J, & Foury F (1998) The role of 3'-5' exonucleolytic proofreading and mismatch repair in yeast mitochondrial DNA error avoidance. *J Biol Chem* 273(37):23690-23697.

128. Chen ML, *et al.* (2009) Erythroid dysplasia, megaloblastic anemia, and impaired lymphopoiesis arising from mitochondrial dysfunction. *Blood* 114(19):4045-4053.

129. Vermulst M, *et al.* (2007) Mitochondrial point mutations do not limit the natural lifespan of mice. *Nat Genet* 39(4):540-543.

130. Vermulst M, *et al.* (2008) DNA deletions and clonal mutations drive premature aging in mitochondrial mutator mice. *Nat Genet* 40(4):392-394.

131. Van Belle TL, Taylor P, & von Herrath MG (2009) Mouse Models for Type 1 Diabetes. *Drug Discov Today Dis Models* 6(2):41-45.

132. Wang J*, et al.* (1999) A mutation in the insulin 2 gene induces diabetes with severe pancreatic beta-cell dysfunction in the Mody mouse. *J Clin Invest* 103(1):27-37.

133. Yoshioka M, Kayo T, Ikeda T, & Koizumi A (1997) A novel locus, Mody4, distal to D7Mit189 on chromosome 7 determines early-onset NIDDM in nonobese C57BL/6 (Akita) mutant mice. *Diabetes* 46(5):887-894.

134. Zuber C, Fan JY, Guhl B, & Roth J (2004) Misfolded proinsulin accumulates in expanded pre-Golgi intermediates and endoplasmic reticulum subdomains in pancreatic beta cells of Akita mice. *FASEB J* 18(7):917-919.

135. Surwit RS, Kuhn CM, Cochrane C, McCubbin JA, & Feinglos MN (1988) Diet-induced type II diabetes in C57BL/6J mice. *Diabetes* 37(9):1163-1167.

136. Surwit RS, Seldin MF, Kuhn CM, Cochrane C, & Feinglos MN (1991) Control of expression of insulin resistance and hyperglycemia by different genetic factors in diabetic C57BL/6J mice. *Diabetes* 40(1):82-87.

Chapter 2

THE MITOCHONDRIAL DNA POLYMERASE EDITING MUTATION, POLGD257A, REDUCES THE DIABETIC PHENOTYPE OF AKITA MALE MICE BY SUPPRESSING APPETITE

2.1 Abstract

Diabetes and the development of its complications have been associated with mitochondrial DNA (mtDNA) dysfunction, but causal relationships remain undetermined. With the objective of testing whether increased mtDNA mutations exacerbate the diabetic phenotype, I have compared mice heterozygous for the Akita diabetogenic mutation (Akita) with mice homozygous for the D257A mutation in mitochondrial DNA polymerase gamma (Polg) or with mice having both mutations (Polg-Akita). The Polg-D257A protein is defective in proofreading and increases mtDNA mutations. At 3-months of age, the Polg-Akita and Akita male mice were equally hyperglycemic. Unexpectedly, as the Polg-Akita males aged to 9 months, their diabetic symptoms decreased. Thus, their hyperglycemia, hyperphagia, and urine output declined significantly. The decrease in their food intake was accompanied by increased plasma leptin and decreased plasma ghrelin, while hypothalamic expression of the orexic gene, neuropeptide Y, was lower and expression of the anorexic gene, proopiomelanocortin, was higher. Testis function progressively worsened with age in the double mutants, and plasma testosterone levels in 9-month old Polg-Akita males were significantly reduced compared to Akita males. The hyperglycemia and hyperphagia returned in aged Polg-Akita males after testosterone administration. Hyperglycemia-associated distal tubular damage in the kidney also returned, and Polg-D257A-associated proximal tubular damage was enhanced. The mild diabetes of female Akita mice was not affected by the Polg-D257A mutation. I conclude that reduced diabetic symptoms of aging Polg-Akita male mice results from appetite suppression triggered by decreased testosterone associated with damage to the Leydig cells of the testis.

2.2 Introduction

Diabetes mellitus is becoming increasingly common worldwide. A large body of data demonstrates links between mitochondrial dysfunction, insulin resistance, and diabetes (1, 2). Deleterious mitochondrial DNA (mtDNA) mutations have their greatest effect in cells that require high energy production, or already have high oxidative stress, including neurons, hair cells of the inner ears, heart and skeletal myocytes, pancreatic beta cells, as well as gut and kidney epithelial cells (3-9). Complications of diabetes also involve damage to these metabolically active cell types, leading to a hypothesis that mtDNA mutations contribute to the complications. Consistent with this, our lab has previously demonstrated in mice that a genetic absence of the bradykinin B2 receptor (B2R) combined with diabetes caused by the Akita mutation, $Ins2^{C96Y}$, progressively increases modifications to kidney mtDNA, including 8-hydroxy-2'-deoxyguanosine content, point mutations, and deletions (3, 4). The mtDNA mutations in these mice are also associated with enhanced nephropathy and senescence-related phenotypes in multiple tissues (3, 4). However, it remains unclear whether the mtDNA mutations act causally with respect to diabetes and its complications, or are consequences of these conditions.

The enzymes required for mitochondrial biogenesis are encoded in the nuclear genome, including mtDNA polymerase gamma (*Polg*), which replicates and proofreads the mitochondrial genome. *Polg* is essential for life, and its complete absence leads to early embryonic death (10). An amino acid substitution, D257A, in the exonuclease domain II of *Polg* ablates proofreading without significantly affecting the capacity of the polymerase to replicate mtDNA (11, 12). Mice homozygous for the D257A mutation (Polg) die prematurely by 13 months of age displaying a series of aging-associated phenotypes due to increased

random accumulations of mtDNA mutations which lead to increased apoptosis particularly in tissues containing cells that are metabolically active (11, 12). The D257A mutation, which does not itself induce diabetes, consequently provides a tool that can be used to determine whether an increased frequency of mtDNA mutations can influence the pathophysiology of diabetes and its complications.

In the present work, I take advantage of this tool to examine the effects of the Polg-D257A mutation in mice that are diabetic because of the dominant Akita mutation ($Ins2^{C96Y}$) in the *Ins2* gene. The C96Y mutation prevents the formation of an important disulfide bond in insulin and leads to mis-folding of the protein. The mis-folded protein has impaired transport through the endoplasmic reticulum (ER), which triggers an ER stress reaction leading to pancreatic β cell apoptosis (13). Males heterozygous for the Akita mutation, but not females, develop hyperglycemia beginning at around 3 weeks of age and becoming progressively more severe with age. Surprisingly, our experiments show that the diabetic symptoms of Akita male mice which also have the $Polg^{D257A}$ mutation (Polg-Akita) become progressively less severe after 3 months age. I demonstrate that the overall improvement in the diabetic phenotype of the Polg-Akita mice is at least in part due to a reduction in the Akita-induced hyperphagia triggered by a *Polg*-induced decrease in testis production of testosterone. Glomerular changes were mild in all the diabetic mice. Proximal tubular damage occurred only in aged double mutant males. Distal tubular damage occurred in all hyperglycemic males.

2.3 Methods

Mice. All mice were maintained on normal chow containing 5.3% fat and 0.019% cholesterol (Prolab Isopro RMH 3000, ref 5P76; Agway Inc., Syracuse, NY, USA). The experimental animals were Akita heterozygous males homozygous for the $Polg^{D257A}$ mutation. Controls were male Akita littermates that were either wild type at the *Polg* locus ($Polg^{+/+}$Akita) or heterozygous for the mutation ($Polg^{D257A/+}$Akita). Heterozygous $Polg^{D257A}$ mutants are phenotypically indistinguishable from wild type mice (11). Both male and female animals were monitored for diabetes and characterized at 3, 6, and 9 months of age. The breeding process to generate doubly mutant and control mice is described in Figure 2.1. All animal experiments were performed in accordance with the Institutional Animal Care and Use Committee at The University of North Carolina at Chapel Hill.

Plasma Analyses. Animals were fasted in the morning, 4 hrs prior to the collection of blood. Plasma glucose was measured using a colorimetric kit (#439-90901, Wako Chemical Co., Richmond, VA). Plasma levels of leptin, insulin, and ghrelin were measured using ELISA kits (#90030 and #90080, Crystal Chem, Inc., Downers Grove, IL and #EZRGRT-91K, LINCO Research, St. Charles, MO). Testosterone levels were measured in plasma pooled from 3 mice per sample with RIA kits (#TKTT2 Siemens Medical Solutions Diagnostics, Los Angeles, CA) by the Reproductive Biology Core at the University of Virginia.

Mitochondrial DNA Mutations. Mitochondria was isolated from 200 mg of liver samples pooled from 3 to 5 mice of each genotype by differential centrifugation in a sucrose gradient as described (14). DNA was purified using standard isolation protocols and fragmented by

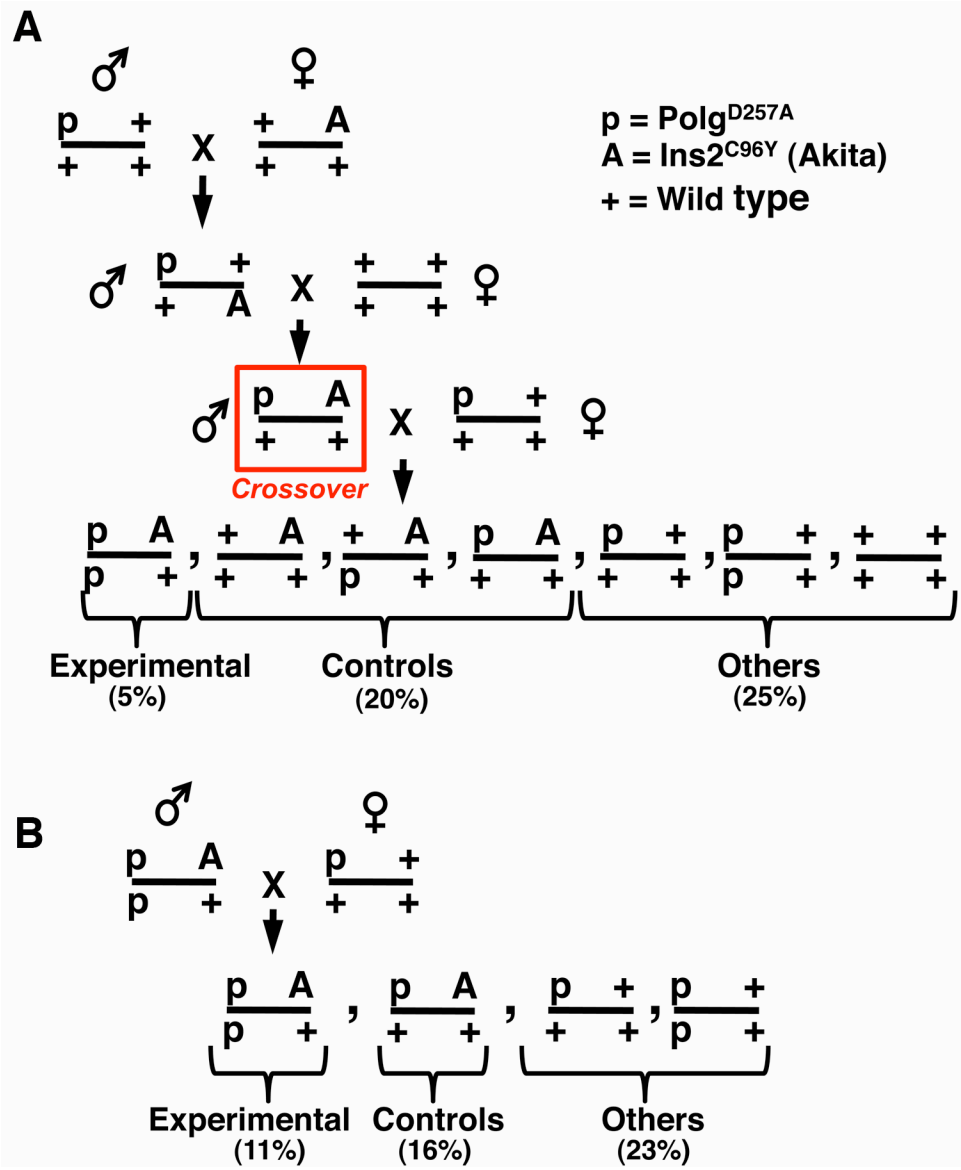

Figure 2.1: Mouse Breeding scheme. C57BL/6J mice heterozygous for the *Polg*^{D257A} mutation were crossed to C57BL/6J-*Ins2*$^{C96Y/+}$ heterozygotes (Akita, #003548, Jackson Lab). (A) Multi-step breeding used to generate both Polg-Akita and Akita mice. Both *Polg* and *Ins2* loci are located on chromosome 7. A male *Polg*$^{D257A/+;}$*Ins2*$^{+/+}$ mouse was crossed to a female *Polg*$^{+/+}$*; Ins2*$^{C96Y/+}$ mouse to generate *Polg*$^{D257A/+}$*;Ins2*$^{+/C96Y}$ progeny in which the mutations are on the two parental chromosomes. A second generation breeding cross was then setup between a male *Polg*$^{D257A/+}$*;Ins2*$^{+/C96Y}$ mouse and a female *Polg*$^{+/+}$*;Ins2*$^{+/+}$ mouse. Due to crossover, both mutations are on the same chromosome. A third cross of a male *Polg*$^{D257A/+}$*;Ins2*$^{C96Y/+}$ to a female *Polg*$^{D257A/+;}$*Ins2*$^{+/+}$ mouse yields the experimental *Polg*$^{D257A/D257A}$*;Ins2*$^{C96Y/+}$ mice with a frequency of 5%; slightly less than expected (6.25%) because of crossing over. (B) Adjusted breeding scheme used to generate additional Polg-Akita and Akita mice. The numbers in parentheses are the percent of male offspring with the genotype obtained from each cross. *Polg*$^{D257A/D257A}$*;Ins2*$^{C96Y/+}$ males younger than 6 mo. of age were used in scheme B. This cross eliminates any effects of crossovers, and ensures that the mitochondria inherited from the mother are initially normal.

Covaris S220 adaptive focused acoustic apparatus (MA, USA) into 300 bp in length, and subjected to high throughput sequencing of 5,000-27,000 reads per base using Illumina GAII. DNA sequence was processed through the band led Solexa image extraction pipeline and aligned with ELAND software against murine mitochondrial genome sequence (NCBL Build 36) as a reference. Default quality score was adjusted to allow 2 mismatches per 36 bp reads. The uniquely mapped reads were used for further analyses.

Gene Expression. Total RNA was purified from hypothalamus and pancreas samples using Trizol (#15596-026 Invitrogen, Carlsbad, CA) as previously described (15). Total RNA from other tissues was purified using an Automated Nucleic Acid Workstation ABI 6700. Real-time PCR was performed in an ABI PRISM 7700 Sequence Detector (Applied Biosystems, Foster City, CA). β-Actin mRNA was used for normalization.

Glucose Tolerance Tests. Male mice of each genotype were fasted for 4 **hrs** prior to oral gavage of glucose (2g/kg BW). Plasma was collected for glucose measurement at time points of 0, 15, 30, 60, and 120 minutes after gavage.

Urine Analyses. Mice were housed in metabolic cages, allowed to acclimate to the new environment for 24 hrs, and urine samples were collected over a second period of 24 hrs. Body weight, food, and water were measured before and at the end of the second period of 24 hrs. Urinary Albumin and creatinine were measured using kits (Albuwell, #1011 and Creatinine Companion, #1012 Exocell, Inc., Philadelphia, PA). Urinary levels of Na, K, and Cl were measured using an Automatic Chemical Analyzer (VT250, Johnson & Johnson).

Histology. Tissues were fixed in 4% paraformaldehyde (PFA). Paraffin sections at 5 μm were stained with Hematoxylin and Eosin, Periodic acid-Schiff, or Masson's Trichrome. For

transmission electron microscopy (JOEL USA, Inc.), small tissue fragments were post-fixed in 2% osmium tetroxide and one-micron thick sections were stained with uranyl acetate followed by lead citrate.

Testosterone Replacement. Six month old Polg-Akita and Akita mice were implanted with 12.5 mg/90 Day Testosterone time-release pellet (Innovative Research America, Sarasota, FL). This dose was shown to normalize plasma testosterone levels in orchidectomized mice (16).

Data Analysis. Values are reported as mean ± SEM. Statistical analyses were conducted with JMP 6.0.2 software (SAS Institute, Cary, NC). P values less than 0.05 were considered significant.

2.4 Results

Mitochondrial mutations in Polg-Akita mice. The reported median lifespan of Polg mice homozygous for Polg-D275A mutation is 13 months, and the amount of mtDNA mutations accumulating in Polg mice has been estimated to be as high as $1x10^{-3}$ mutations/bp in most tissues compared to $<5x10^{-4}$ mutations/bp in wild type mice (11, 12, 17, 18). Because untreated Akita diabetic mice deteriorate quickly after 9 months (19), I determined mtDNA mutation load in the liver of 9 month old mice, which are histologically intact at this age. As expected, the average number of base substitution per site per hundred mtDNA molecules, without correcting for errors associated with deep sequencing and heteroplasmic polymorphisms, was significantly higher in the Polg mice than in their wild type (WT) littermates (0.425±0.005 mutations per site per hundred molecules sequenced versus 0.375±0.004; $P \leq 0.001$). Diabetes, again as expected, further increased base substitution rate ($P < 0.001$), with the Polg-Akita mice having significantly more mutations than their Akita littermates (0.557±0.007 versus 0.494±0.008; $P \leq 0.001$). I conclude that the mtDNA of 9-month-old Polg-Akita mice has accumulated significantly more mutations than the mtDNA of their Akita siblings.

The expressions of mitochondrial transcription factor A (*Tfam*), mtDNA polymerase gamma (*Polg*), and cytochrome b (*CytB*) have been correlated respectively with mitochondrial biogenesis (20), replication (21), and function (22). However, renal and hepatic gene expression of *Tfam*, *Polg*, and *CytB* did not differ significantly among the groups (Table 2.1). Similarly, mtDNA content in these tissues was not significantly different between the two genotypes (Fig. 2.2). I conclude that the Polg mutation did not change mitochondrial biogenesis and replication in our diabetic mice. mtDNA damage associated with diabetes also includes an increased incidence of deletions (3, 4). However I found no significant differences

Table 2.1: Renal and Hepatic Gene Expression at 9 Months of Age

	Renal 9 months			Hepatic 9 Months		
	WT	Akita	Polg-Akita	WT	Akita	Polg-Akita
n=	7	6	7	4	3	4
Polg	1.00±0.19	1.06±0.28	0.98±0.15	1.00±0.07	2.55±0.65	1.00±0.10
Tfam	1.00±0.13	0.90±0.32	1.39±0.24	1.00±0.27	1.10±0.7	0.28±0.13
Cyb	1.00±0.08	1.28±0.28	1.32±0.13	1.00±0.25	1.70±0.38	1.00±0.18

mRNA levels were determined by Real time PCR and expressed relative to the mean levels in the wild type kidneys as 1.00. Data are expressed as Mean ± SEM. No statistical differences were observed by Tukey-Kramer HSD.

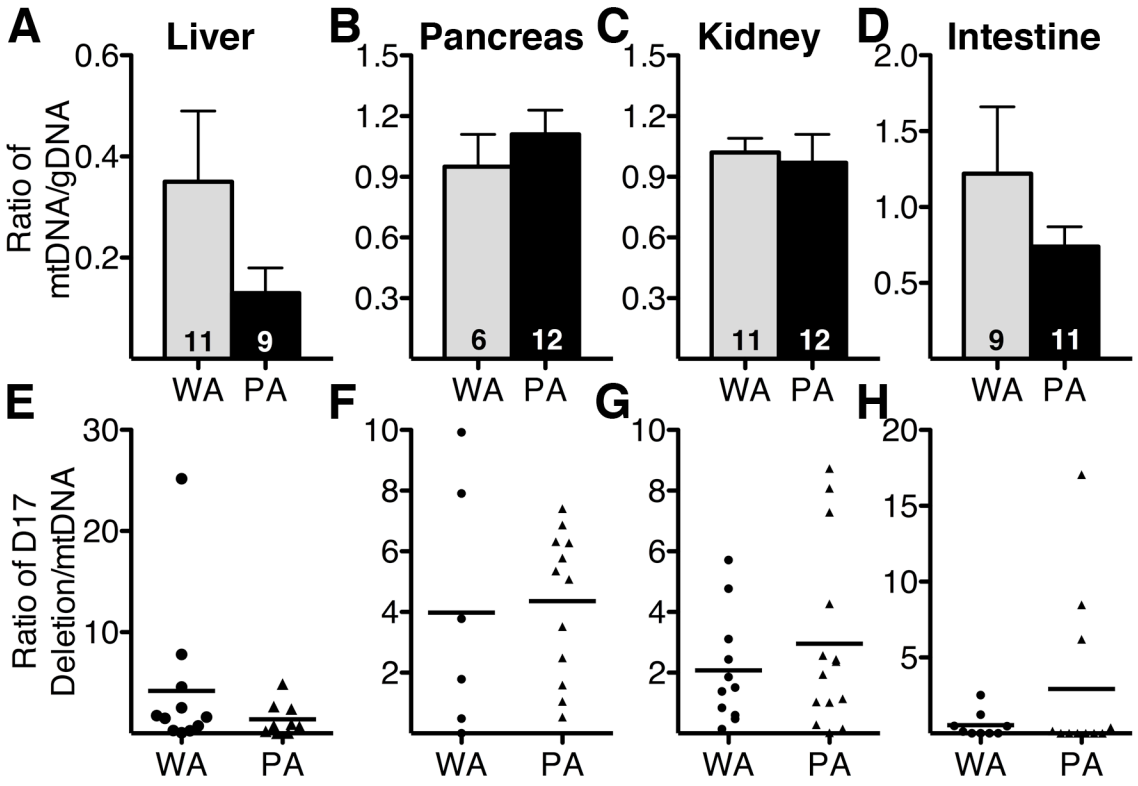

Figure 2.2: Mitochondrial DNA in the liver (A, E), pancreas (B, F), kidney (C, G), and small intestine (D, H). DNA was isolated from tissues and Real-time PCR amplification for the Cytochrome b gene was performed to assay mitochondrial DNA content using amplification of the Na-K-Cl cotransporter 2 gene (*NKCC2)* as an indicator of the content of nuclear DNA. A deletion of ~3.8kb in relation to the D-loop of mtDNA was assayed using a primer probe set that recognizes the loss of the D-17 region in the mtDNA genome (A, B, C, D) Mitochondrial DNA content relative to genomic DNA and (E, F, G, H) D17 deletions in the pancreas, kidney, and small intestine, respectively, of 9 month old Akita (WA) and Polg-Akita (PA) mice. The extent of D-17 deletions was expressed relative to the mtDNA gene coding for Cytochrome b in each animal. All data are represented as Mean ± SEM. (n≥6) Numbers in the bars indicate the number of animals. * $P < 0.05$ PA versus WA.

in the incidence of D-17 deletions in the liver, pancreas, kidneys and small intestine of the Polg-Akita mice compared to the Akita mice (Fig. 2.2).

Improved diabetic symptoms in aging male Polg-Akita mice. At 3 months of age, both Akita and Polg-Akita male mice exhibited all the symptoms normally associated with type 1 diabetes. Thus, both had markedly elevated plasma glucose levels (491±33 mg/dl, Fig. 2.3A) and food intake (8.5g/day, Fig. 2.3B) compared to their non-diabetic counterparts. In contrast, at 6 months of age, plasma glucose and food consumption in the Polg-Akita mice began to show significant decreases relative to the Akita mice. By 9 months of age, the fasting plasma glucose levels in the Polg-Akita mice (280±50 mg/dL) had decreased still further compared to their littermate Akita mice (475±54 mg/dl), although they were still significantly higher than in non-diabetic wild type (167±10 mg/dL) and Polg mutant (151±10 mg/dL) mice. The food intake of the Polg-Akita mice was dramatically lower than that of littermate Akita mice, and was no longer different from that of non-diabetic mice. In contrast, the body weight of the Polg-Akita mice increased steadily with age, and at 9 months they were significantly heavier than their Akita littermates (26.3±1.2 g versus 21.6±1.2 g; $P \leq 0.01$, Fig. 2.3C). The weight gain in the Polg-Akita mice was associated with significantly larger amounts of subcutaneous and visceral fat (Fig. 2.3D), although still below the amount observed in wild type mice. Diabetes in our female Akita mice was mild, as has been reported previously (19); it was not affected by the $Polg^{D257A}$ mutation (Fig. 2.4). Thus, plasma glucose levels are similar in Akita (276±15 mg/dL) and Polg-Akita females (282±20 mg/dL) through 9 months of age. Likewise, food consumption is similar in Akita (3.78±0.16 g/Day) and Polg-Akita females (3.71±0.27 g/Day) through 9 months of age. Together, these data show that, starting around 3 months of

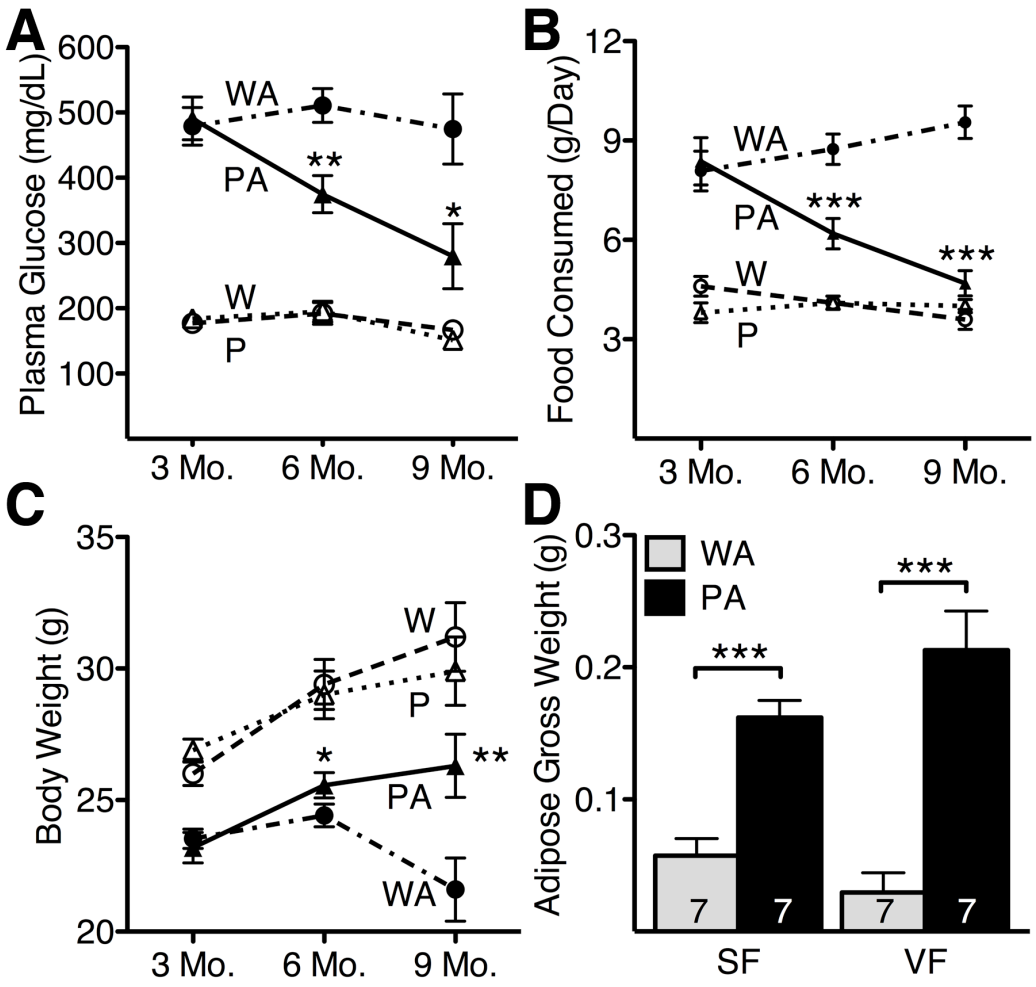

Figure 2.3: Amelioration of diabetic profiles in Polg-Akita mice. (A) Plasma glucose, (B) Food consumption, and (C) Body weight in male wild type (W), Polg (P), Akita (WA), and Polg-Akita (PA) mice. Gross weight of subcutaneous (SF) and visceral (VF) fat in (D) 9 months old Akita (WA) and Polg-Akita (PA) male mice. All data are represented as Mean ± SEM. * $P < 0.05$, ** $P < 0.01$, and *** $P < 0.001$ between Polg-Akita and Akita mice at each time point by Student's t-test. $n \geq 20$, $n \geq 10$, and $n \geq 7$ at 3, 6 and 9 months, respectively.

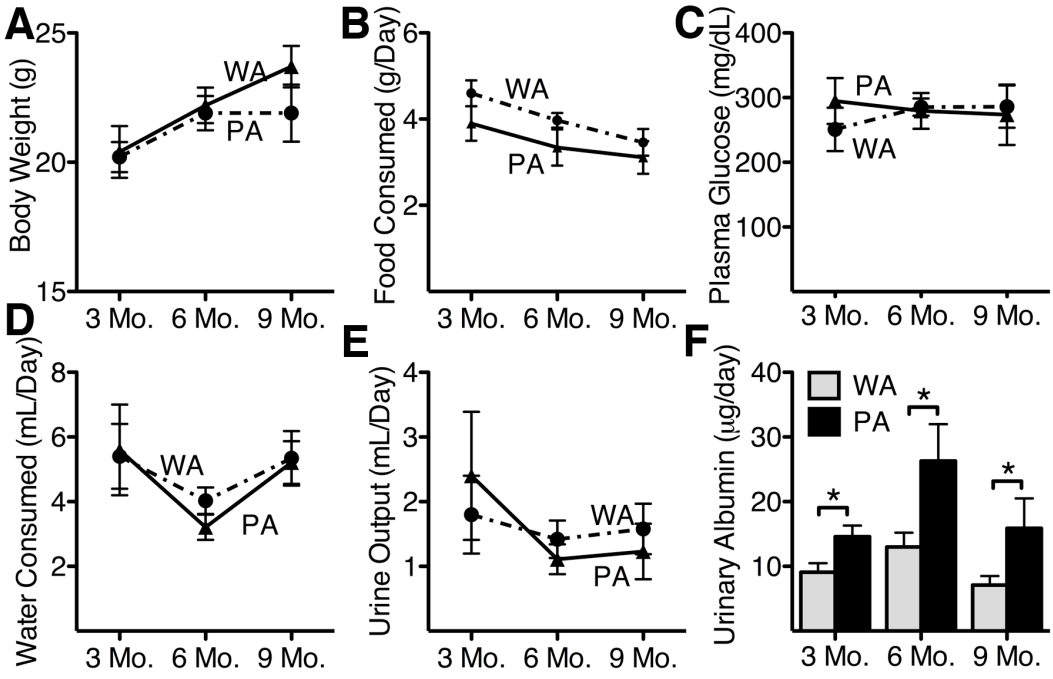

Figure 2.4: Diabetes in female Akita and Polg-Akita mice. (A) Body Weight, (B) Food Consumption, (C) Plasma Glucose, (D) Water Consumption, (E) Urine output, and (F) Urinary Albumin in Akita(WA) and Polg-Akita (PA) mice at 3, 6, and 9 months of age. All data are represented as Mean ± SEM. * $P < 0.05$ indicate significant difference.

age, the *Polg*^{D257A} mutation causes an age-dependent and male-specific amelioration of the Akita diabetic phenotype.

Kidney function. At 3 months of age, Polg-Akita males had small but significant decreases (~20%) in water consumption (Fig. 2.5A) and urine output (Fig. 2.5B) compared to Akita mice, although both variables were markedly higher than in non-diabetic mice. Urine glucose levels at 3 months of age (Fig. 2.5C) were comparable in Polg-Akita and Akita mice. However, as the hyperglycemia of the male Polg-Akita mice improved with age, their water consumption, urine output, and urinary glucose also declined, and at 9 months of age they were no longer different from those of non-diabetic mice. Urinary potassium, sodium, and chloride levels did not differ in the diabetic mice regardless of the presence of the *Polg*^{D257A} mutation. Despite the improvement of hyperglycemia, daily urinary albumin excretion was similar in the Polg-Akita and Akita males although it was only modestly greater than in non-diabetic males throughout the 9 months of study (Fig. 2.5D).

The glomeruli showed no notable differences between the diabetic Akita mice and the Polg-Akita mice under both light microscopy (Figs. 2.5E and 2.5F) and electron microscopy (Fig. 2.6). No evidence of fibrosis or areas of necrosis were found. In the distal tubular epithelial cells, glycogen deposits in the central portion of nuclei were present in both the Akita and Polg-Akita kidneys, but were more prominent in the Akita mice than in Polg-Akita mice (Figs. 2.5E, 2.5F, long arrows). In the proximal tubular epithelial cells, in contrast, cytoplasmic clear foamy inclusions were present only in the Polg-Akita kidneys (Fig. 2.5F, arrow heads), while no such changes were seen in either the Akita kidneys or in non-diabetic Polg kidneys of the same age. Ultra-structurally, the foamy cytoplasmic inclusions seen by light microscopy in the proximal tubular cells of the Polg-Akita kidneys proved to be markedly enlarged lysosomes

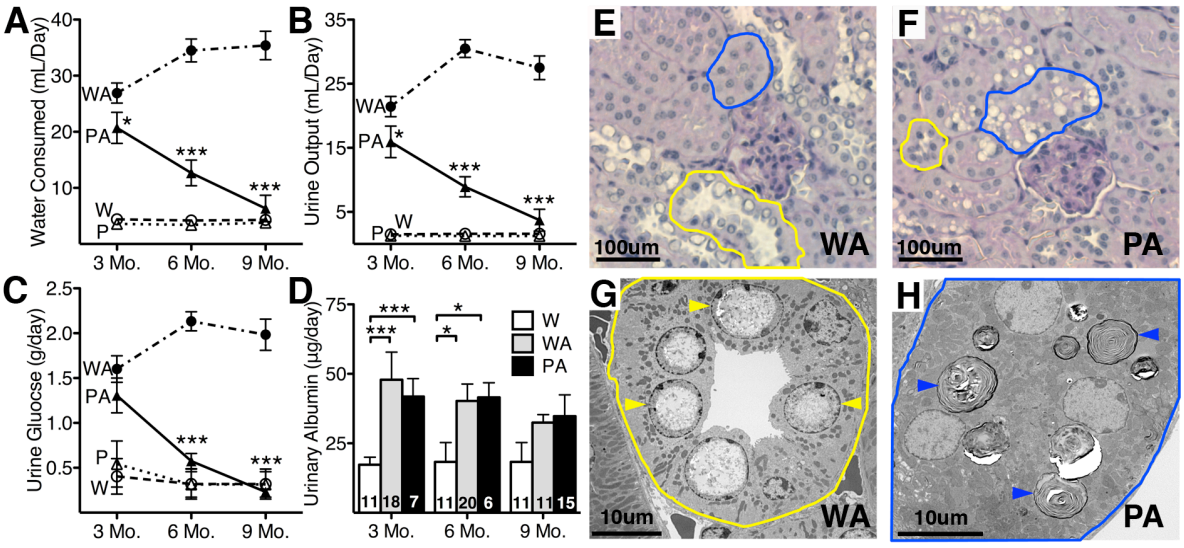

Figure 2.5: Renal function and histology in 9-month-old Polg-Akita mice. (A) Water consumption, (B) urine output, (C) urine glucose, and (D) urinary albumin in Wild type (W), Polg (P), Akita (WA), and Polg-Akita (PA) mice. Renal histology of diabetic (E) Akita and (F) Polg-Akita mice with proximal tubules (blue outline) and distal tubules (yellow outline). (G) Electron micrograph of Akita distal tubular cells with glycogen deposits (yellow arrow heads) within the nuclei. (H) Electron micrograph Polg-Akita proximal tubular cells with mitochondria and lamellated inclusions (blue arrow heads) in the cytoplasm. All data are represented as Mean ± SEM. * $P < 0.05$ and *** $P < 0.001$ between Polg-Akita and Akita mice at each time point by Student's t-test. n ≥ 6 at 3, 6 and 9 months.

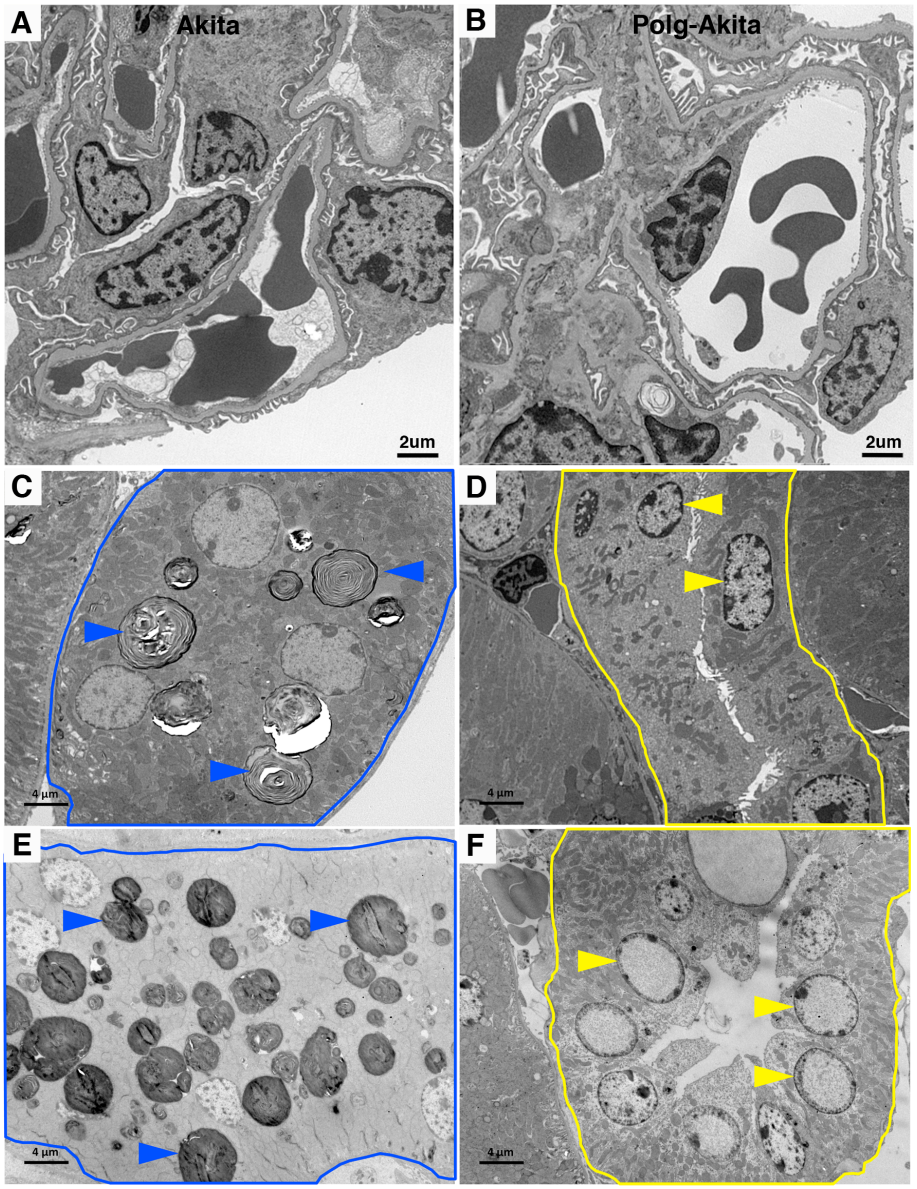

Figure 2.6: Kidney electron micrographs of Akita and Polg-Akita. Glomeruli of (A) Akita mice and (B) Polg-Akita mice show no discernible differences in glomerular basement membrane and podocyte morphology. The proximal tubular cells of Polg-Akita kidneys (C, outlined in blue) contain lamellated inclusions (blue arrow heads) throughout the cytoplasm. The distal tubular cells (D, outlined in yellow) appear normal with normal nuclei appearance (yellow arrow heads). In this section of proximal tubular cells from Polg-Akita supplemented with testosterone for 90 days (E, outlined in blue) show a marked increase in lamellated inclusion bodies (blue arrow heads) compared to un-supplemented Polg-Akita kidneys (C). Like wise, the distal tubular cells form Polg-Akita supplemented with testosterone (F, outlined in yellow) shows a marked increase in glycogen deposits in the nuclei (yellow arrow heads) compared to un-supplemented Polg-Akita kidneys (D).

containing electron-dense material and calcifications (Fig. 2.5H). Lamellated inclusions of glycolipids in lysosomes are correlated with increased damage and turnover of mitochondria within cells, and some inclusions can be seen in Polg-Akita kidneys, although most of the mitochondria appeared normal except for some variations in sizes and density. No inclusions were seen in the Akita littermates (Fig. 2.5G). Taken together, these data show that the distal renal tubular damage, which occurs in the Akita mice in association with their severe hyperglycemia, disappears in the Polg-Akita mice, in association with their markedly decreased hyperglycemia, but proximal tubular damage is now apparent because of mitochondrial damage caused by the *Polg* mutation.

Plasma insulin and insulin sensitivity. Insulin mRNA amounts in the pancreas of both Akita and Polg-Akita mice were similar, at 20–30% of the levels in non-diabetic wild type mice (Fig. 2.7A). Plasma insulin levels in the Akita and Polg-Akita mice were also approximately 20% of those in non-diabetic mice. Plasma insulin levels in the Polg-Akita mice were slightly higher than those in the Akita littermates, but the difference was not significant (Fig. 2.7B). No differences in the morphology and numbers of pancreatic islet cells were found between the Akita (Fig. 2.7C) and Polg-Akita (Fig. 2.7D) mice. At 9 months, both the Akita and Polg-Akita males exhibited impaired clearance of oral glucose loads (Fig. 2.7E). However, plasma insulin levels after the oral glucose challenge did not differ significantly in the Akita and Polg-Akita mice (Fig 2.7F). Taken together, these data demonstrate that adding the $Polg^{D257A}$ mutation did not significantly change the already impaired beta-cell function of the Akita mice, and that the impaired glucose handling exhibited by the Akita mice was likewise not changed by the *Polg* mutation.

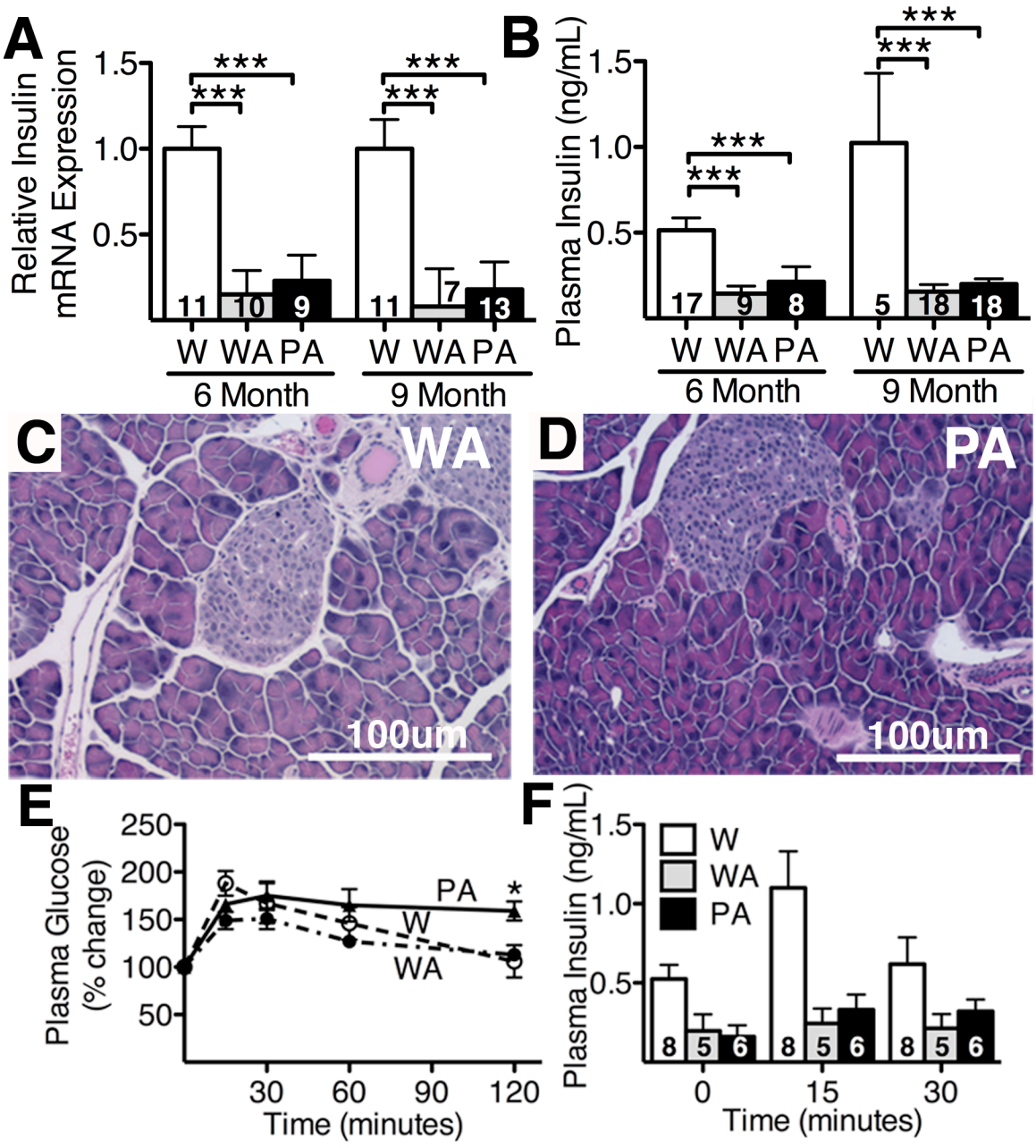

Figure 2.7: Insulin levels in Akita and Polg-Akita mice. (A) Insulin mRNA levels and (B) Plasma insulin in wild type (W), Akita (WA), and Polg-Akita (PA) mice at 6 and 9 months of age. All data are represented as Mean ± SEM. (C) Pancreas (H&E) from 9-month-old Akita and (D) Polg-Akita mice. (E) Glucose tolerance test (GTT) and (F) plasma insulin during GTT at 9 months of age in W, WA, and PA. ** $P < 0.01$ between Polg-Akita and Akita, *** $P < 0.001$ compared to wild type by Student's t-test.

Small intestine function. In agreement with a previous report (11), I find that the *Polg*^{D257A} mutation causes an increase in apoptosis within the villi of the small intestine of the Polg-Akita mice relative to Akita mice. Additionally, I find an increase in apoptosis and a decrease in cell proliferation in the small intestine crypts of the Polg-Akita mice relative to Akita mice (Fig. 2.8). However, these profiles were found at similar levels in non-diabetic Polg mice, indicating that these *Polg*^{D257A} effects were not altered by diabetes. In agreement with this, the gross morphology of the small intestine remained unchanged in 9-month old Polg-Akita mice relative to Akita mice. The mRNA levels of intestinal transporters that affect glucose uptake were also similar in the Polg-Akita and Akita mice (Table 2.2). Pancreatic expression of mRNAs for amylase, trypsinogen, chymotrypsinogen, and lipase in 9-month old Polg-Akita mice was not significantly affected by the *Polg*^{D257A} mutation (Fig. 2.8). Taken together, these observations show that the Polg-Akita mice at 9 months of age display no significant indications of digestive problems or nutrient mal-absorption that might account for the amelioration of their diabetic hyperphagia and hyperglycemia.

Appetite control. Prompted by the decrease in food consumption which developed in the Polg-Akita mice as they aged, I measured two known regulators of appetite: leptin (a suppressor of appetite) and ghrelin (a stimulator of appetite). At 9 months of age, the plasma leptin levels in Polg-Akita mice were significantly higher (Fig. 2.9A), while circulating ghrelin levels were significantly lower, relative to Akita littermates (Fig. 2.9B). Expression in the hypothalamus of the anorexic gene, *Pomc* (coding for proopiomelanocortin), and the orexic gene, *Npy* (coding for Neuropeptide Y), are critical for controlling appetite (23), and I found that hypothalamic expression of the orexic *Npy* gene was significantly increased in Akita diabetic mice relative to non-diabetic wild type mice (Fig. 2.9C), while expression of the

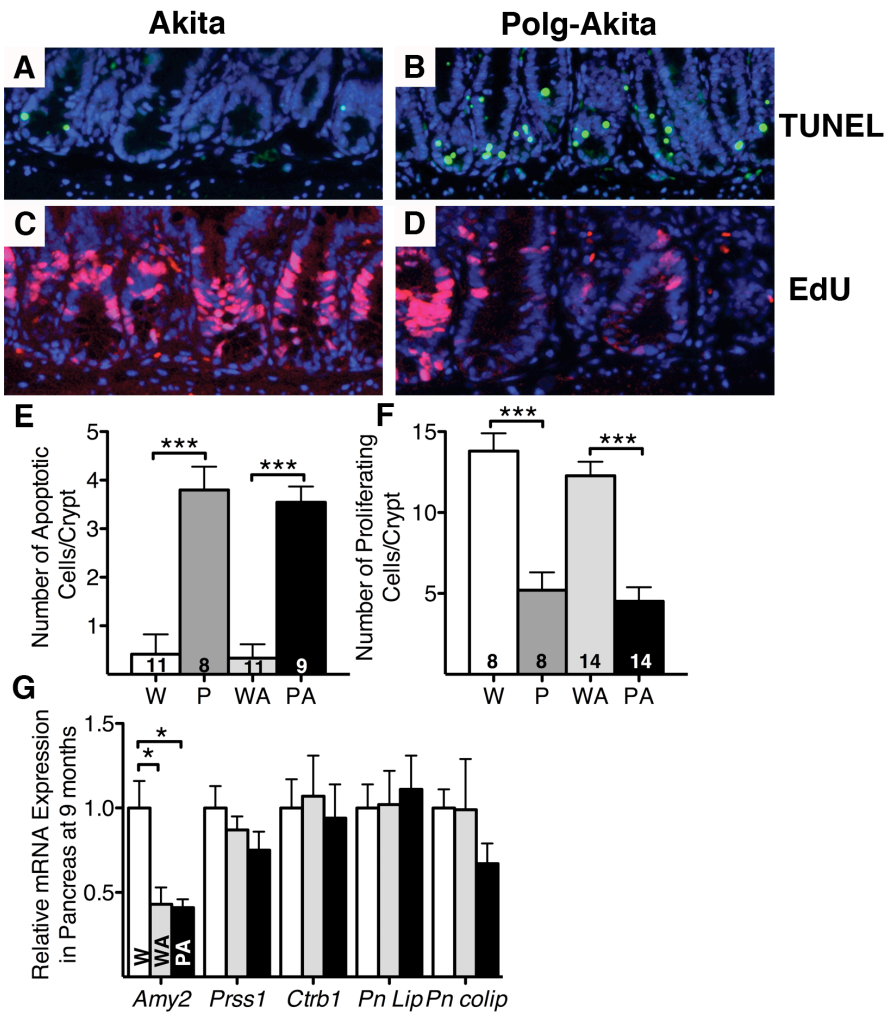

Figure 2.8: Polg-D257A mutation affects small intestine apoptosis and proliferation. Small intestines were isolated, flushed with 10mls of ice cold PBS and fixed in 4% paraformaldehyde at 4°C for at least 24 hours. Intestines were then cut length wise and rolled for sectioning. Apoptosis was evaluated using a commercially available kit (ApopTag S7110; Chemicon Int.). Proliferation was determined using a commercially available kit (Click-iT EdU C10084, Molecular Probes, Inc., Eugene, OR). The small intestine of 9 month old (A) Akita and (B) Polg-Akita mice were stained using the TUNEL assay for apoptosis. Cellular proliferation by EdU staining of the intestinal crypts from 9 months old mice comparing (C) Akita and (D) Polg-Akita small intestines. (E) Quantification of apoptotic cells in the crypt region of the small intestine for wild type, Polg, Akita, and Polg-Akita. Increased apoptotic cells in the crypts were evident in Polg-Akita intestines. (F) Quantification of proliferating cells in the crypt region of the small intestine for wild type, Polg, Akita, and Polg-Akita. Decreased proliferating cells in the crypts were evident in Polg-Akita intestines. Pancreatic gene expression of digestive enzymes at 9 months of age (G) in W (wild type), WA (Akita), and PA (Polg-Akita) mice. All data are represented as Mean ± SEM. * $P < 0.05$ and *** $P < 0.001$ indicate significant difference in Polg-Akita compared to Akita mice and wild type compared to Polg mice by Tukey-Kramer HSD.

Table 2.2: Gene Expression in Small Intestine of Glucose Transporters at 9 Months of Age

	WT	Polg	Akita	Polg-Akita
n=	5	4	4	6
NaK ATPase α1	1.00±0.30	0.85±0.09	0.87±0.50	1.08±0.35
NaK ATPase β1	1.00±0.37	0.73±0.17	0.67±0.24	0.76±0.20
Glut2	1.00±0.23	0.26±0.11	0.82±0.42	0.45±0.08
Sglt	1.00±0.29	0.86±0.19	0.87±0.43	0.70±0.20

mRNA levels were determined by Real time PCR and expressed relative to the mean levels in the wild type intestines as 1.00. Data are expressed as Mean ± SEM. No statistical differences were observed by Tukey-Kramer HSD.

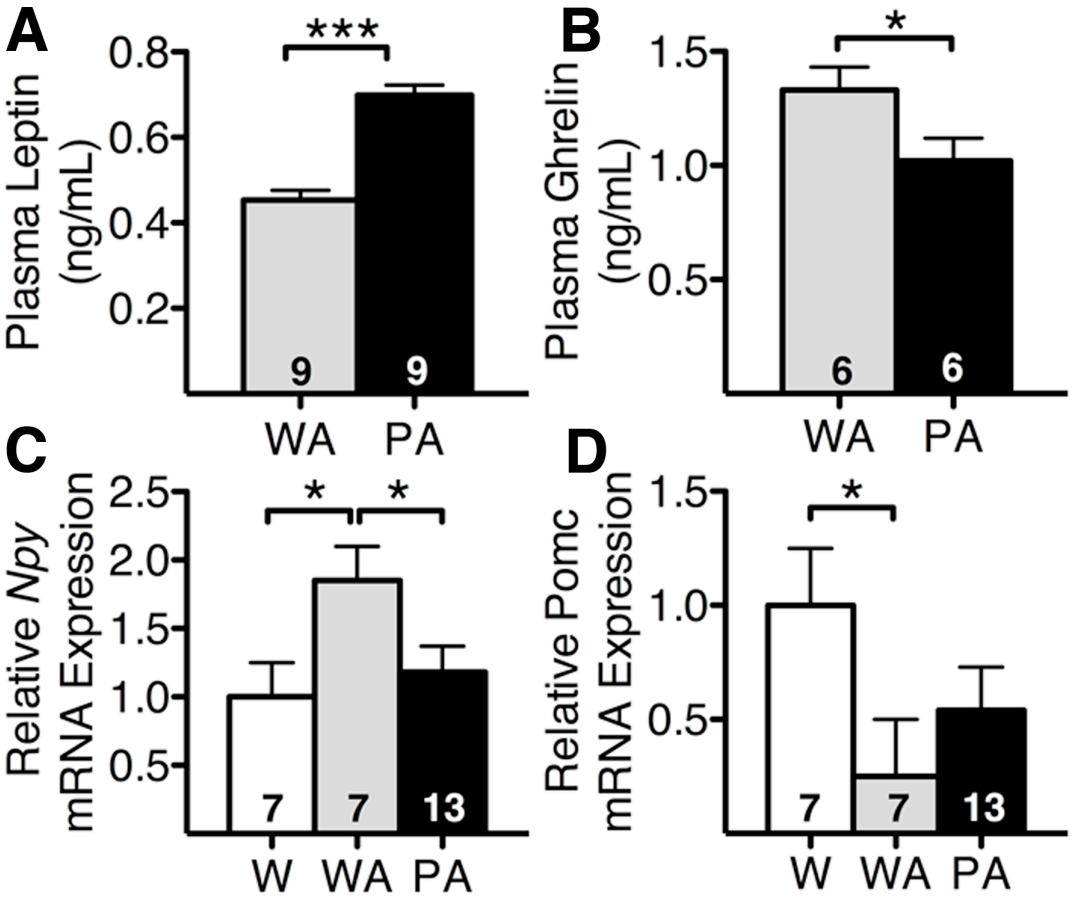

Figure 2.9: Appetite. (A) Plasma leptin, (B) plasma ghrelin, and hypothalamic gene expression of (C) Neuropeptide Y and (D) Proopiomelanocortin in wild type (W), Akita (WA), and Polg-Akita (PA) mice at 9 months of age. All data are represented as Mean ± SEM. * $P < 0.05$ and *** $P < 0.001$ indicate significant difference by Student's t-test.

anorexic *Pomc* gene was significantly decreased (Fig. 2.9D). However, in the Polg-Akita mice these diabetes-associated shifts in *Npy* and *Pomc* expression were reversed, returning to levels not significantly different from those in non-diabetic wild type mice. Thus, adding the $Polg^{D257A}$ mutation to the Akita mutation increases plasma leptin, decreases plasma ghrelin, decreases hypothalamic expression of *Npy* and increases hypothalamic expression of *Pomc.* It is likely that these changes in modulators of food intake, all known to suppress appetite, result in the decreased appetite I observed in Polg-Akita mice relative to Akita mice.

Testicular function. The testis is severely affected by the $Polg^{D257A}$ mutation (11), but not by diabetes. Thus, light microscopy showed that the testes of 9-month-old Akita mice (Fig. 2.10C) were not notably different from those of non-diabetic wild type mice (Fig. 2.10A). In contrast, the seminiferous tubules of the Polg (Fig. 2.10B) and Polg-Akita (Fig. 2.10D) mice were severely atrophic and contained vacuoles. Marked loss of germ cells and spermatogenesis was evident within the seminiferous tubules of both Polg and Polg-Akita mice. Light microscopy showed a significant increase in the number of Leydig cells per cluster in the Polg mice relative to WT and in the Polg-Akita mice relative to Akita, although the increase was less in the diabetic mice (Fig. 2.10E). Ultra-structurally, Leydig cells of the testis in Polg-Akita mice have a markedly degenerative morphology compared to Akita mice, including the presence of lipofuscin indicative of mitochondrial damage (Fig. 2.11).

Plasma testosterone in wild type mice at 9 months of age was 220±12 ng/dL. Plasma testosterone in the Akita mice was not demonstrably different from this at 6 months age, but had decreased to about 50ng/dL at 9 months age (Fig. 2.10F). The Polg-Akita mice had significantly lower plasma testosterone levels than the Akita mice at both ages (~30%; $P < 0.01$). Together, these data demonstrate that the $Polg^{D257A}$ mutation has a strong and direct

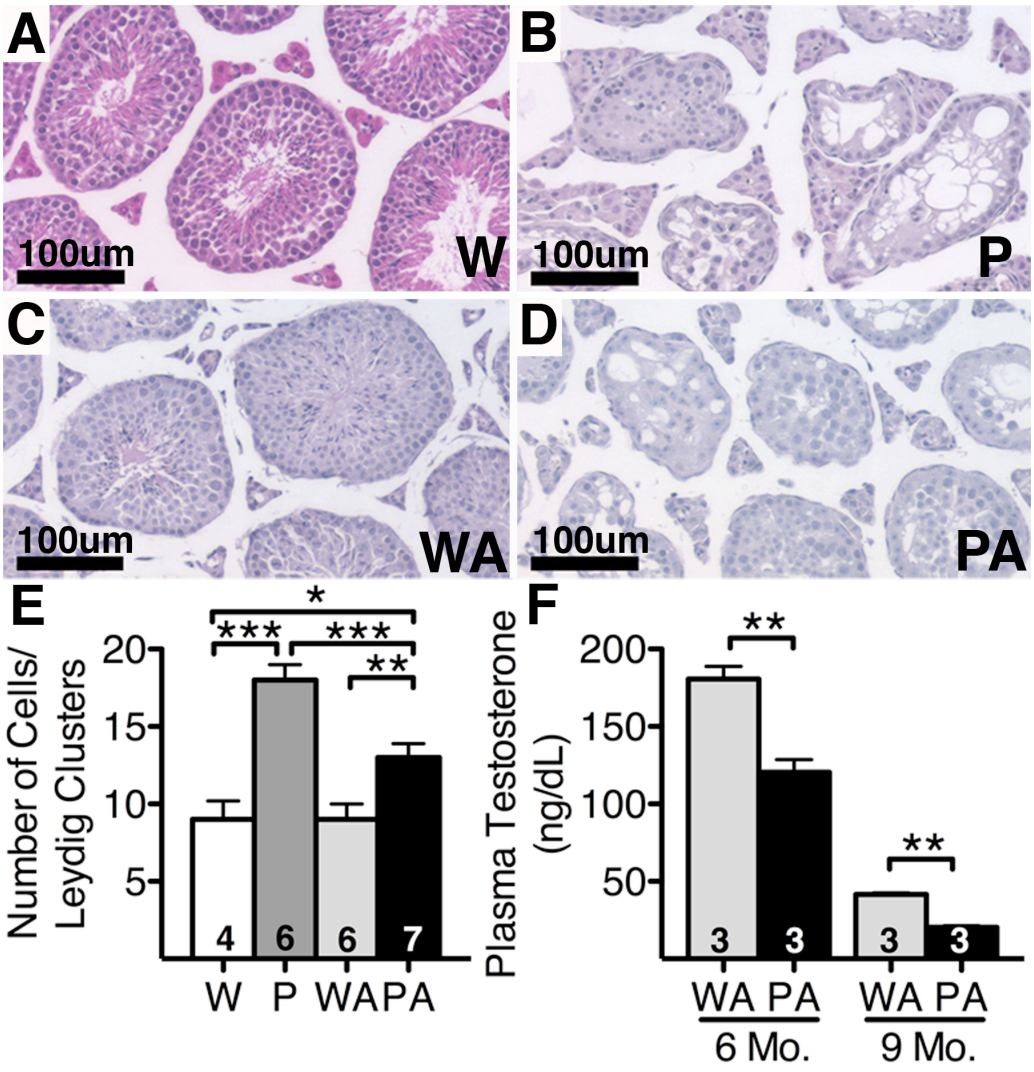

Figure 2.10: Diminished testis function in Polg-Akita mice. Comparable histology sections of the testis of 9 month old (A) Wild type - W, (B) Polg - P, (C) Akita - WA and (D) Polg-Akita - PA mice. (E) Total number of cells/ Leydig cluster and (F) plasma testosterone. All data are represented as Mean ± SEM. * $P < 0.05$, ** $P < 0.01$, and *** $P < 0.001$ indicate significant difference by Student's t-test.

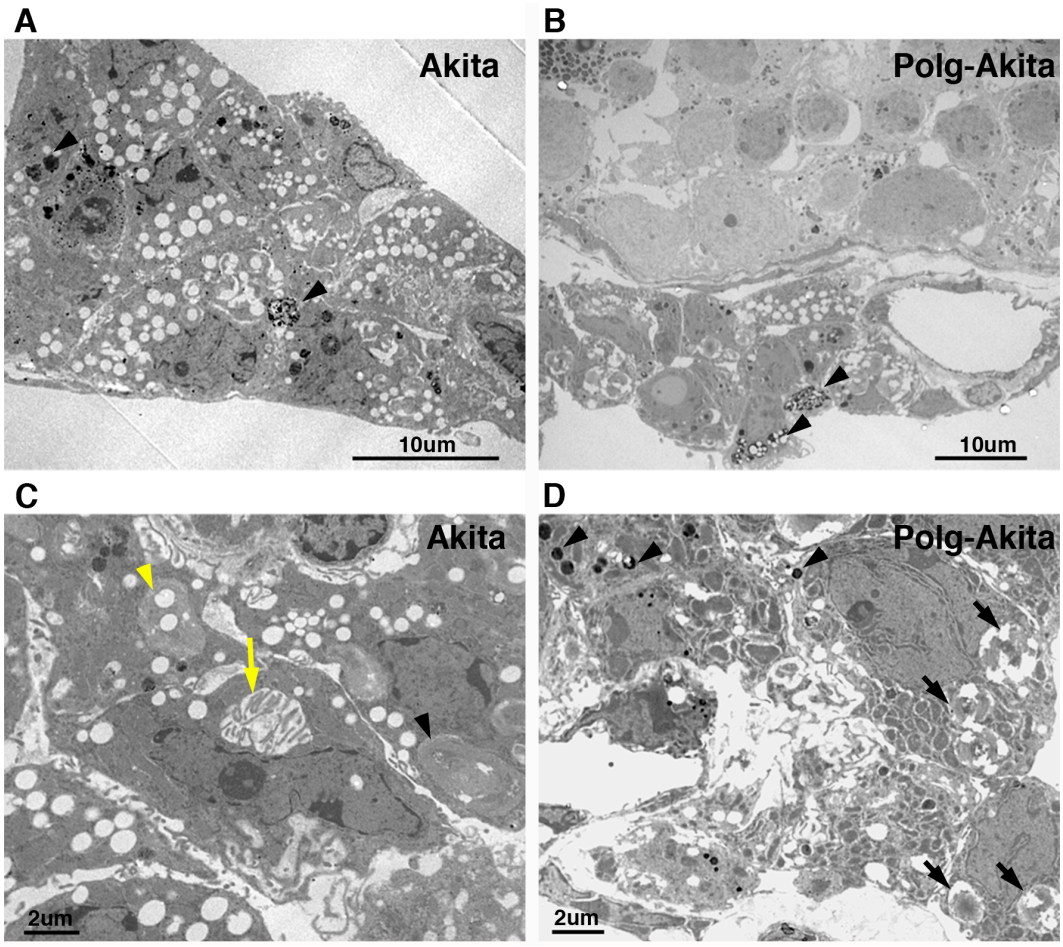

Figure 2.11: EM of Leydig cells.

(A, C) Akita – The Leydig cell clusters are composed of tightly packed cells that have short villi on the cell surface. The nuclei are oval to angulated and have marginated chromatin. Nearly all cells contain lipid droplets (small round clear spaces) in the cell cytoplasm and a few contain lipofuscin deposits (A, Arrows). One Leydig cell appears to contain a small lumen within the cytoplasm (C, yellow arrow). Other cells contain whorled aggregates of smooth endoplasmic reticulum (C, yellow arrow heads).

(B, D) Polg-Akita – In this cluster of Leydig cells, the cells are loosely aggregated and the cytoplasm of some cells contains lipid droplets. The cells have an angulated shape with chromatin clumps and thin marginated chromatin. Lipofuscin is present within the cytoplasm (black arrow heads). Poorly formed whorles of smooth endoplasmic reticulum are present (D, black arrows). (Although not shown in this photograph, the amount of collagen within the Leydig cell clusters appeared to be increased in Polg-Akita mice.)

Note: There are also some additional findings in the Leydig cells that are shown in these photographs but are less clear. These are the "whorled" arrangements of endoplasmic reticulum. These were present more often in Leydig cells from PP and Polg-Akita. The mitochondria in all mice appeared to be similar in number and size.

negative impact on testosterone levels and testicular function in the Polg-Akita mice.

Testosterone replacement. To test whether decreased testosterone levels are responsible for the reduced appetite and hyperglycemia, I implanted pellets into 6-month old Polg-Akita mice (n=3) that deliver the physiological dose of testosterone (0.14mg/day) commonly used in replacement therapy in mice (16). Within 15 days after implantation of the testosterone pellet, plasma glucose in the Polg-Akita mice increased from 300 mg/dl to 500 mg/dl, indistinguishable from the level in Akita mice without testosterone supplementation (Fig. 2.12A). Their food consumption also increased compared to untreated Polg-Akita mice, and were essentially the same level as in untreated Akita mice (Fig. 2.12B). Taken together, these data show that testosterone is a key component that directly regulates food consumption and thereby influences the hyperglycemia of Akita male mice. Surprisingly, however, despite the return of hyperglycemia in the Polg-Akita mice treated with testosterone, their daily urine output, glucose excretion and urine albumin excretion were not increased (Figs. 2.12C-E). This indicates that the testosterone treated Polg-Akita mice are reabsorbing substantial amounts of glucose, and suggested to us that the kidneys of these animals were likely to be metabolically stressed. In support of this idea, I found that the ultrastructure of the proximal tubules of the Polg-Akita mice treated with testosterone for 3 months showed considerably more lamellated inclusions (Fig. 2.6E) than were present in the untreated Polg-Akita mice of the same age (Fig. 2.6C).

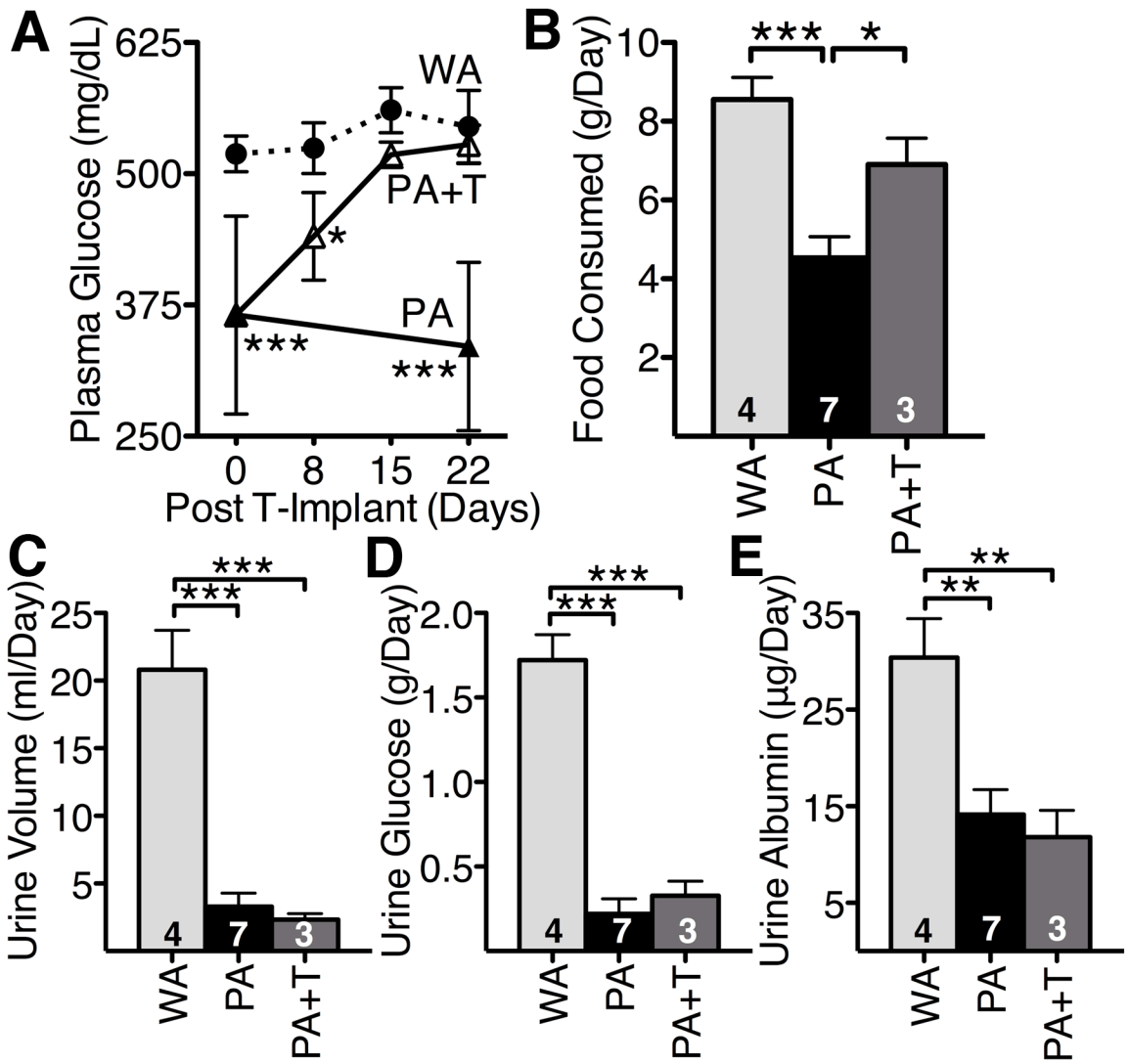

Figure 2.12: Testosterone replacement in Polg-Akita mice. (A) Plasma glucose levels in Testosterone implanted Akita (WA+T) and Polg-Akita (PA+T) mice and Control Akita (WA or WA-T) and Polg-Akita (PA or PA-T). (B)Food Consumption, (C) Urine Volume, (D) Urine Albumin, and (E) Urine Glucose in WA, PA, and PA-T at 22 days post implant. All data are represented as Mean ± SEM. Scale bar=100µm * $P < 0.05$, ** $P < 0.01$, and *** $P < 0.001$ indicate significant difference by Student's t-test.

2.5 Discussion

Because of the importance of mitochondria in metabolism, I expected that the *Polg*^{D257A} mutation, which leads to an accumulation of random mtDNA mutations, would exacerbate the diabetes exhibited by male Akita mice and would increase the severity of their diabetic complications. Surprisingly, I found the opposite result: a dramatic improvement of diabetic symptoms (hyperglycemia, food consumption, and water consumption) in the Polg-Akita male mice as they aged. Accompanying these changes, I found alterations in the expression of anorexic (*Pomc*) and orexic (*Npy*) genes in the hypothalamus indicating that the *Polg* mutation had caused appetite suppression. I did not find any improvement in the overall function of either the pancreas or small intestine that would be sufficient to alter the diabetes so markedly. However, there was a dramatic aging-associated increase in testicular damage in the Polg-Akita mice relative to the Akita mice, including damage to the Leydig cells, and a reduction in plasma testosterone. Testosterone replacement increased food consumption in the double mutants, and their hyperglycemia returned, confirming the influence of testosterone and appetite in the development of the diabetic symptoms of Akita male mice.

In non-diabetic animals, an increase in plasma glucose after a meal stimulates the release of insulin. Insulin binds to insulin receptors in peripheral tissues and triggers glucose uptake via insulin-sensitive glucose transporters. Insulin, together with the amylin released by the beta cells simultaneously with insulin (24), plays an important role in the regulation of appetite by suppressing orexic genes within the hypothalamus (25, 26). In Akita mice, mis-folded insulin protein causes ER stress and β cell death, resulting in reduced insulin production (13). Insufficient insulin production initiates two pathways that accelerate hyperglycemia in Akita mice (Fig. 2.13A). First, it reduces the ability of peripheral tissues to take up glucose.

Second, the reduced insulin impairs appetite suppression in the hypothalamus causing hyperphagia. The increased food intake induces an increased demand for insulin, which increases the problems of the already stressed insulin-producing β cells leading to further β cell death. This damaging feedback can be partly interrupted by reducing food intake, as illustrated by the well-documented benefits of reduced food intake in the management of type 1 diabetes before the discovery of insulin (27).

In the present study, I have demonstrated that the mtDNA mutator, Polg-D257A, can break the self-induced cycle of hyperglycemia and hyperphagia of Akita male mice as they age (Fig. 2.13B). The most striking age-dependent damage in the Polg-Akita males is in the testis, accompanied with a decrease in circulating testosterone. Recent studies have suggested that aging-related reduction of food consumption may in part result from reduced testosterone and a consequent increase in leptin production (28). Epidemiological studies have also demonstrated an association between these factors (29). In addition, testosterone administration has been shown to suppress the elevated leptin levels in older hypogonadal men (30, 31), and dihydrotestosterone suppresses both leptin mRNA levels and leptin secretions in adipocytes *in vitro* (32). Leptin, produced in adipose tissues, is crucial in the regulation of appetite by signaling through the hypothalamus (33). Our observations in aged Polg-Akita males show the involvement of these factors in the changes in food consumption and appetite induced by the Polg mutation. Thus, as they age, Polg-Akita mice develop significant increases in plasma leptin, increased *Pomc* and decreased *Npy* gene expression compared to Akita males. Furthermore, both hyperglycemia and hyperphagia returned in Polg-Akita males after testosterone administration. I conclude that the age-dependent decline of testis function and testosterone production caused by $Polg^{D257A}$ underlies the reduced diabetic phenotypes of the

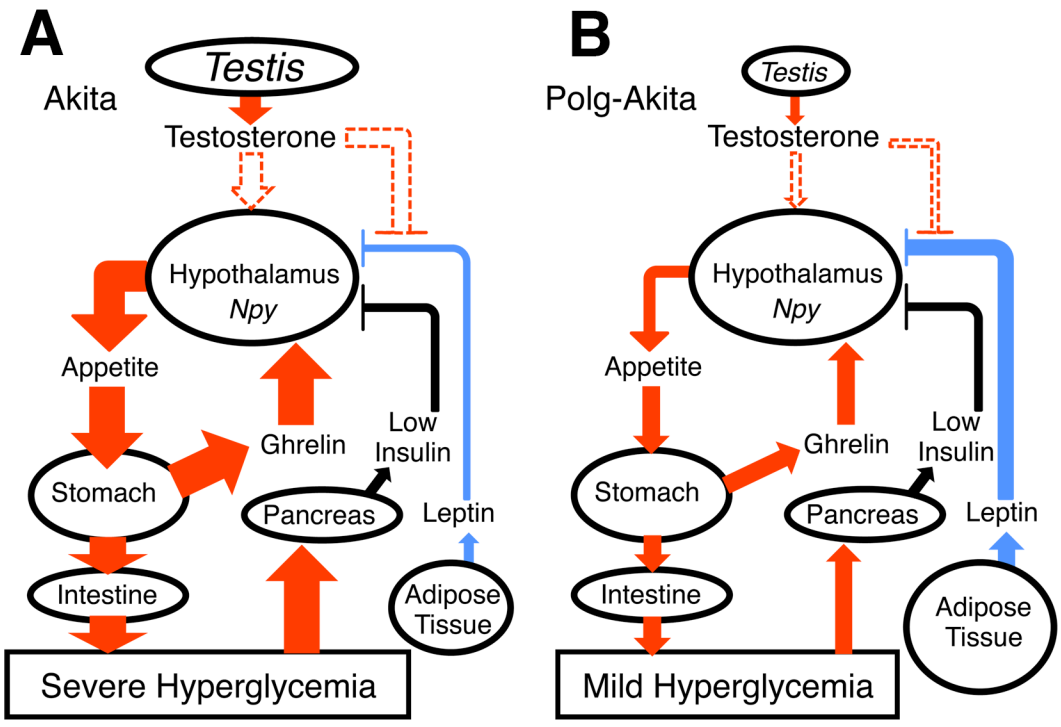

Figure 2.13: Hyperphagic model of diabetic Akita mice (A) and the mechanism of reversal in Polg-Akita mice (B). (A) In Akita mice, low levels of insulin no longer suppresses appetite, normal testosterone levels increases appetite by either directly increasing *Npy* or through suppressing leptin while ghrelin, released from the stomach, also works in unison with testosterone and leptin to increase appetite through the hypothalamus. (B) In Polg-Akita mice, low levels of insulin and amylin no longer suppresses appetite, reduced testosterone levels decrease appetite by either directly decreasing *Npy* or allowing leptin to suppress *Npy* while reduced ghrelin also reduces appetite. Red lines – appetite stimulating affect, blue lines – appetite suppressing affect, black lines – no change between genotypes. Line thickness indicates magnitude of affect.

Polg-Akita mice. This interpretation is supported by a recent report that gonadectomy causes a marked reduction of hyperglycemia in diabetic Akita males and normalizes *Pomc* and *Npy* mRNA levels within their hypothalamus, and that reducing the food intake of Akita mice also reduces their hyperglycemia (23).

Testosterone increases appetite in castrated rats and appears to do so independently of its conversion to estrogen (34). Whether testosterone acts on adipocytes to regulate production of leptin, circulating leptin, or directly on the genes in the hypothalamus remains to be elucidated. In addition, since plasma testosterone levels also declined in aged diabetic Akita mice without apparent loss of appetite, other factors must be also involved. For example, a significant reduction in circulating ghrelin works in unison with the testosterone-leptin mechanism to reduce appetite. I also note that this aging-related amelioration of diabetes caused by the $Polg^{D257A}$ mutation could be exaggerated in the Akita model of diabetes in which β cell destruction is directly tied to insulin production. Whether it is applicable to other animal models of diabetes remains to be determined.

The nephropathy in our experimental diabetic Akita mice was mild, in part because of their C57BL/6J genetic background, which confers resistance to diabetic nephropathy (35, 36). Concordant with the dramatic improvement of hyperglycemia and reduced urine output, the Polg-Akita mice no longer had glycogen deposits in the nuclei of their distal tubular cells. Instead, despite the lessening of their hyperglycemia, the Polg-Akita mice now had abnormalities in their proximal tubular cells. Formation of enlarged lysosomes filled with lamellated inclusions and calcifications indicate that the increase in mtDNA mutations induced by the $Polg^{D257A}$ mutation leads to increased mitochondrial destruction in the proximal tubular cells, which have high-energy requirements and are highly packed with mitochondria. I note

that diabetes is necessary to cause the observed abnormalities in the proximal tubular epithelial cells, because they were not present either in non-diabetic Polg males or in mildly diabetic Polg-Akita females of the same age. Our observation that the urine volumes and glucose excretion of testosterone treated Polg-Akita mice remained low, despite a return of hyperglycemia, further emphasizes this interaction. Thus, the treated mice are reabsorbing sufficient amounts of filtered glucose to avoid osmotic diuresis and glycosuria even with plasma glucose levels exceeding 500mg/dL, which requires a large amount of energy. Accompanying this high-energy demand, I find an accumulation of laminated bodies in the proximal tubules of the testosterone treated hyperglycemic Polg-Akita mice exceeding that in the euglycemic untreated Polg-Akita mice.

In conclusion, I have demonstrated that the mtDNA editing mutation, $Polg^{D257A}$, causes an age-dependent reduction of the diabetic phenotype of Akita male mice. I have shown that this reduction is, at least in part, due to appetite suppression caused by a premature decline in testosterone production associated with increased damage to Leydig cells. Since female Akita and Polg-Akita mice are both only moderately hyperglycemic and their food consumption remains similar throughout 9 months of age, the Polg-D257A does not affect the severity of their diabetes. The accumulation of mitochondrial debris in the proximal tubules of the Polg-Akita males, even when euglycemic, demonstrates clearly that increased mutations in mtDNA exacerbate the kidney pathology in untreated type 1 diabetes.

REFERENCES

1. de Andrade PB*, et al.* (2006) Diabetes-associated mitochondrial DNA mutation A3243G impairs cellular metabolic pathways necessary for beta cell function. *Diabetologia* 49(8):1816-1826.

2. Patti ME & Corvera S (2010) The Role of Mitochondria in the Pathogenesis of Type 2 Diabetes. *Endocr Rev* .

3. Kakoki M*, et al.* (2006) Senescence-associated phenotypes in Akita diabetic mice are enhanced by absence of bradykinin B2 receptors. *J Clin Invest* 116(5):1302-1309.

4. Kakoki M, Takahashi N, Jennette JC, & Smithies O (2004) Diabetic nephropathy is markedly enhanced in mice lacking the bradykinin B2 receptor. *Proc Natl Acad Sci U S A* 101(36):13302-13305.

5. Simmons RA, Suponitsky-Kroyter I, & Selak MA (2005) Progressive accumulation of mitochondrial DNA mutations and decline in mitochondrial function lead to beta-cell failure. *J Biol Chem* 280(31):28785-28791.

6. Someya S*, et al.* (2008) The role of mtDNA mutations in the pathogenesis of age-related hearing loss in mice carrying a mutator DNA polymerase gamma. *Neurobiol Aging* 29(7):1080-1092.

7. Trifunovic A & Larsson NG (2008) Mitochondrial dysfunction as a cause of ageing. *J Intern Med* 263(2):167-178.

8. Wang J, Markesbery WR, & Lovell MA (2006) Increased oxidative damage in nuclear and mitochondrial DNA in mild cognitive impairment. *J Neurochem* 96(3):825-832.

9. Zhang D*, et al.* (2003) Mitochondrial DNA mutations activate the mitochondrial apoptotic pathway and cause dilated cardiomyopathy. *Cardiovasc Res* 57(1):147-157.

10. Hance N, Ekstrand MI, & Trifunovic A (2005) Mitochondrial DNA polymerase gamma is essential for mammalian embryogenesis. *Hum Mol Genet* 14(13):1775-1783.

11. Kujoth GC*, et al.* (2005) Mitochondrial DNA mutations, oxidative stress, and apoptosis in mammalian aging. *Science* 309(5733):481-484.

12. Trifunovic A*, et al.* (2004) Premature ageing in mice expressing defective mitochondrial DNA polymerase. *Nature* 429(6990):417-423.

13. Wang J*, et al.* (1999) A mutation in the insulin 2 gene induces diabetes with severe pancreatic beta-cell dysfunction in the Mody mouse. *J Clin Invest* 103(1):27-37.

14. Graham JM (2001) Isolation of mitochondria from tissues and cells by differential centrifugation. *Curr Protoc Cell Biol* Chapter 3:Unit 3 3.

15. Chomczynski P & Sacchi N (1987) Single-step method of RNA isolation by acid guanidinium thiocyanate-phenol-chloroform extraction. *Anal Biochem* 162(1):156-159.

16. Nathan L*, et al.* (2001) Testosterone inhibits early atherogenesis by conversion to estradiol: critical role of aromatase. *Proc Natl Acad Sci U S A* 98(6):3589-3593.

17. Vermulst M*, et al.* (2007) Mitochondrial point mutations do not limit the natural lifespan of mice. *Nat Genet* 39(4):540-543.

18. Vermulst M*, et al.* (2008) DNA deletions and clonal mutations drive premature aging in mitochondrial mutator mice. *Nat Genet* 40(4):392-394.

19. Yoshioka M, Kayo T, Ikeda T, & Koizumi A (1997) A novel locus, Mody4, distal to D7Mit189 on chromosome 7 determines early-onset NIDDM in nonobese C57BL/6 (Akita) mutant mice. *Diabetes* 46(5):887-894.

20. Ekstrand MI*, et al.* (2004) Mitochondrial transcription factor A regulates mtDNA copy number in mammals. *Hum Mol Genet* 13(9):935-944.

21. Foury F (1989) Cloning and sequencing of the nuclear gene MIP1 encoding the catalytic subunit of the yeast mitochondrial DNA polymerase. *J Biol Chem* 264(34):20552-20560.

22. Blakely EL*, et al.* (2005) A mitochondrial cytochrome b mutation causing severe respiratory chain enzyme deficiency in humans and yeast. *FEBS J* 272(14):3583-3592.

23. Toyoshima M*, et al.* (2007) Dimorphic gene expression patterns of anorexigenic and orexigenic peptides in hypothalamus account male and female hyperphagia in Akita type 1 diabetic mice. *Biochem Biophys Res Commun* 352(3):703-708.

24. Moore CX & Cooper GJ (1991) Co-secretion of amylin and insulin from cultured islet beta-cells: modulation by nutrient secretagogues, islet hormones and hypoglycemic agents. *Biochem Biophys Res Commun* 179(1):1-9.

25. Morris MJ & Nguyen T (2001) Does neuropeptide Y contribute to the anorectic action of amylin? *Peptides* 22(3):541-546.

26. Mayer CM & Belsham DD (2009) Insulin directly regulates NPY and AgRP gene expression via the MAPK MEK/ERK signal transduction pathway in mHypoE-46 hypothalamic neurons. *Mol Cell Endocrinol* 307(1-2):99-108.

27. Westman EC, Yancy WS, Jr., & Humphreys M (2006) Dietary treatment of diabetes mellitus in the pre-insulin era (1914-1922). *Perspect Biol Med* 49(1):77-83.

28. Morley JE (2001) Decreased food intake with aging. *J Gerontol A Biol Sci Med Sci* 56 Spec No 2:81-88.

29. Baumgartner RN*, et al.* (1999) Serum leptin in elderly people: associations with sex hormones, insulin, and adipose tissue volumes. *Obes Res* 7(2):141-149.

30. Kapoor D, Clarke S, Stanworth R, Channer KS, & Jones TH (2007) The effect of testosterone replacement therapy on adipocytokines and C-reactive protein in hypogonadal men with type 2 diabetes. *Eur J Endocrinol* 156(5):595-602.

31. Sih R*, et al.* (1997) Testosterone replacement in older hypogonadal men: a 12-month randomized controlled trial. *J Clin Endocrinol Metab* 82(6):1661-1667.

32. Gupta V*, et al.* (2008) Effects of dihydrotestosterone on differentiation and proliferation of human mesenchymal stem cells and preadipocytes. *Mol Cell Endocrinol* 296(1-2):32-40.

33. Friedman JM & Halaas JL (1998) Leptin and the regulation of body weight in mammals. *Nature* 395(6704):763-770.

34. Gentry RT & Wade GN (1976) Androgenic control of food intake and body weight in male rats. *J Comp Physiol Psychol* 90(1):18-25.

35. Gurley SB*, et al.* (2006) Impact of genetic background on nephropathy in diabetic mice. *Am J Physiol Renal Physiol* 290(1):F214-222.

36. Qi Z*, et al.* (2005) Characterization of susceptibility of inbred mouse strains to diabetic nephropathy. *Diabetes* 54(9):2628-2637.

Chapter 3

THE EFFECT OF MITOCHONDRIAL DNA POLYMERASE EDITING MUTATION, POLGD257A, ON THE CELL CYCLE OF THE SMALL INTESTINE

3.1 Abstract

Changes in nutritional absorption in the intestine are an important aspect of the aging process yet few comprehensive studies have been carried out addressing this issue. I used mitochondrial DNA mutator mice homozygous for a D257A mutation in polymerase gamma (PolgD257A mouse) as a genetic tool to increase mitochondrial DNA mutations and answer questions regarding aging in the small intestine. The small intestines of relatively young 7-month-old PolgD257A mice have morphological changes such as increased villus height/width and increased crypt depth/width that mimic the aged human small intestine. I find a general increase in apoptosis in the small intestine crypts of Lieberkühn that has not been reported or studied previously in aging mice, rats, or humans. Immunohistochemically, the PolgD257A mutants maintained the same number of actively dividing cells in the proliferating region of the crypt, yet cell migration along the crypt-villus axis was diminished and a lesser proportion of cells are in S-phase of the cell cycle than the wild type littermates. *In vitro*, I find that the stem cells from crypts proliferate at a slower rate and produce less budding via symmetric division in the PolgD257A mice than those in wild type mice. I conclude that the PolgD257A mutation causes age-associated changes in the morphology of the small intestine correlated with increased apoptosis of progenitor and stem cells, a slower cell cycle in the proliferating progenitor cells, and a proliferation defect in the stem cells located in the crypts of Lieberkühn.

3.2 Introduction

With the growing elderly population and its ramifications on the health care system, a clear understanding of the mechanisms behind the aging process in individual organs is important. Aging has been widely accepted as the root cause of organ degeneration and dysfunction. For instance, elderly subjects are prone to malnutrition and mal-absorption, both of which are associated with intestinal dysfunction (1, 2). Morphological changes in the small intestine villi and crypts of elderly subjects have been reported to include enlarged height and width of villi and crypts (3, 4). However, there are no comprehensive studies demonstrating how these changes in villi shape affect function. In agreement with these findings in humans, studies of both mice and rats have shown similar changes with age. The small intestines of aged rats have increased size of the villi and crypt compartments (5). A histological comparison between young and old mice also provides evidence for the increased size of the villi and crypt compartments in old mice compared to young mice (6).

Aging of the human small intestine is also characterized by increased apoptosis and increased proliferation of the enterocytes (3, 7). Increased proliferation has also been associated with the aging rat small intestine, and apoptosis is initially high in young rats and diminishes to low levels in aging rats (8, 9). However, comprehensive studies on the age-related changes in the levels of apoptosis in the villi and crypt compartments of humans, rats, and mice are lacking. In addition, whether any of these morphological or molecular changes lead to dysfunction of the aging intestine has not been determined.

Mitochondrial dysfunction is known to affect basic cellular function, initiate apoptosis, and lead to aging (10). Insertions, deletions and point mutations in the mitochondrial genome have their greatest effect in cells that require high energy production including neurons, hair

cells of the inner ears, heart and skeletal myocytes, pancreatic beta cells, as well as gut and kidney epithelial cells (11-15). Mitochondrial DNA mutations in the colon of elderly subjects have been shown to cause a decrease in cellular proliferation and an increase in apoptosis (16). Yet, a mechanism behind the cause of increased proliferation and decreased apoptosis has not been determined due to a lack of an appropriate aging model that mimics these findings in humans.

Mitochondrial DNA polymerase gamma (*Polg*) is responsible for replicating the mitochondrial genome. An introduction of an amino acid substitution, D257A, in the exonuclease domain II disrupts the proofreading ability of Polg without significantly affecting the replicating capacity of the polymerase (17, 18). Mice homozygous for the PolgD257A mutation have a reduced lifespan of 13 months, and display a series of aging-associated phenotypes at 10 months of age as a consequence of increased random accumulations of mtDNA mutations (17, 18). These include graying and loss of hair, kyphosis, and decreased bone density. Hence, the homozygous PolgD257A mouse is an animal model of premature aging with all the visible signs of human aging.

Previous reports have shown that several tissues in PolgD257A mice, including thymus, small intestine, and testes, have elevated levels of apoptosis at 3 months of age (17). Consequently, the D257A mutation provides a genetic tool that can be used to determine if an increased frequency of mtDNA mutations in the small intestine will contribute to an aging phenotype, including apoptosis.

In the present work, I have investigated PolgD257A mice as a means to accelerate aging in the small intestine. Previous work utilizing the PolgD257A mouse has shown that the villi of the small intestine undergoes two distinct changes: (i) increased villi epithelial cell

apoptosis; and (ii) morphology changes, such as elaborate branching and fusion (17). However, it is not clear if the increase in apoptosis and the change in morphology of the villi causes any other molecular changes. How the small intestine phenotype affects the whole body metabolism when fed a high fat western diet is described in Chapter 4. In this chapter, I characterized the small intestine phenotype of 3 and 7 month old mice homozygous for the PolgD257A mutation, and I demonstrate that 7-month-old PolgD257A mice have morphological changes to the villi and crypt compartments that mimic human small intestine aging. Surprisingly, I found an increase in apoptosis in the small intestine crypts of Lieberkühn, which has not been reported in these mice. The PolgD257A mutant small intestine maintained the same number of cells in the proliferating region of the crypt, however cell migration along the crypt-villus axis was diminished and correlated with a disruption of the cell cycle. While morphological changes of human aging of the small intestine are similar in PolgD257A mice, the changes in the cell cycle and apoptosis found in the crypts are novel findings in the context of premature aging.

3.3 Materials and Methods

Mice. All mice were maintained on normal chow containing 5.3% fat and 0.019% cholesterol (Prolab Isopro RMH 3000, ref 5P76; Agway Inc., Syracuse, NY, USA). The experimental animals were males homozygous for the *Polg*^{D257A} mutation that have been extensively backcrossed onto a C57BL/6 background. Littermate controls were wild type at the *Polg* locus. Male animals were monitored and characterized at 3 and 7 months of age. All animal experiments were performed in accordance with the Institutional Animal Care and Use Committee at The University of North Carolina at Chapel Hill.

Isolation of Small Intestines. Mice were lethally anesthetized animals with an over dose of 2,2,2 Tribromoethanol and the small intestine was removed from the stomach to the cecum of the large intestine. Isolated intestines were placed in ice cold PBS, and subsequently flushed with 10 mLs of ice cold PBS. The intestines were split into two sections, duodenum to jejunum and jejunum to ileum. Each section was placed in 4% paraformaldehyde at 4°C for at least 24 hours. Intestines were then cut length wise and rolled for sectioning.

Histology. Paraffin sections were cut at a thickness of 5 μm and stained with Hematoxylin and Eosin, Periodic acid-Schiff, or Masson's Trichrome. Analysis of villus length & width, crypt length & width, intestinal length, and intestinal diameter were measured on digitally scanned slides using ImageScope Software.

Apoptosis and S-Phase Detection. Terminal deoxynucleotidyl transferase dUTP nick end labeling (*TUNEL*) was used to detect DNA fragmentation caused by apoptosis signaling. A commercially available TUNEL kit was used to determine apoptosis (ApopTag S7110; Chemicon Int.). To determine cells in S-phase, animals were injected with 50 μg/ml of 5-

ethynyl-2′-deoxyuridine (EdU) and sacrificed 2 hours after injection. Cells in S-Phase were determined as previously described (19) using a commercially available kit (Click-iT EdU C10084, Molecular Probes, Inc., Eugene, OR).

Cell Migration. For EdU pulse time course, mice were injected once with 50 μg/ml of EdU. Mice were sacrificed at 2, 24, and 48 hours after injection. For EdU washout time course, mice were injected 3 times per day for 4 consecutive days with 75 μg/ml EdU. Mice were sacrificed at 2, 24, 48, and 96 hours after the last injection. EdU was detected as described previously.

Cell Cycle Immunostaining. Small intestine was resected, flushed of fecal contents with ice cold PBS, cut open along the longitudinal axis, and fixed in 4% paraformaldehyde for 16 hours at 4 °C. Prior to immunostaining, the sections underwent antigen retrieval using Reveal Decloaker (Biocare Medical, Concord, CA) in a pressure cooker set at 120°C for 30 seconds and then 90°C for 30 seconds. The sections were allowed to cool in the Reveal Decloaker for 20 minutes at room temperature and washed three times with excess water for 2 minutes each. The sections were stained first for EdU as described above using Alexafluor 488 azide, and then blocked with DAKO Blocking Solution (DAKO, X0909, Carpinteria, CA) for 5 minutes prior to antibody staining. All primary antibodies were diluted in DAKO Antibody Diluent (Dako, S0809). For all proliferating cells, sections were stained with KI67 (1:500; Dako, #M7249). For mitosis, sections were stained with Anti-phospho Histone H3 (1:500; Ser10, 06-570, Millipore, Temecula, CA) Cells at G1 phase were visualized with Anti-Minichromosome maintenance 2 (1:200; MCM2, N-19, SC-9839, Santa Cruz Biotechnology, Santa Cruz, CA). All primary antibodies were incubated with tissue at 4°C for 16 hours. The tissues were then washed three times with Tris-wash buffer (0.05 M, pH7.6) for 3 minutes each wash. Secondary

antibodies (Ki67: donkey anti-rat biotinylated, 712-067-003/streptavidin-405, 016-470-084; PH3: donkey anti-rabbit-dylight 549, 711-505-152; MCM2: donkey anti-goat-dylight 647, 705-496-147) conjugated to fluorophores that facilitated co-localization were diluted in DAKO diluent at 1:250, and applied to tissue sections for 45 minutes at 21°C. The tissues were then washed three times with Tris-wash buffer for 3 minutes each. For nuclear staining, Bis-benzimide (Sigma, B2883, St. Louis, MO) was diluted to 5 µg/ml in Tris-wash buffer and applied to tissue sections for 5 minutes. The tissue was then washed once with Tris-wash buffer, and cover slip was mounted with Hydromount (National Diagnostics, HS-106, Atlanta, GA).

Crypt Isolation, IESC FACS Enrichment, and Culturing. Crypts were isolated as previously described (20). The crypts were placed in crypt culturing medium (Advanced DMEM/F12 (Gibco, #12634) supplemented with 1X B27 w/o Vitamin A (Invitrogen # 12587010), 1X N2 (Invitrogen # 17502048), 10 mM HEPES (Gibco # 15630-106), 100 µg/mL Penicillin/Streptomycin, 2 mM L-Glutamine), and 10 µl were counted to determine the concentration of crypts/ml of solution. A volume containing five-hundred crypts was removed and pelleted at 500 x g for 5 minutes at 4°C. The medium was removed and the crypt pellet was lightly and carefully resuspended in 5 µl of crypt culturing medium. Matrigel culturing conditions were conducted essentially as described (20) with the exception that whole crypts were placed in 50 µl of Matrigel containing R-spondin (1 µg/mL first day, 500 ng/mL thereafter), Noggin (100 ng/mL, Peprotech, Rocky Hill, New Jersey, #250-38), EGF (50 ng/mL), Jagged (1µM), and Wnt-3a (2.5 ng/mL, first day only, R&D Systems, #1324-WN/CF).

For FACS, intestinal epithelium was isolated and dissociated to single cells as described (20). Single cell preparations were stained in crypt culture medium with antibodies that would facilitate the enrichment of CD44+ IESCs. Doublets were discriminated and excluded using SSC-Height and SSC-Area parameters. CD45 lymphocytes and CD31 endothelial cells were excluded using antibodies against these cell surface proteins and subsequent FACS exclusion gating (1:500; CD45, Biolegend; San Diego, CA); 1:500; CD31, Biolegend). Anti-CD44 (1:1000, Biolegend) was used to enrich the CD31-CD45- fraction for CD44+ IESCs. Cells that underwent downstream applications were sorted into crypt culturing medium that was maintained on ice for the 1 hour FACS sort period. ATP was measured using the CellTiter-Glo Luminescent Cell Viability Assay per manufacturer's instructions (G7570, Promega Corporation, Madison, WI).

Data Analysis. Values are reported as mean ± SEM. Statistical analyses were conducted with JMP 6.0.2 software (SAS Institute, Cary, NC). P values less than 0.05 were considered significant.

3.4 Results

Cell Apoptosis and Proliferation in the Small intestines of PolgD257A Mice. At 7 months of age, both wild type mice (Fig. 3.1A) and PolgD257A mice (Fig. 3.1B) have apoptosis in the epithelial cells found in the tips of the villi. I confirmed the previous report (17) that epithelial cells in the column of the villi of PolgD257A mice contain significantly increased apoptotic cells compared to wild type mice (Fig. 3.1B). Quantification of the apoptotic cells of the villus indicates a two-fold increase in cell death in PolgD257A mice (19.4 ± 1.2 cells/villus) compared to wild type mice (9.9 ± 1.0 cells/villus, Fig. 3.1C). Interestingly, PolgD257A mice showed a significant increase in apoptosis found within the crypts of Lieberkuhn (indicated by yellow arrowheads in Fig. 3.1B), where both intestinal stem cells and progenitor cells are present. High magnification (40x) of the crypts of Lieberkühn reveals a low level of apoptosis in wild type mice (Fig. 3.2A) compared to the increases seen in PolgD257A mice (Fig. 3.2B). Quantification of the apoptotic crypt cells indicates a ten-fold increase in cell death in PolgD257A mice (3.8 ± 0.5 cells/crypt) compared to wild type mice (0.4 ± 0.06 cells/crypt, Fig. 3.2E).

EdU is incorporated into DNA during the S-phase of the cell cycle and represents a marker of cell proliferation. In a marked contrast, visualization of EdU was more robust in the crypt region of wild type mice than in PolgD257A mice. The number of EdU labeled cells in the crypts of Lieberkühn was significantly less in PolgD257A (5.2 ± 1.3 cells/crypt, Fig. 3.2C) mice than in wild type mice (13.8 ± 1.2 cells/crypt, Fig. 3.2D) demonstrating a reduction in S-phase cell proliferation. Similar degrees of increase in apoptotic cells and decrease in proliferating cells were observed in the crypts of 3-month-old PolgD257A mice. From this data, I also conclude that the PolgD257A mutation is associated with a dramatic increase in

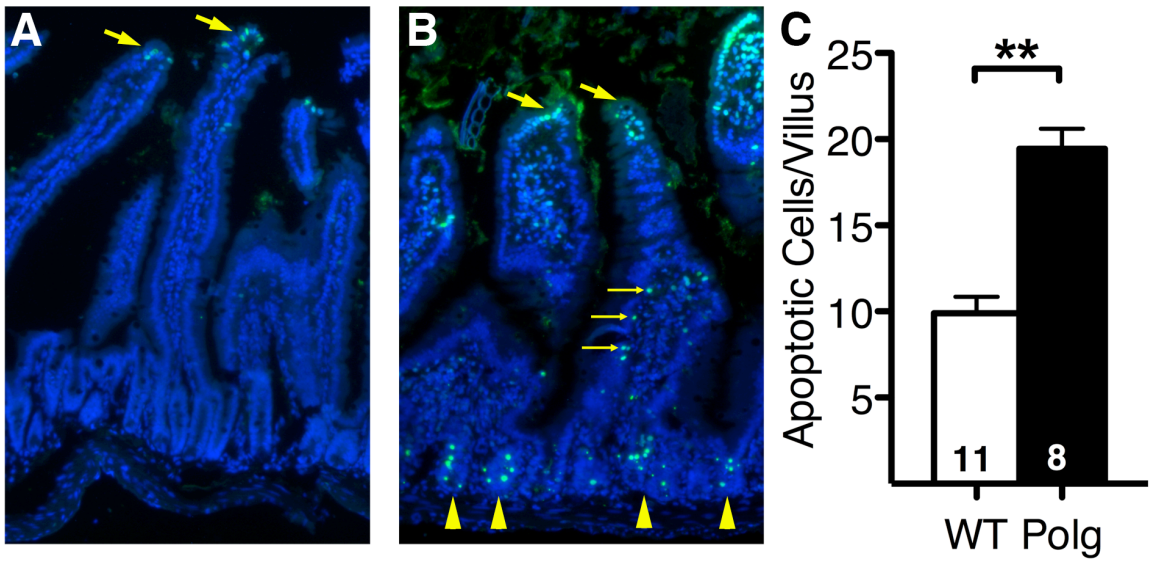

Figure 3.1: Apoptosis in wild type and PolgD257A small intestines. (A) wild type small intestine with apoptosis located at tip of each villus with large yellow arrows indicating apoptotic cells. (B) Polg small intestines have similar levels of apoptosis at the tip of each villus indicated with large yellow arrows. Small yellow arrows indicate an increase in apoptotic cells in the columnar epithelial cells along the length of the villi. An increase in apoptosis was found at the basis of the villi in the crypts of Lieberkühn. (C) Quantification of apoptosis found in the villi. All data are represented as Mean ± SEM. ** $P < 0.01$ between WT (n = 11) and Polg (n = 8) by Student's t-test. Nuclei staining – blue and Apoptosis – green

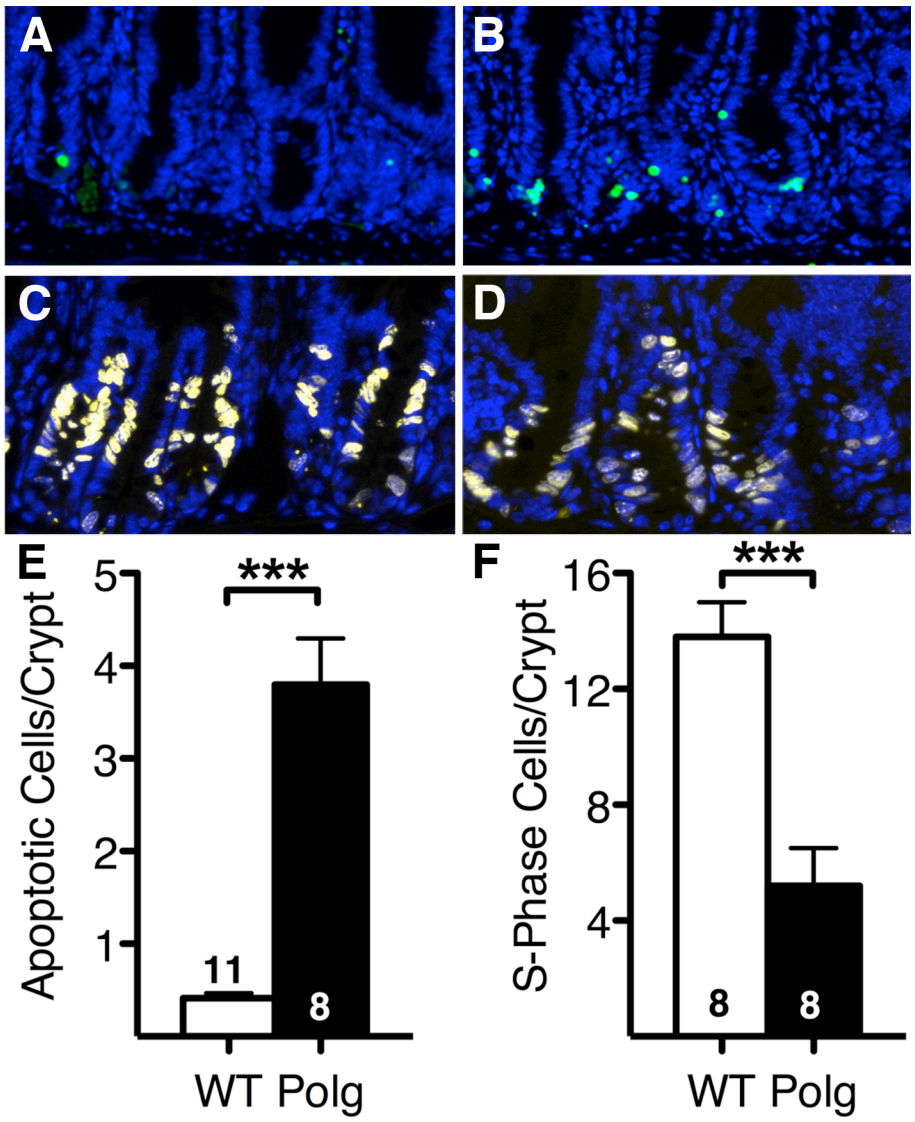

Figure 3.2: Apoptosis and S-phase proliferation in wild type and PolgD257A crypts of Lieberkuhn. Apoptosis is located in the region of the transit amplifying cells of wild type (A) and Polg (B) crypts. Wild type crypts have few apoptotic cells in this region while Polg mice have numerous apoptotic cells. EdU incorporation in S-phase cells in the transit amplifying region is found in the crypts of wild type (C) and Polg (D) mice. Wild type mice have numerous and robust staining of S-phase cells in this region while Polg mice have fewer and less intense staining of S-phase cells in this region. Quantification of apoptotic cells per crypt (E) and S-phase proliferating cells per crypt (F) comparing wild type and Polg mice. All data are represented as Mean ± SEM. *** $P < 0.001$ between WT ($n \geq 8$) and Polg ($n = 8$) by Student's t-test. Nuclei staining – blue, Apoptosis – green, and S-phase cells – yellow

apoptosis and a decrease in cell proliferation particularly in the crypts of Lieberkühn.

Intestinal Cell Migration. To test whether the change in cell proliferation alters migration in the intestine, I conducted a pulse study with EdU in both wild type and PolgD257A mice and followed the migration of the labeled cells 2 hrs, 24 hrs, and 48 hrs after injection. EdU labeled intestinal epithelial cells of wild type mice were robustly labeled and displayed a highly coordinated migration pattern at 2 hrs (Fig. 3.3A), 24 hrs (Fig. 3.3B), and 48 hrs (Fig. 3.3C) post injection. In contrast, the EdU labeled intestinal epithelial cells of PolgD257A mice were sparsely labeled and displayed a random migration pattern at 2 hrs (Fig. 3.3D), 24 hrs (Fig. 3.3E), and 48 hrs (Fig. 3.3F) post injection. The epithelial cells in PolgD257A mice are clearly migrating at a slower rate than in wild type mice. At 48 hrs post injection, cell migration was measured by the distance from the base of the crypt to the nearest EdU labeled cell. I found a significant reduction in epithelial cell migration in PolgD257A mice (median distance of migration 260 ± 4.6 μm) compared to wild type mice (median distance of migration 343 ± 3.4 μm, Fig. 3.3G, $P < 0.001$). Furthermore, the lack of robust labeling in 2 hrs post injection PolgD257A sections is suggestive of slower DNA synthesis during the cell cycle.

To confirm a delayed cell migration of PolgD257A intestinal epithelial cells, PolgD257A and wild type mice were injected with EdU three times per day for four consecutive days. The EdU labeled cells were followed at 2, 24, 48, and 96 hrs after the last EdU injection. The epithelial cells of wild type mice were completely labeled 2 hrs post injection by this method (Fig. 3.4A) whereas the epithelial cells of PolgD257A mice were labeled in the lower two thirds of the crypt-villus axis but sparsely labeled the cells at the tips of the villi (Fig. 3.4E). At 24 hrs post-injection, labeled wild type epithelial cells had completely migrated out of the crypts and started to migrate up the villi (Fig. 3.4B) whereas

most of the PolgD257A epithelial cells migrated out of the crypts but not up the villi (Fig. 3.4F). At 48 hrs post-injection, labeled wild type epithelial cells had migrated half way up the villi (Fig. 3.4C), whereas the PolgD257A epithelial cells migrated out of the crypts and started to migrate up the villi (Fig. 3.4G). The labeled PolgD257A section at 48 hrs post-injection had the same pattern as the labeled wild type sections at 24 hrs post-injection. At 96 hrs post-injection, labeled wild type epithelial cells had completely migrated out of the villi and were no longer visible (Fig. 3.4D). In contrast, labeled PolgD257A epithelial cells still remained near the distal end of the villi (Fig. 3.4H). Taken together, these data show that the epithelial cell migration in the small intestines of PolgD257A mice is significantly impaired compared to wild type mice.

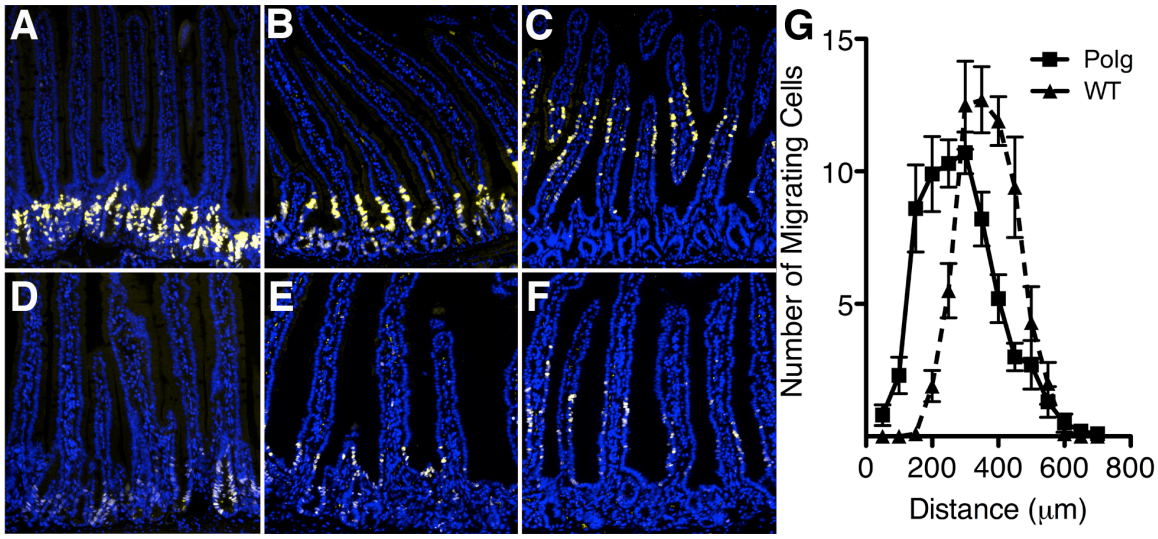

Figure 3.3: Cell migration by EdU pulse is reduced in PolgD257A small intestines. Migration of EdU labeled cells at 2 hrs. post-injection in wild type (A) and Polg (D), 24 hrs. post-injection in wild type (B) and Polg (E), and 48hrs post-injection in wild type (C) and Polg (F). At 48 hrs post-injection of EdU, the length of migrating cells were measured from the base of the crypt to the first labeled cell in each villus. All data are represented as Mean ± SEM. Nuclei staining – blue and S-phase cells – yellow

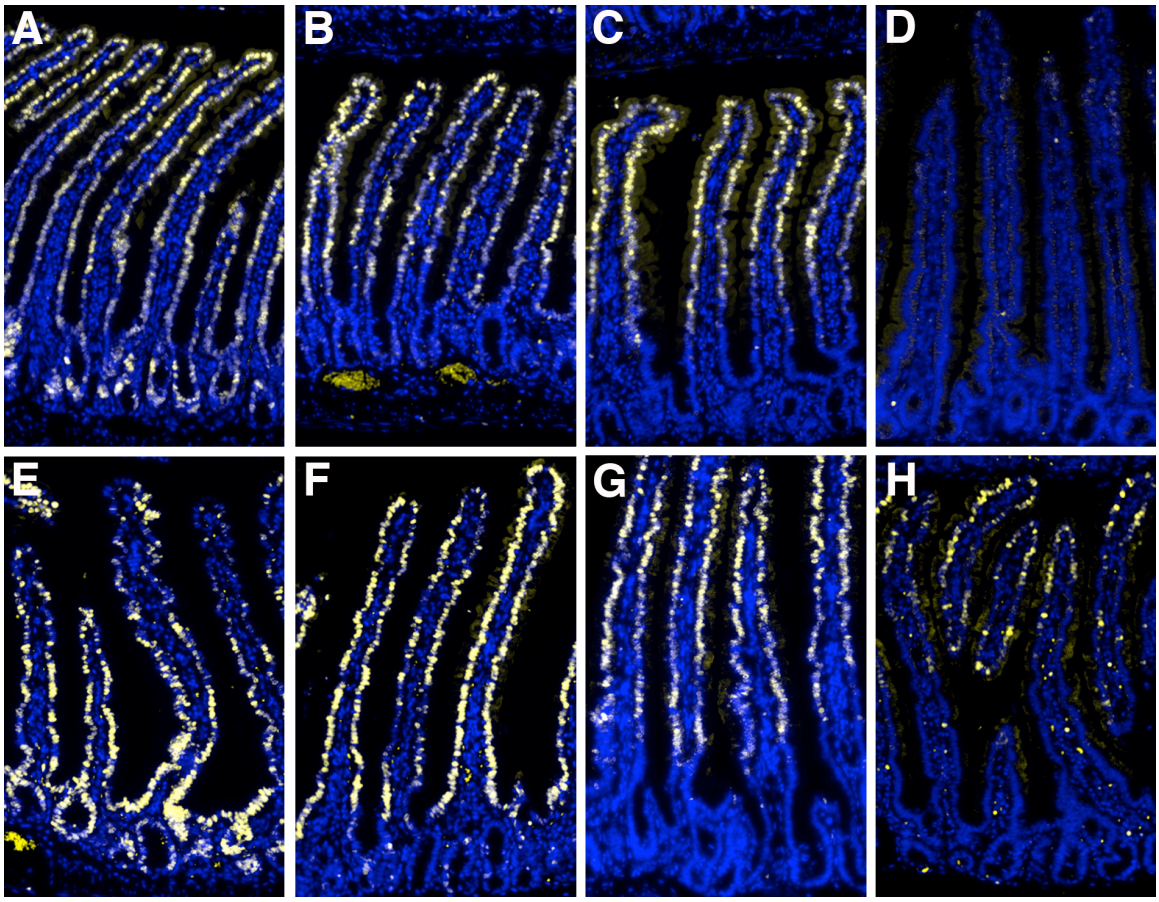

Figure 3.4: Cell migration by EdU washout is slower in PolgD257A small intestines. Animals were injected with EdU three times per day for four consecutive days. Migration of EdU labeled cells at 2 hrs. post-injection in wild type (A) and Polg (E), 24 hrs. post-injection in wild type (B) and Polg (F), 48 hrs post-injection in wild type (C) and Polg (G) and 96 hrs post-injection in wild type (D) and Polg (H). Nuclei staining – blue and S-phase cells – yellow

Measurements of Small Intestine Dimensions. Histological sections of the small intestine were examined to evaluate differences in gross morphology between wild type and PolgD257A mice. Villi length was comparable in the small intestine of PolgD257A mice compared to wild type mice (Fig. 3.5A). Villi width (Fig. 3.5B), crypt length (Fig. 3.5C), and crypt width (Fig. 3.5D) were all significantly larger in PolgD257A mice compared to wild type mice. Thickness of the smooth muscle, measured at 50 random locations from the proximal to distal end of the small intestine, was significantly smaller in Polg D257A mice compared to wild type mice (Fig. 3.5E). The small intestine was slightly longer in PolgD257A mice compared to wild type mice (Fig. 3.5F), however the difference was not significant. These data show that the PolgD257A mutation affects the gross morphology of the small intestines and mimics changes in dimension found in the aging human small intestine.

Alteration of Cell Cycle in Intestinal Crypts. Epithelial cells in the crypt region of both PolgD257A and wild type mice were labeled with a proliferation marker (KI67 – red) and cell cycle markers for S phase (EdU - green), G1 phase (MCM2 - blue), and M phase (pH3 - white). The numbers of proliferating cells detected by KI67 were similar in wild type (Fig. 3.6A) and PolgD257A (Fig. 3.6G) crypts. As previously shown and reconfirmed here by EdU labeling, there are 2.5 times more crypt transit amplifying cells (progenitor cells) in S-phase (DNA synthesis) of wild type mice (Fig. 3.6B) than in PolgD257A mice (Fig. 3.6H). As measured by Anti-MCM2 staining, there are slightly fewer crypt epithelial cells in G1 phase (growth arrest prior to DNA synthesis) of wild type (Fig. 3.6C) than in PolgD257A (Fig. 3.6I) mice however the difference is not significant. There are significantly fewer crypt epithelial cells in late G2 (growth arrest prior to mitosis) and M-phase (Mitosis) of wild type mice (Fig.

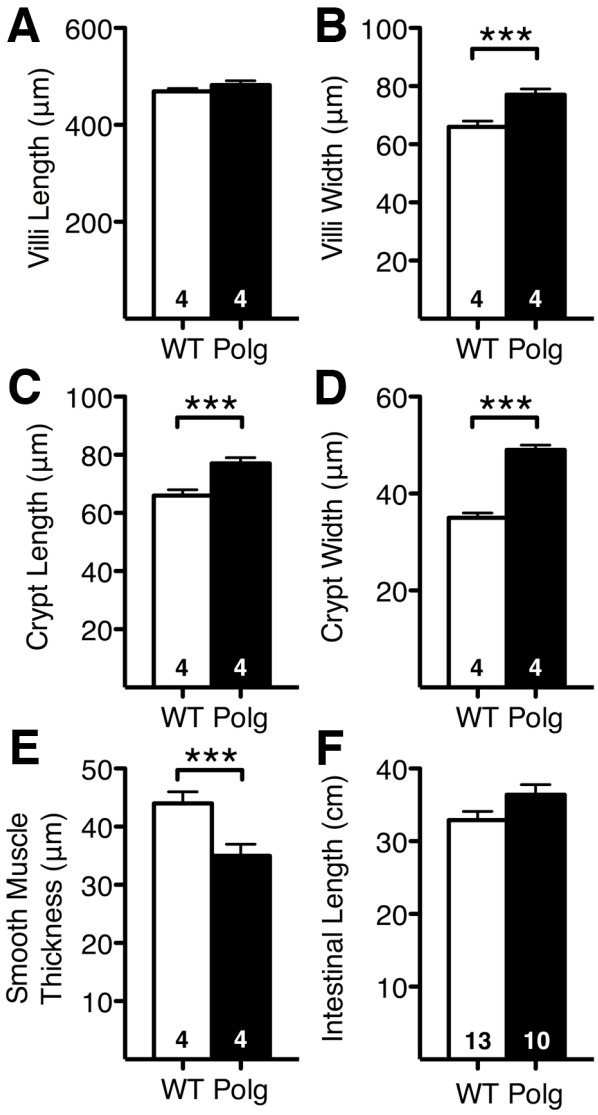

Figure 3.5: Measurements of intestinal morphology. Approximately 25 villi and 25 crypts were measured per animal. A comparison of villus length (A) and width (B), crypt length (C) and width (D), smooth muscle thickness (E), and small intestine length (F) between wild type and Polg mice. All data are represented as Mean ± SEM. *** $P < 0.001$ between WT ($n \geq 4$) and Polg ($n \geq 4$) by Student's t-test.

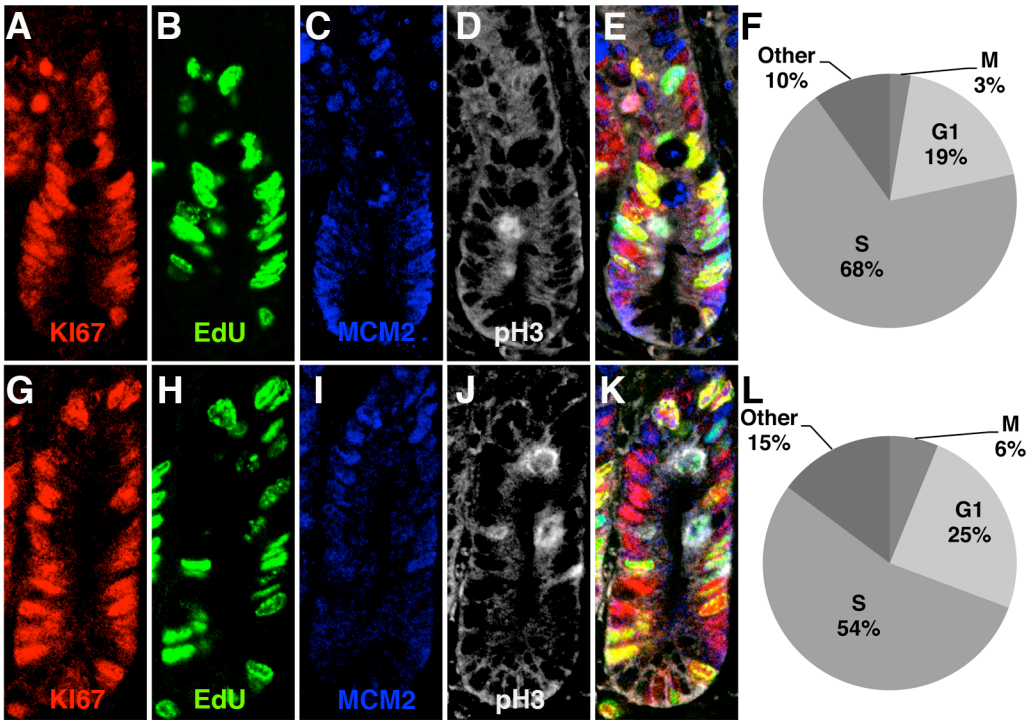

Figure 3.6: Cell cycle changes in PolgD257A crypt cells. Cell proliferation by KI67 (red) staining is equivalent in wild type (A) and Polg (G) crypts. S-phase labeling by EdU (green) is significantly higher ($P < 0.001$) in wild type (B) than in Polg (H). G1-phase labeling by MCM2 (blue) are slightly lower ($P = 0.057$) in wild type (C) than in Polg (I). M-phase labeling by pH3 (white) are lower ($P < 0.01$) in wild type (D) than in Polg (J). (E) Merge of A-D for wild type crypt and (K) merge of G-J for Polg crypt. The percentages of cells in each phase of the cell cycle were determined in wild type (F) and Polg (L) crypts. At least 50 crypts from 2 mice were used to generate percentage of cells in each phase. "Other" represents cells either in G2 or apoptosis. All statistics calculated based on Student's t-test.

3.6D) than in PolgD257A mice (Fig. 3.6J) as measured by anti-pH3 staining. The percentage of cells in S-phase is significantly higher in wild type mice (Fig. 3.6F) than in PolgD257A mice (Fig. 3.6L). The decrease in S-phase cells in PolgD257A mice corresponds to a significant increase in M-phase cells suggesting that these cells are stalling in M-phase. There was a modest increase in the number of cells in both G1-phase ($P = 0.057$) and G2-phase ($P = 0.077$) in PolgD257A mice compared to wild type mice. I conclude that the PolgD257A mutation does not change the number of proliferating cells in the crypt region. However, the PolgD257A mutation not only disrupts the synchronization of the cell cycle in the proliferating cells by decreasing cells in S-phase but also increases the percentage of cells in other phases of the cell cycle, suggesting a slowing of the cell cycle.

Culturing of Isolated Crypts. Crypts were isolated from small intestines of 3-month-old PolgD257A and wild type mice to assess their ability to grow in culture. When in culture, isolated crypts lose the transit amplifying cells, and form a ball of cells that consist of the stem cells and paneth cells. The paneth cells provide many of the growth factors required by the stem cells, allowing effective growth of the stem cell population *in vitro* (21). During the first four days in culture, both wild type and PolgD257A populations of cells appeared to multiple at a similar rate and maintained a similar size (Fig. 3.7A). However by 8 days, the wild type cryptoid cultures (Fig. 3.7B) began to multiple at a faster rate and became larger than the PolgD257A cryptoids (Fig. 3.7C). Fourteen days after plating, the size of the wild type cryptoids (Fig. 3.7D) significantly increased and began to show multiple buddings (formation of new stem cells formed by symmetric cell division), while budding of the PolgD257A cryptoids were rarely found (Fig. 3.7E). Twenty days after plating, the wild type cryptoids (Fig 3.7F) continued to increase in size and extent of budding while growth was arrested in the

PolgD257A cryptoids (Fig. 3.7G). After 20 days in culture, 7 of the 9 independent wild type crypts monitored continued to grow. In contrast, only 3 of the 13 independent PolgD257A crypts monitored continued to grow to limited degrees. Similar results were seen in crypts isolated from 7-month-old wild type and PolgD257A mice in culture (Data not shown). Thus, the *in vitro* culturing of intestinal crypts demonstrates that intestinal stem cells of the PolgD257A mice have a dramatic decrease in the ability to proliferate compared to those of wild type mice. I conclude that the PolgD257A mutation specific decrease in cell proliferation originates from the decreased growth potential of stem cells in the crypts.

ATP Content in Isolated Intestinal Epithelial Cells. Epithelial cells were isolated from 3-month-old PolgD257A and wild type mice. Sorting for CD44+, CD31- and CD45- yielded the stem and progenitor cells while sorting for CD44-, CD31- and CD45- yielded the terminally differentiated epithelial cells. In the stem and progenitor population of cells isolated from the crypt region, the content of ATP in PolgD257A (18.9 ± 0.3 fM ATP/cell) and wild type (19.5 ± 0.6 fM ATP/cell) cells were similar (Fig. 3.8). In the terminally differentiated epithelial cells isolated from the villus region, the content of ATP in PolgD257A (6.2 ± 0.2 fM ATP/cell) cells were increased compared to wild type (5.4 ± 0.1 fM ATP/cell) cells (Fig. 3.8). This data suggests that the PolgD257A mutation does not affect the content of ATP of the intestinal stem and progenitor epithelial cells, but production of ATP in terminally differentiated cells are higher in PolgD257A mice than in wild type mice.

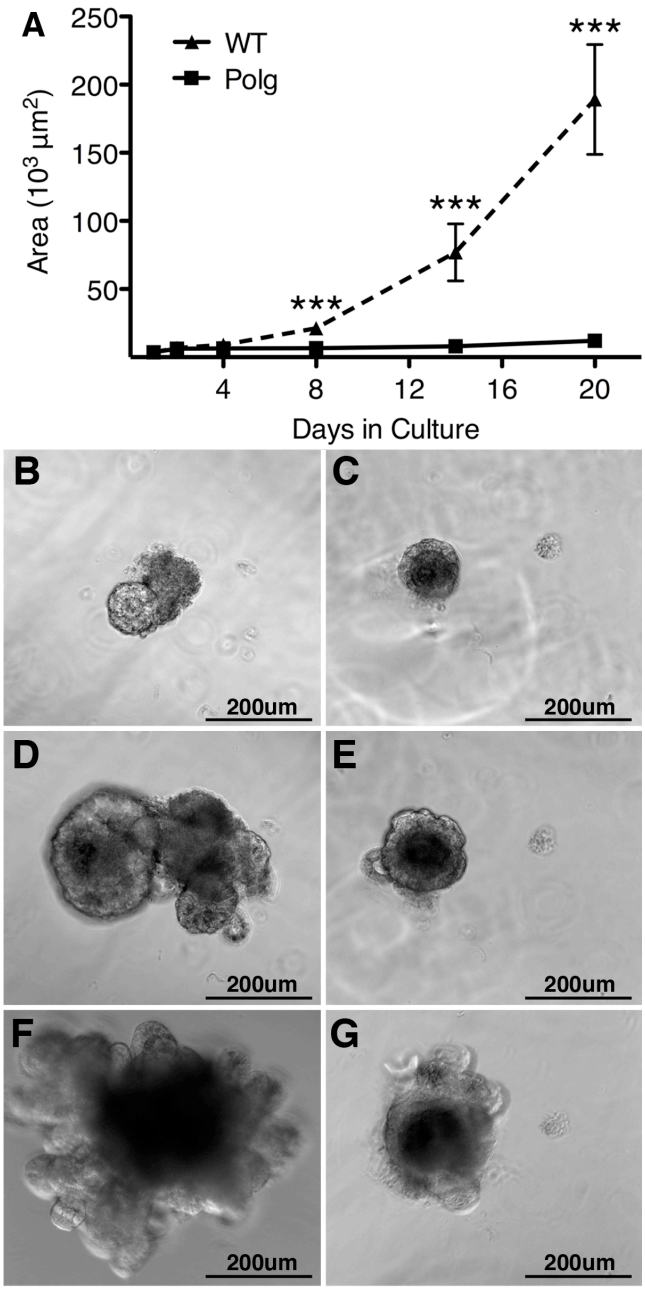

Figure 3.7: PolgD257A mutation impairs the culturing of isolated crypts. (A) Area of cell mass was determined on marked crypt cultures at days 1, 2, 4, 8, 14, and 20 after plating. Wild type cultures (▲) grew at an exponential rate starting at day 4 in culture while Polg cultures (■) only moderately increased in area through day 20. Wild type cultures at Days 8, 14, and 20 (B, D, F, respectively) have increased cellular mass with significant budding occurring at Days 14 and 20. Polg cultures at Days 8, 14, and 20 (C, E, G, respectively) have reduced cellular mass with very few buds developing. All data are represented as Mean ± SEM. *** $P < 0.001$ between WT (n =9) and Polg (n = 13) by Student's t-test.

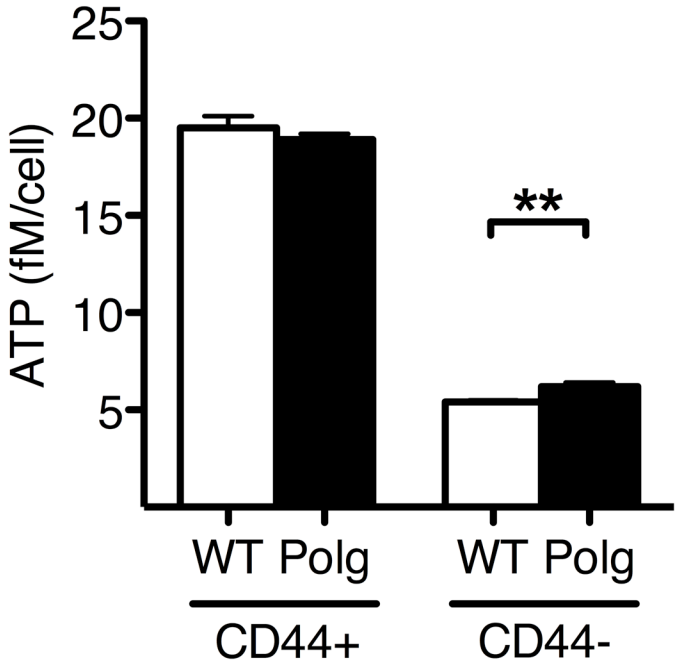

Figure 3.8: ATP content in isolated intestinal epithelial cells. Intestinal epithelial cells were isolated from wild type (n=2) and PolgD257A (n=2) mice. Single cell suspension was sorted for CD44. Positive CD44 cells contain stem and progenitor cells while negative CD44 cells contain terminally differentiated cells. All data are represented as Mean ± SEM. ** $P < 0.01$ between WT and Polg by Student's t-test.

3.5 Discussion

Mice homozygous for the PolgD257A mutation have been described as a model for premature aging with reduced lifespan and characteristics associated with human aging such as thinning of skin, graying and loss of hair, and kyphosis (17, 18). I characterized the small intestines of PolgD257A mice to determine if the intestines undergo a similar aging process as seen in humans. I confirmed that PolgD257A mice have increased apoptosis in the epithelial cells lining the villi and at the tip of the villi, but I find apoptosis was also significantly increased in the crypts. The increase in apoptotic cells in the crypt has not been described in humans, but may exist in the aging small intestine. In support of the increased apoptosis in the crypts, I find that the PolgD257A mutation causes a decrease in S-phase labeling in the transit amplifying cells and significantly reduced epithelial cell migration along the crypt-villus axis. I also find that the premature aging of the small intestine caused by the PolgD257A mutation are characterized by increased dimensions of both villi and crypt compartments. The number of proliferating cells in the small intestine of PolgD257A and wild type mice were similar. Despite these similarities, the number of cells in S-phase was significantly reduced and significantly more cells were in G1, M, or G2 phases of the cell cycle. Furthermore, isolated crypts *in vitro* revealed a proliferation defect that is linked to the stem cell population found in the crypts.

It has been well documented that human small intestine undergoes an increase in villi and crypt dimensions with age (3, 4). Previous studies in aged mice and rats have provided further confirmation that aging leads to increased dimensions of villi and crypts (5, 6). Our observations that the histological changes of the villi and crypts occurs in mice at 7 months of age supports the premature aging of the small intestine initiated by the PolgD257A mutation.

The PolgD257A mutation was also shown to dramatically alter the histology of the small intestine at 10 months of age, with significant fusion and branching of the villi (17). The exaggerated branching seen in old PolgD257A small intestine villi may be unique to this aging model, since it has not been described in aged humans or rodents. While the branching of the villi was not a prominent feature in our 7-month-old PolgD257A mice, the histological changes such as increased height and width of the villi and crypt compartments in the premature aging PolgD257A small intestine closely mimic the aging induced changes seen in the human small intestine.

Apoptosis is found at the tips of the villi in the small intestine, and is a normal event due to the high rate (3.3 days) of epithelial cell turnover (22, 23). The novel finding that PolgD257A mice have increased apoptosis in the crypt region suggests that these cells are undergoing a damage response induced by the increased mtDNA mutations produced by the PolgD257A mutation. The crypt region houses both stem and progenitor cells which are required to replenish epithelial cells lost during apoptosis. Under normal circumstances, there is a low level of spontaneous apoptosis in the crypt region that is thought to maintain the stem cell population by removing excess or damaged stem cells (24). Furthermore, damaging insults such as irradiation causes a significant increase in apoptosis particularly in the stem cell population in the crypt region (24). However, there are no reports of increased apoptosis in the transit amplifying cells (progenitors) of the crypt in aging humans and rodents. This suggests that stem and progenitor cells in the crypt are particularly susceptible to mitochondrial DNA damage triggered by the PolgD257A mutation, and prompt the need of further studies of apoptosis in the crypt in aging humans and rodents.

In conjunction with the increase in apoptosis, the PolgD257A small intestine was found to have a decreased number of S-phase cells. However, staining with KI67 (a marker of cell proliferation in all phases of the cell cycle) was similar in both PolgD257A and wild type mice. This observation indicates that the number of cells in a proliferating state was not affected by the PolgD257A mutation, yet the decrease S-phase labeling suggests that the PolgD257A mutation affects the cell cycle of these rapidly dividing transit-amplifying cells. Mitochondria have been shown to have an instrumental role in apoptosis (25-28), however the same can be said about cell division. Inhibition of mitochondrial protein synthesis leading to G1 arrest attenuates DNA replication (29, 30), whereas increasing mitochondrial DNA increases the transition from G1 to S and G2 to M thereby accelerating the progression through the cell cycle in yeast (31). Hence, mitochondria are critical to DNA replication. During Gap1 (G1) phase, all proteins required during DNA replication are synthesized. DNA synthesis occurs during the S-phase of the cell cycle and requires pools of ATP for incorporation into DNA and energy for the cellular processes of DNA replication. After the completion of S-phase, the cell enters Gap2 (G2) phase where ATP is synthesized for mitosis (32). Cells exit G2 and enter Mitosis (M) phase during which the physical separation of chromosomes occurs through ATP mediated movement of kinesin down the microtubule and cell division takes place (33). Hence, ATP produced by the mitochondria is an essential requirement to drive the cell cycle. Analysis of markers for cell cycle, MCM2 for G1, pH3 for M, and EdU for S confirmed a shift in the percentage of cells in each phase of the cell cycle in the PolgD257A mice. PolgD257A mice had significantly more cells in phases G1, M and other (possibly G2) compared to wild type mice. I examined whether cells contain ATP at a reduced rate in PolgD257A mutants. However, no significant difference in ATP levels were seen in the isolated intestinal stem and

progenitor cells of PolgD257A and wild type mice. It is possible that this pool of cells contains a majority of cells undergoing typical cell cycling and a smaller population cells undergoing atypical cell cycling, which could explain the similar ATP levels. Collectively, the data suggests the PolgD257A mutation is consistent with mitochondrial dysfunction in some of the progenitor cells likely causing a decrease in ATP levels in just this subset of cells. A depletion of ATP in a subset of the progenitor cells would explain the slower cell cycle in the PolgD257A mutants and possible stalling at multiple stages during the cell cycle. However, further investigation into the subset of poorly dividing cells is necessary to determine the extent of stalling in the PolgD257A mutants.

Two separate experiments showed that the migrations of epithelial cells from the crypt to the tip of the villi are severe in the mice with the PolgD257A mutation. The slower migration of PolgD257A epithelial cells is likely the result of two important contributions: (i) increased apoptosis in the crypts and (ii) the disruption of the cell cycle. The increase in apoptosis occurred mainly in the transit amplifying (TA) cells of the crypt. The sole function of TA cells are to increase the total number of cells for differentiation to enterocytes, goblet, enteroendocrine, and paneth cells, and to replenish lost or damaged epithelial cells. The actively dividing TA cells are essential in supporting cell migration by providing the push necessary to replenish the epithelial cells along the villi. The reduction in the actively dividing TA cells due to apoptosis contributes to a slower cell migration, reduced shedding of epithelial cells, and a prolonged presence of the epithelial cells in the villi. Prolonging the time the epithelial cells are in the villi may hamper epithelial cell function, yet this remains to be determined. Secondly, the observation that there are more cells in the stages other than S-phase of the cell cycle suggests that the cycling time of the cells in this region is longer than normal,

which contributes to the slower migration seen in the PolgD257A intestines compared to wild type intestines. Interestingly, these patterns were observed in PolgD257A mice at both 3 and 7 months of age, suggesting that the PolgD257A mutation itself have a large impact on the small intestine regardless of age.

In addition to TA cells, the crypt compartment contains intestinal stem cells, and I cannot eliminate the possibility that the PolgD257A mutation has a detrimental effect on the stem cell population. The isolation and culturing of crypts allows for the evaluation of the intestinal stem cell population *in vitro* since after plating the TA cells die and the only cells that remain are stem cells and paneth cells. *In vitro* the paneth cells provide the necessary factors required by the stem cells for maintenance and growth. In this *in vitro* system, the stem cells are capable of both symmetric and asymmetric division (20, 21, 34). Asymmetric division leads to progenitor cells while symmetric division leads to new stem cells that form a bud off the mass of growing cells. The observation of slower cell migration and increased apoptosis in the crypt region is supported by our results of a marked decrease in stem cell proliferation in PolgD257A mice compared to wild type mice. These results confirm that dysfunction at the stem cell level is a contributing factor involved in passing deleterious mutations on to progenitor cells leading to progenitor cell apoptosis and the decreased cell migration found in the PolgD257A small intestine.

In conclusion, the PolgD257A mutation causes changes in the morphology of the small intestine similar to the age-associated changes in small intestine morphology of aging humans and mice. The changes in morphology are the result of increased apoptosis and a slower cell cycle in the proliferating progenitor and stem cells located in the crypts of Lieberkuhn. Histologically, the premature aging in the small intestines of the PolgD257A mice closely

mimics aging of the small intestine in humans, rats, and mice. However, the PolgD257A mutation appears to cause significantly more damage in the stem and progenitor cells located in the crypts. Whether this increase in damage is associated with intestinal dysfunction or found in aging humans remains to be determined.

REFERENCES

1. Thomson AB (2009) Small intestinal disorders in the elderly. *Best Pract Res Clin Gastroenterol* 23(6):861-874.

2. Drozdowski L & Thomson AB (2006) Aging and the intestine. *World J Gastroenterol* 12(47):7578-7584.

3. Corazza GR*, et al.* (1998) Proliferating cell nuclear antigen expression is increased in small bowel epithelium in the elderly. *Mech Ageing Dev* 104(1):1-9.

4. Webster SG & Leeming JT (1975) The appearance of the small bowel mucosa in old age. *Age Ageing* 4(3):168-174.

5. Holt PR, Pascal RR, & Kotler DP (1984) Effect of aging upon small intestinal structure in the Fischer rat. *J Gerontol* 39(6):642-647.

6. Martin K, Kirkwood TB, & Potten CS (1998) Age changes in stem cells of murine small intestinal crypts. *Exp Cell Res* 241(2):316-323.

7. Ciccocioppo R*, et al.* (2002) Small bowel enterocyte apoptosis and proliferation are increased in the elderly. *Gerontology* 48(4):204-208.

8. Mandir N, FitzGerald AJ, & Goodlad RA (2005) Differences in the effects of age on intestinal proliferation, crypt fission and apoptosis on the small intestine and the colon of the rat. *Int J Exp Pathol* 86(2):125-130.

9. Xiao ZQ*, et al.* (2001) Aging is associated with increased proliferation and decreased apoptosis in the colonic mucosa. *Mech Ageing Dev* 122(15):1849-1864.

10. Lee HC & Wei YH (2000) Mitochondrial role in life and death of the cell. *J Biomed Sci* 7(1):2-15.

11. Simmons RA, Suponitsky-Kroyter I, & Selak MA (2005) Progressive accumulation of mitochondrial DNA mutations and decline in mitochondrial function lead to beta-cell failure. *J Biol Chem* 280(31):28785-28791.

12. Someya S, *et al.* (2008) The role of mtDNA mutations in the pathogenesis of age-related hearing loss in mice carrying a mutator DNA polymerase gamma. *Neurobiol Aging* 29(7):1080-1092.

13. Trifunovic A & Larsson NG (2008) Mitochondrial dysfunction as a cause of ageing. *J Intern Med* 263(2):167-178.

14. Wang J, Markesbery WR, & Lovell MA (2006) Increased oxidative damage in nuclear and mitochondrial DNA in mild cognitive impairment. *J Neurochem* 96(3):825-832.

15. Zhang D, *et al.* (2003) Mitochondrial DNA mutations activate the mitochondrial apoptotic pathway and cause dilated cardiomyopathy. *Cardiovasc Res* 57(1):147-157.

16. Nooteboom M, *et al.* (2010) Age-associated mitochondrial DNA mutations lead to small but significant changes in cell proliferation and apoptosis in human colonic crypts. *Aging Cell* 9(1):96-99.

17. Kujoth GC, *et al.* (2005) Mitochondrial DNA mutations, oxidative stress, and apoptosis in mammalian aging. *Science* 309(5733):481-484.

18. Trifunovic A, *et al.* (2004) Premature ageing in mice expressing defective mitochondrial DNA polymerase. *Nature* 429(6990):417-423.

19. Salic A & Mitchison TJ (2008) A chemical method for fast and sensitive detection of DNA synthesis in vivo. *Proceedings of the National Academy of Sciences of the United States of America* 105(7):2415-2420.

20. Gracz AD, Ramalingam S, & Magness ST (2010) Sox9 expression marks a subset of CD24-expressing small intestine epithelial stem cells that form organoids in vitro. *Am J Physiol Gastrointest Liver Physiol* 298(5):G590-600.

21. Sato T, *et al.* (2011) Paneth cells constitute the niche for Lgr5 stem cells in intestinal crypts. *Nature* 469(7330):415-418.

22. Shibahara T, *et al.* (1995) The fate of effete epithelial cells at the villus tips of the human small intestine. *Arch Histol Cytol* 58(2):205-219.

23. Cheng H & Leblond CP (1974) Origin, differentiation and renewal of the four main epithelial cell types in the mouse small intestine. I. Columnar cell. *Am J Anat* 141(4):461-479.

24. Potten CS (1992) The significance of spontaneous and induced apoptosis in the gastrointestinal tract of mice. *Cancer Metastasis Rev* 11(2):179-195.

25. Srinivasula SM*, et al.* (2001) A conserved XIAP-interaction motif in caspase-9 and Smac/DIABLO regulates caspase activity and apoptosis. *Nature* 410(6824):112-116.

26. Harris MH & Thompson CB (2000) The role of the Bcl-2 family in the regulation of outer mitochondrial membrane permeability. *Cell Death Differ* 7(12):1182-1191.

27. Joza N*, et al.* (2001) Essential role of the mitochondrial apoptosis-inducing factor in programmed cell death. *Nature* 410(6828):549-554.

28. Shi Y (2001) A structural view of mitochondria-mediated apoptosis. *Nat Struct Biol* 8(5):394-401.

29. Gattermann N*, et al.* (2004) Severe impairment of nucleotide synthesis through inhibition of mitochondrial respiration. *Nucleosides Nucleotides Nucleic Acids* 23(8-9):1275-1279.

30. van den Bogert C, van Kernebeek G, de Leij L, & Kroon AM (1986) Inhibition of mitochondrial protein synthesis leads to proliferation arrest in the G1-phase of the cell cycle. *Cancer Lett* 32(1):41-51.

31. Blank HM*, et al.* (2008) An increase in mitochondrial DNA promotes nuclear DNA replication in yeast. *PLoS Genet* 4(4):e1000047.

32. Chapman JD, Webb RG, & Borsa J (1971) ATP pool levels in synchronously growing Chinese hamster cells. *J Cell Biol* 49(1):229-233.

33. Rice S*, et al.* (1999) A structural change in the kinesin motor protein that drives motility. *Nature* 402(6763):778-784.

34. Barker N*, et al.* (2007) Identification of stem cells in small intestine and colon by marker gene Lgr5. *Nature* 449(7165):1003-1007.

Chapter 4

A MITOCHONDRIAL DNA POLYMERASE EDITING MUTATION PREVENTS DIET INDUCED OBESITY

4.1 Abstract

Nutrient mal-absorption by the small intestine is prevalent problem in the elderly. Aging is thought to be the main contributing factor leading to the apparent mal-absorption yet the exact mechanism behind the dysfunction of the small intestine is not known. With the objective to determine if premature aging due to increased mitochondrial DNA mutations cause a mal-absorption phenotype, I examined mice homozygous for the PolgD257A mutation, which causes increased mitochondrial DNA mutations, for evidence of mal-absorption. PolgD257A mutant and wild type mice were administered a normal rodent chow (NC) or a high fat-high carbohydrate western-type diet (HFW). The PolgD257A mice on NC were indistinguishable from wild type mice on NC with regards to body weight, plasma measurements, and Respiratory exchange ration (RER). However on HFW, RER was increased in wild type mice while PolgD257A mice showed a slight increase. These mice also show increased excretion of fat in the feces and reduced fat absorption compared to wild type HFW mice. Triglyceride absorption was reduced in HFW mice compared to NC mice in both genotypes but mutant HFW mice show significantly lower triglyceride absorption. In the villi and crypt compartments, apoptosis was increased and proliferation was decreased in PolgD257A mice compared to wild type mice regardless of the diet. The only mitochondrial defect seen was a decrease in State III (ADP stimulated) respiration in PolgD257A HFW mice compared to wild type HFW mice. PolgD257A mice on HFW did not gain weight compared to wild type mice on HFW. Insulin resistance was observed in wild type HFW mice, but not in PolgD257A HFW mice. Together, these results show, under conditions of high dietary lipid load, that a mutant Polg protein results in an impaired ability to absorb lipid that is likely triggered by the increase in apoptosis and decrease in proliferation seen in the small intestines.

4.2 Introduction

Intestinal dysfunction leading to mal absorption is common in the elderly (1, 2). The exact mechanism behind the dysfunction of the small intestine is not known, but aging is thought to be the main contributing factor leading to the apparent mal-absorption. In humans, a compensatory increase in cell proliferation in the small intestines has been observed in the aging population correlating with increased size of the small intestine villi and crypt compartments (3, 4). Furthermore, aging in humans causes increased proliferation and apoptosis in enterocytes (5). Similarily, in aging rodents, increases in length and width of villi and crypt dimensions have been reported (6, 7). Additionally, cell proliferation in the small intestines of rats increases with age (8, 9), and while apoptosis is high in young rats, it decreases to low levels with age (9). However, there have been no comprehensive studies demonstrating how these changes in morphology and proliferation affect function.

An instrumental role which mitochondrial DNA mutations play in the aging process is highlighted by the increase in the number of mutations found in aging individuals (10-14). Mitochondria are essential organelles responsible for generating energy in the form adenosine triphosphate (ATP) that is necessary for maintaining cellular function. Most efficient synthesis of ATP is the electron transport chain within the matrix of the mitochondria, coupled with oxidation of the reduced hydrogen carriers, $NADH+H^+$ and $FADH_2$, supplied by the tricarboxylic acid (TCA) cycle. During periods of high-energy demand, the number of mitochondria in the cell increases by fission in order to meet the energy demands (15, 16). Accumulations of mtDNA mutations and/or deletions, causes mitochondria dysfunction and leads to multiple disorders and that mainly affect metabolically active cell populations (17-23). Maintenance of the mitochondrial genome, both replication and repair, is carried out by the

nuclear gene, DNA polymerase gamma (*Polg*). *Polg* is essential for life as evidenced by the embryonic lethality of knock-out mice (24). D257A in exonuclease domain II disrupts the proofreading function of Polg, and causes an increase in mitochondrial DNA mutations. Mice homozygous for the PolgD257A mutation exhibit phenotypes consistent with premature aging (25, 26). Consequently, the PolgD257A mice provide a genetic means to study the effects of increased mitochondrial DNA mutations in the small intestine.

Previous studies have shown that the small intestine has increased mitochondrial DNA mutations leading to increased apoptosis (25, 26). However, it is not known whether increases in apoptosis will affect intestinal absorption. I have shown in Chapter 3 that the PolgD257A mutation alters the cell cycle of the progenitor (transit amplifying) cells located in the crypts of Lieberkühn. I observed a reduced migration of epithelial cells along the crypt-villus axis which suggests that the PolgD257A mutation causes a slower than normal cell cycling. I have also shown that the increased apoptosis is not confined to the columnar epithelial cells of the villus, but also occurs in the stem and progenitor cells found in the crypts. Whether alterations to cell cycle and apoptosis in $Polg^{D257A}$ mice affects absorption by the small intestine remains a mystery.

The goal of the experiments described in this chapter is to elucidate the effect of increasing mtDNA mutations in the small intestine on nutritional absorption, and on obesity and type 2 diabetes. I used the prematurely aging $Polg^{D257A}$ mice as a genetic tool to answer this question, and determine the role of mitochondrial DNA mutations in the functionality of the small intestine. I found that the $Polg^{D257A}$ mice on a normal rodent chow (NC) are not affected by the changes in cell cycle and apoptosis in the small intestine. However, $Polg^{D257A}$ mice on a high fat-high carbohydrate western-type diet (HFW) are protected against diet-

induced obesity and insulin resistance. I demonstrate that the changes in apoptosis and cell cycle in the small intestine of *Polg*^{D257A} mice impairs the ability to absorb dietary lipids preventing the accumulation of fat without disturbing nutritional balance.

4.3 Methods

Mice. The experimental animals were males homozygous for the *Polg*^{D257A} mutation (Polg) from crosses between heterozygotes that have been extensively backcrossed onto a C57BL/6 background. Controls were male littermates that are wild type at the *Polg* locus. Mice were fed *ad libitum* either NC [5.3% (w/w) fat and 0.019% (w/w) cholesterol, Prolab Isopro RMH 3000, ref 5P76; Agway Inc., Syracuse, NY] or HFW [21% (w/w) fat and 0.2% (w/w) cholesterol, TD88137; Teklad, Madison, WI] for 14 weeks. The diet was administered starting at 4 months of age and continued throughout the course of the experiment.

Plasma Analyses. Animals were fasted in the morning, 4 hrs prior to the collection of blood. Plasma glucose, 3-hydroxybutyrate (3-HB), and cholesterol were measured using colorimetric kits (#439-90901, #417-73501/601, and #439-17501, respectively, Wako Chemical Co., Richmond, VA). Plasma triglyceride was measured using a colorimetric kit (#2150, Stanbio Laboratory, Boerne, TX). Plasma insulin, leptin, and 25(OH)-Vitamin D were measured using ELISA kits (#90080 and #90030, Crystal Chem, Inc., Downers Grove, IL and #K2109, ALPCO Immunoassays, Salem, NH). Liver and plasma vitamin E were measured as previously described (27).

Glucose and Insulin Tolerance Tests. For oral glucose tolerance tests (GTT), male mice of each genotype were fasted for 4 hrs prior to oral gavage of glucose (2g/kg BW). Plasma was collected for glucose measurement 0, 15, 30, 60, or 120 minutes after gavage. For insulin tolerance tests (ITT), male mice of each genotype were fasted for 4 hrs prior to intraperitoneal injection of insulin (0.25U/kg BW). Plasma was collected for glucose measurement 0, 15, 30, 60, or 120 minutes after injection.

Measurement of Metabolic Parameters and Energy Expenditure. Mice were housed in metabolic cages for 48 hrs. Mice were allowed to acclimate to the new environment for 24 hrs before data and sample collection. Starting the second 24 hrs, body weight, food intake, water intake, and urine output was measured. Urine and feces samples were collected over 24 hrs. For energy expenditure, indirect calorimetry and physical activity were measured using the Labmaster system (TSE Systems GmbH, Bad Homburg, Germany) as previously described (28, 29). Briefly, 3-month-old and 7-month-old mice were individually housed in a laboratory animal monitoring system that allows the continuous measurement of these parameters. Mice were monitored for 96 hrs with the first 24 hrs discarded to allow for acclimation to the cages. During the first 48 hrs, animals were fed NC. After 48 hrs, the diet was switched to HFW and monitored was continued for an additional 48 hrs. The final 24 hrs on either NC or HFW were used for all comparisons.

Acid Steatocrit and Fecal Lipase. Acid steatocrit was measured as described previously (30) with minor modification. In short, 0.02 g of powdered specimen was mixed in 200 µl of 1 N perchloric acid. One drop of 0.5% Oil Red O was added and mixed. Specimens were placed in non-heparinized capillary tubes and spun. Steatocrit and daily fat absorption were calculated as previously described (31, 32). For lipase activity in the feces, 0.05 g of powdered specimen was mixed with 200 µL phosphate buffered saline (PBS). Specimens were centrifuged and supernatant was transferred to a clean tube. The supernatant was assayed for enzymes using an Automatic Chemical Analyzer (Johnson & Johnson's VT250).

Isolation of Small Intestines. Anesthetized animals were dissected and the small intestines exposed. The small intestine was removed from the stomach to the cecum of the large

intestine. Isolated intestines were placed in ice cold PBS, and subsequently flushed with 10mls of ice cold PBS. The intestines were split into two sections, duodenum to jejunum and jejunum to ileum. Each section was placed into 4% PFA at 4°C for at least 24 hrs. Intestines were then cut length wise and rolled for sectioning. Apoptosis was evaluated using a commercially available kit (ApopTag S7110; Chemicon Int.). Cells in S-Phase were determined as previously described (33) using a commercially available kit (Click-iT EdU C10084, Molecular Probes, Inc., Eugene, OR).

Immunostaining. Small intestine was resected, flushed of fecal contents with ice cold PBS, cut open along the longitudinal axis, and fixed in 4% PFA for 16 hrs at 4 °C. The sections remained hydrated for the remainder of the immunostaining procedure. Prior to immunostaining, the sections were blocked with 5% Normal Donkey Serum in PBS/0.1% TritonX (blocking buffer). The primary antibody was diluted in blocking buffer. For lymphatic staining, sections were stained with LYVE-1 (1:200; #70R-LR005, Fitzgerald), and incubated with tissue at 4°C for 16 hrs. The tissues were then washed three times with PBS for 5 minutes. Cy2 conjugated secondary antibodies (#715-225-150, Jackson Immunoresearch Laboratories) were diluted in blocking buffer at 1:200, and applied to tissue sections for 45 minutes at 21°C. The tissues were then washed three times with PBS for 3 minutes each. For nuclear staining, DAPI was added to Flouromount-G (#0100-01, SouthernBiotech) and mounted with a cover slip.

Histology. Tissues were fixed in 4% PFA. Paraffin sections of 5 μm were stained with Hematoxylin and Eosin, Periodic acid-Schiff, or Masson's Trichrome. For transmission electron microscopy (JOEL USA, Inc.), small tissue fragments were post-fixed in 2% osmium

tetroxide and one-micron thick sections were stained with uranyl acetate followed by lead citrate.

Gene Expression. Total RNA was purified from hypothalamus and pancreas using Trizol (#15596-026 Invitrogen, Carlsbad, CA) as previously described (34). Total RNA from other tissues was purified using an Automated Nucleic Acid Workstation ABI 6700. Real-time PCR was performed in an ABI PRISM 7700 Sequence Detector (Applied Biosystems, Foster City, CA). β-Actin mRNA was used for normalization.

Enterokinase. Enterokinase activity was determined as previously described (35). Briefly, isolated small intestine from duodenum was homogenized on ice for 2 minutes in extraction buffer: 20 mM Tris-HCl, 150 mM NaCl, 1% Triton X-100. 20 μL of homogenized tissue was added to 80 μL of reaction buffer: 125 nM trypsinogen, 0.07 M sodium succinate, and incubated 30 minutes at room temperature. The reaction was stopped with 2 μL 2 M HCl. The amount of trypsin generated from trypsinogen during the reaction is correlated to the amount of enterokinase present in the homogenized tissue. The amount of trypsin was determined by addition of 100 μL of detection buffer: 40 mM Tris-HCl (pH-8.0), 300 mM NaCl, 10 mM $CaCl_2$, 200 μM chromogenic substrate S-2765 (Chromogenix). An increase in absorbance at 405 nm was monitored immediately following the addition of the detection buffer.

TG secretion, TG absorption, and Vitamin E absorption. The rate of triglyceride secretion from the liver was determined as previously described by Johnson et al (36). At 7 months of age, male mice of each genotype fed either NC or HFW were fasted for 4 hrs prior to injection of Tyloxapol (Triton WR-1339; Sigma Chemical Co., St. Louis, Missouri, USA) via retro-orbital injection at a dose of 0.7 mg/g body weight. Plasma was collected for triglyceride

measurement at time points of 0, 15, and 30 minutes after injection. Immediately following the 30 minutes plasma collection, the animals were challenged with 250 μL/30 g body weight of Olive oil with (1 mg/kg) deutrated vitamin E. Plasma was collected for triglyceride measurement at 60, 120, and 180 minutes after oral gavage. Pooled plasma samples were measured for Vitamin E as previously described (37).

Oxygen Consumption in Small Intestine Homogenates. Briefly, small intestines were removed and flushed with ice cold PBS. A ~200 mg section of intestine was gently homogenized in SET buffer (250 mM Sucrose, 1 mM EDTA, 10 mM Tris-HCl, 2 mM ATP pH 7.4). Total protein was measured using a BCA protein assay kit (cat. 23227, Thermo Fisher Scientific, Inc), and samples were normalized to total protein. Intestinal homogenate was placed into a BD Oxygen Biosensor System and O_2 was measured. A 2X Reaction buffer, containing 125 mM Sucrose, 25 mM K_2HPO_4, 200 mM KCl, 2.5 mM MgCl2, 2.5 mM L-Carnitine, 0.25 mM Malic Acid, 20 mM Tris-HCl, 2.5 mM DTT, 0.25 mM NAD^+, 4.0 mM ATP, and 0.125 mM CoA, was prepared and added to the plates with homogenates. Fluorescence was measured using a FLUOstar microplate fluorometer (BMG LabTech) with excitation at 485 nm and emission at 612 nm every 3 minutes over a period of 120 minutes.

Isolation and Assessment of Mitochondria. Mitochondria were isolated from livers as previously described (38). Isolated liver mitochondria (5 μg protein) in buffer (70 mM sucrose, 220 mM mannitol, 10 mM KH_2PO_4, 2 mM $MgCl_2$, 2 mM HEPES, 1 mM EDTA, 0.1% BSA, 5 mM succinate, and 2 μM rotenone) were loaded onto XF24 plates. The rate of O_2 consumption was measured according to the manufacturer's instructions with a Seahorse XF24 Analyzer (Seahorse Bioscience; North Billerica, MA) during the consecutive addition at 6 minute

intervals of 0.5 mM ADP, 2 μM oligomycin, 4 μM FCCP, and 2 μM antimycin A. For each experiment, mitochondria from one mouse was isolated, and assayed in triplicate. The experiment was repeated with another mouse and produced essentially the same results.

Analysis of Mitochondrial DNA Copy Number and D17 Deletions. DNA was isolated from tissues and Real-time PCR amplification for the Cytochrome b gene was performed to assay mitochondrial DNA content using amplification of the Na-K-Cl cotransporter 2 gene (*NKCC2)* as an indicator of the content of nuclear DNA. A deletion of ~3.8 kb in relation to the D-loop of mtDNA was assayed using a primer probe set that recognizes the loss of the D-17 region in the mtDNA genome. The extent of D-17 deletions was expressed relative to the mtDNA gene coding for Cytochrome b in each animal.

Data Analysis. Values are reported as mean ± SEM. Statistical analyses were conducted with JMP 6.0.2 software (SAS Institute, Cary, NC). P values less than 0.05 were considered significant.

4.4 Results

PolgD257A mutation protects against obesity. Wild type and PolgD257A mice were followed monthly starting at one month of age. At four months of age, wild type and PolgD257A mice were either continued on NC or switched to HFW and followed for three additional months. While on NC, both wild type and PolgD257A mice gained equal body weight throughout the study. Wild type mice fed a HFW diet gained significantly more body weight compared to wild type mice fed a NC. Strikingly, PolgD257A mice fed a HFW diet did not gain additional body weight compared to wild type and PolgD257A mice fed a NC diet (Fig. 4.1A). Accumulation of fat in both inguinal and gondal fat pads contributed to the weight gain of wild type mice fed HFW diet. While on NC, Wild type and PolgD257A mice have similar gross inguinal and gonadal fat weight. Conversely, PolgD257A mice fed a HFW diet had similar inguinal and gonadal fat pads as wild type and PolgD257A mice fed a NC diet (Fig. 4.1B, C). This data shows that PolgD257A mutant mice are refractory to weight gain on a HFW diet.

Insulin resistance in PolgD257A mice. At 3 and 7 months of age, both WT and Polg mice were challenged with an oral gavage of glucose, and monitored for clearance of glucose. At 3 months of age, WT and Polg mice on a NC diet respond similarly to a glucose challenge (Fig. 4.2A). In addition, plasma insulin, in response to the increase in glucose, is stimulated to the same degree in both WT and Polg mice (Fig. 4.2B). At 7 months of age, WT and Polg mice on a NC diet also respond similarly to a glucose challenge (Fig. 4.2C), and plasma insulin is also stimulated to the same degree in both WT and Polg mice (Fig. 4.2D). WT mice on HFW diet for 3 months had a poor response to the glucose challenge, developed mild insulin resistance,

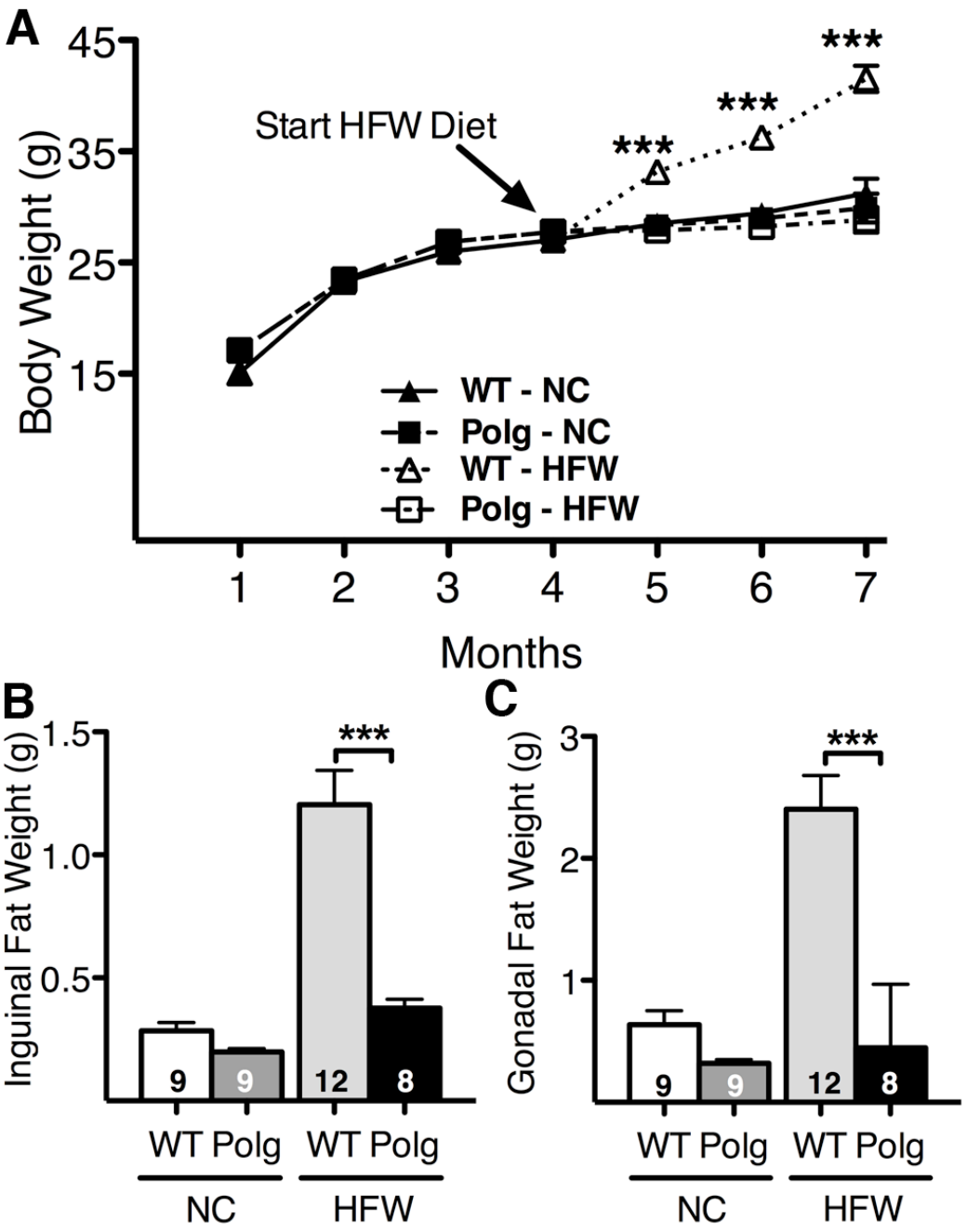

Figure 4.1: PolgD257A mice are protected from diet induced obesity. (A) Body weight prior to and after administering high fat diet. Gross weight of (B) inguinal and (C) gondal fat pads in WT and Polg mice administered either a normal or western diet. All data are represented as Mean ± SEM. *** $P < 0.001$ between WT NC (n = 9), Polg NC (n = 9), WT HFW (n = 12), and Polg HFW (n = 8) by Tukey-Kramer HSD.

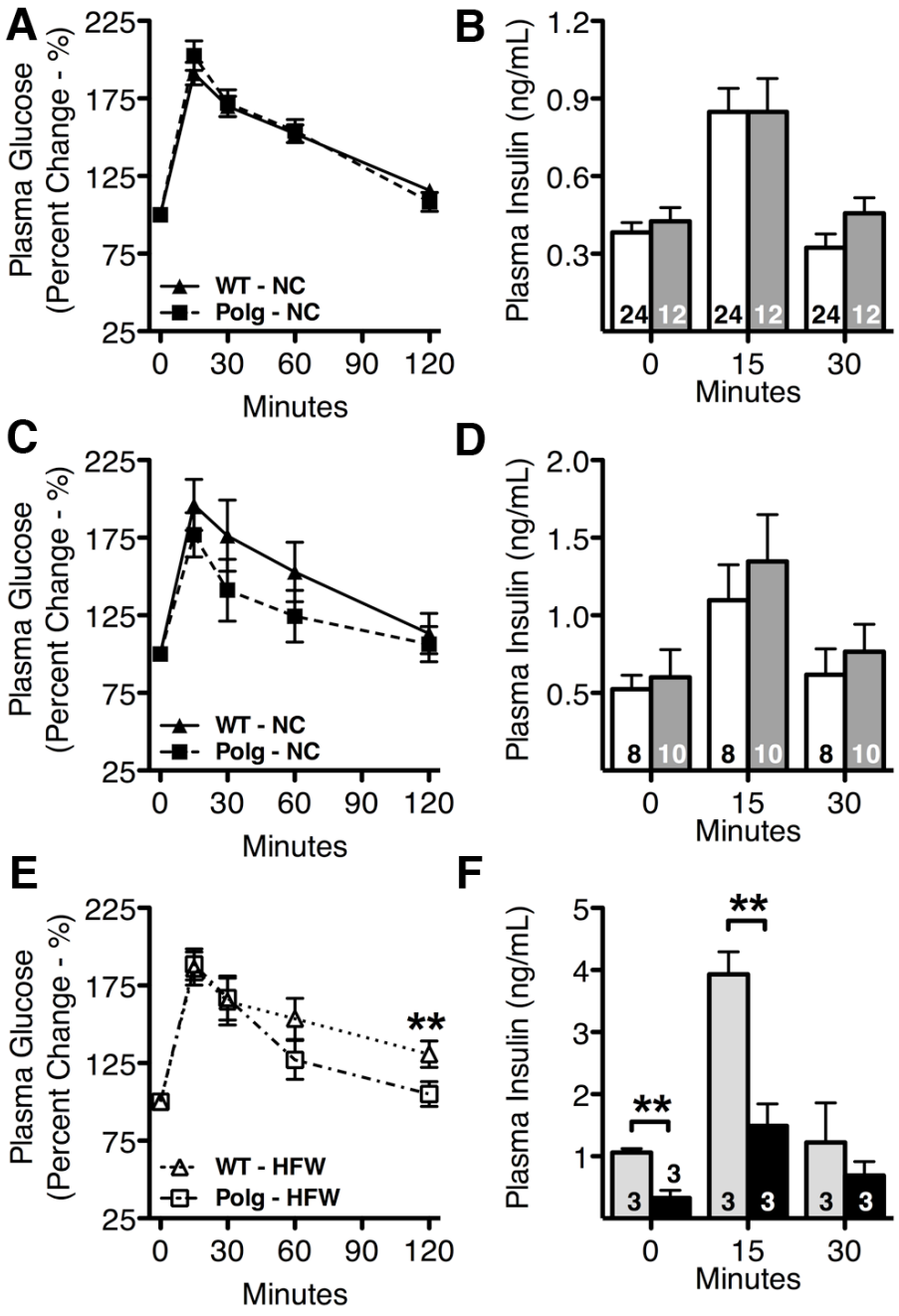

Figure 4.2: Oral glucose tolerance test. (A) Percent change of plasma glucose in 3-month-old following an OGTT in WT NC (n = 24) compared to Polg NC (n = 12) (B) Plasma insulin levels prior to (0 min) and after (15 and 30 min) glucose challenge in 3-month-old WT NC compared to Polg NC. (C) Percent change of plasma glucose in 7-month-old following an OGTT in WT NC (n = 8) compared to Polg NC (n = 10) (D) Plasma insulin levels prior to (0 min) and after (15 and 30 min) glucose challenge in 7-month-old WT NC compared to Polg NC. (E) Percent change of plasma glucose in 7-month-old following an OGTT in WT HFW (n = 7) compared to Polg HFW (n = 8) (D) Plasma insulin levels prior to (0 min) and after (15 and 30 min) glucose challenge in 7-month-old WT HFW (n = 3) compared to Polg HFW (n = 3). All data are represented as Mean ± SEM. ** $P < 0.01$ by Student's t-test.

and elevated plasma insulin levels (Fig. 4.2E, F). However after 3 months of HFW diet, Polg animals did not show a poor response to glucose challenge; rather, they responded similar to WT and Polg mice on NC diet, and did not develop insulin resistance (Fig. 4.2E, F). These results demonstrate that PolgD257A mice on HFW do not develop insulin resistance or glucose intolerance.

Plasma measurements. Metabolic parameters were measured in wild type and Polg mutant mice prior to and after administering a HFW diet. A summary of all metabolic parameters measured throughout the course of this study is shown in Table 4.1. In 3 month old Polg and wild type mice, plasma glucose, plasma cholesterol, and plasma insulin remained the same. At 3 months, Polg mice have lower plasma triglycerides, water consumption, and food consumption compared to wild type mice. By 7 months of age, Polg and WT mice fed a NC diet had similar plasma levels of cholesterol, glucose, insulin, leptin, 3-hydroxybutyrate, and triglycerides. Food consumption, water consumption, Vitamin D, and Vitamin E were the same in 7-month-old WT and Polg mice regardless of the diet. Plasma levels of 3-hydroxybutyrate, triglycerides, Vitamin D, and Vitamin E were similar in HFW diet fed WT and Polg mice. However, plasma leptin, insulin, and glucose were increased in WT HFW diet mice compared to Polg HFW diet mice. A dietary effect, HFW > NC, was observed by two-way ANOVA in plasma cholesterol ($P < 0.001$), plasma insulin ($P < 0.001$), plasma leptin ($P < 0.001$), plasma vitamin E ($P < 0.05$), food consumption ($P < 0.01$), and water consumption ($P < 0.01$). A genotype effect, WT > Polg, was observed by two-way ANOVA in plasma glucose ($P < 0.01$), plasma insulin ($P < 0.001$), plasma leptin ($P < 0.001$), and plasma 3- hydoxybutyrate ($P < 0.05$). A diet- genotype interaction was observed in WT HFW diet mice by two-way ANOVA

Table 4.1: Summary of metabolic data from dietary experiment

	3-Month-Old Normal Chow		7-Month-Old				Two-Way ANOVA (7-Month-Old)		
			Normal Chow		Western Diet				
	WT (n=22)	Polg (n=25)	WT (n=10)	Polg (n=10)	WT (n=12)	Polg (n=12)	Diet	Genotype	Interaction
Plasma Cholesterol (mg/dL)	94 ± 4	106 ± 9	88 ± 6	89 ± 5	185 ± 17[A]	151 ± 10[A]	<0.001	NS	NS
Plasma Glucose (mg/dL)	177 ± 7	184 ± 8	167 ± 12	151 ± 8	197 ± 12[B]	144 ± 5	NS	0.001	NS
Plasma Insulin (ng/mL)	0.4 ± 0.03	0.4 ± 0.1	0.5 ± 0.1	0.5 ± 0.1	1.6 ± 0.3[C]	0.3 ± 0.1	<0.001	<0.001	<0.001
Plasma Leptin (ng/mL)	0.6 ± 0.3	0.2 ± 0.1	3.5 ± 1.0	0.6 ± 0.1	12.1 ± 1.9[C]	1.2 ± 0.2	<0.001	<0.001	<0.01
Plasma 3-hydroxybutyrate (µmol/L)	255 ± 7	267 ± 9	161 ± 22	218 ± 17	202 ± 14	228 ± 17	NS	<0.05	NS
Plasma Triglycerides (mg/dL)	70 ± 8	54 ± 5[D]	45 ± 7	45 ± 8	42 ± 5	31 ± 4	NS	NS	NS
Plasma Vitamin D (nmol/L)	-	-	11 ± 3	18 ± 3	19 ± 3	13 ± 3	NS	NS	NS
Plasma Vitamin E (uM)	-	-	1.6 ± 0.6	2.6 ± 0.6	6.2 ± 2.3	5.9 ± 1.5	<0.05	NS	NS
Food Consumption (g/Day)	4.6 ± 0.3	3.8 ± 0.3[D]	4.1 ± 0.3	4.1 ± 0.2	3.3 ± 0.3	3.7 ± 0.1	<0.01	NS	NS
Water Consumption (mL/Day)	4.4 ± 0.3	3.6 ± 0.3[D]	4.2 ± 0.3	3.4 ± 0.3	3.1 ± 0.4	2.7 ± 0.2[E]	<0.01	NS	NS

Data are given as mean±SEM. All statistics performed using Tukey-Kramer HSD unless otherwise noted.

[A] $P < 0.05$ 7 month Normal chow vs. Western diet

[B] $P < 0.001$ vs. 7 month Normal and Western Polg

[C] $P < 0.001$ vs.all groups

[D] $P < 0.05$ vs 3 month WT by Student t test

[E] $P < 0.05$ vs. 7 month Normal WT

in plasma insulin ($P < 0.001$) and plasma leptin ($P < 0.01$). Together these data show that WT mice administered HFW diet develop many of the metabolic changes seen in obesity such as plasma increases in insulin and leptin yet the PolgD257A mice given HFW diet do not respond in the same way and remain similar to NC administered mice.

Increased daily fecal fat excretion. At 7 months of age, after receiving either NC or HFW diets, feces were collected from WT and Polg mice over a period of 24 hrs. Each sample was analyzed for fat content in feces by acid steatocrit and fecal lipase levels were measured. Daily fat excretion and percentage of fat absorbed were calculated based on food consumption, acid steatocrit, and total feces weight. No significant differences in these parameters were observed between WT and Polg mice fed NC. Acid steatocrit was significantly higher in animals fed the HFW diet compared to animals consuming a NC diet (Diet effect, $P < 0.001$ by ANOVA). Acid steatocrit was significantly higher in Polg mice compared to WT mice (Genotype effect, $P < 0.01$ by ANOVA). A significant diet and genotype interaction ($P < 0.02$) reflects significantly higher acid steatocrit in Polg than in WT after HFW diet for 3 months (Fig. 4.3A). Similarly, the feces collected from HFW diet Polg mice contained elevated active lipase levels compared to HFW diet WT mice (Fig. 4.3B, $P < 0.02$ for a genotype effect and $P < 0.04$ for a diet-genotype interaction). Since dry weights of feces produced by mice administered HFW diet for 3 months were less than those produced by NC fed mice, daily fecal fat excretion of the WT mice fed HFW did not differ from those of the mice fed NC, suggesting that they are absorbing on average four times more fat. In contrast, daily fat excretion was significantly increased in HFW fed Polg mice (Fig. 4.3C). Daily fat absorption is significantly reduced in Polg HFW diet mice than in WT HFW diet mice (Fig. 4.3D, no effects or interactions by

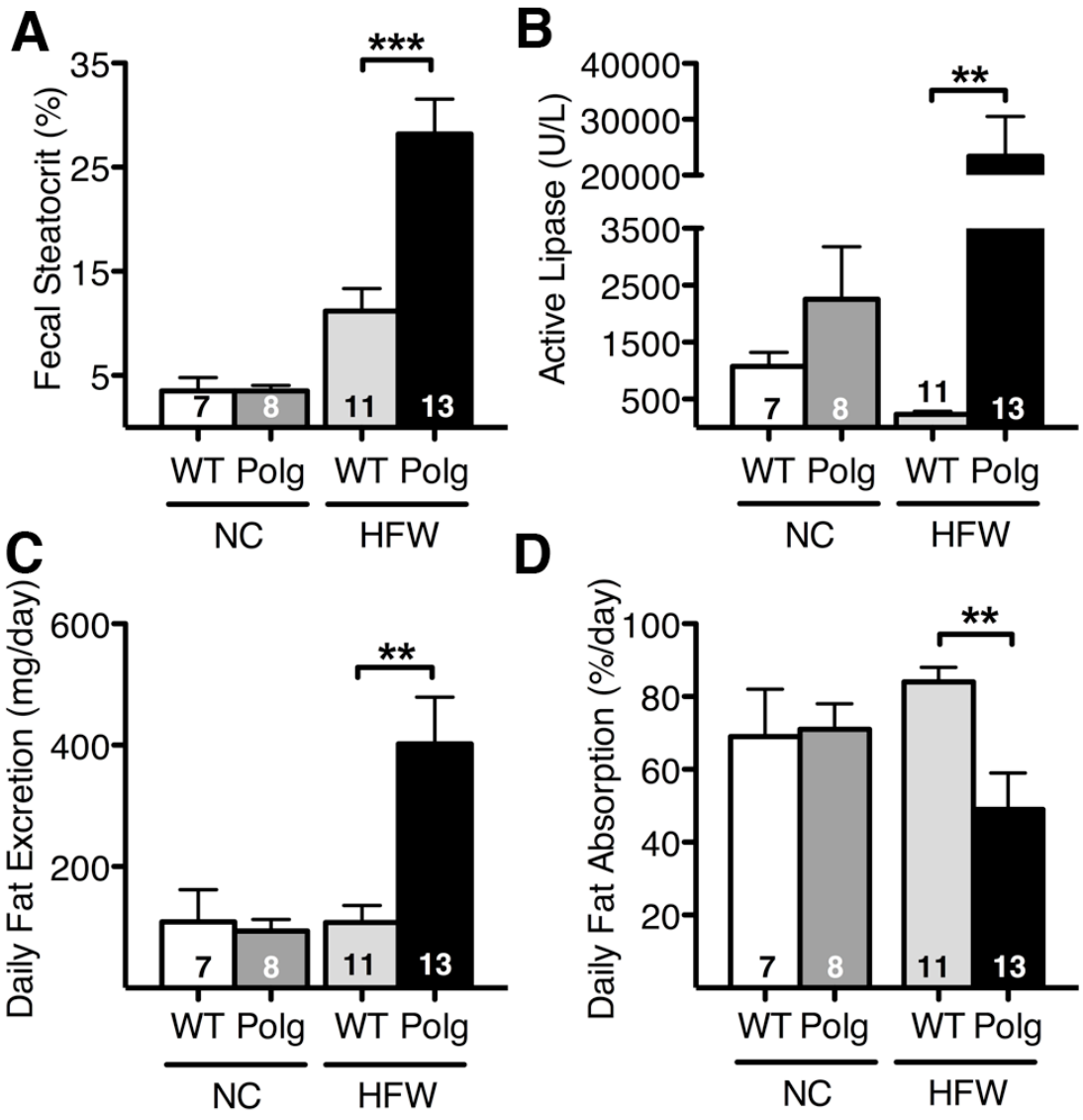

Figure 4.3: Fecal steatocrit in PolgD257A mice. (A) Fecal steatocrit, (B) Fecal lipase, (C) Daily fat excretion, and (D) Daily fat absorption in 7-month-old WT NC (n = 7), Polg NC (n = 8), WT HFW (n = 11), and Polg HFW (n = 13). All data are represented as Mean ± SEM. *** $P < 0.001$, ** $P < 0.01$, and * $P < 0.05$ by Tukey-Kramer HSD.

ANOVA), although these mice still absorbed about 2.7 times more fat per day compared to NC fed mice. These data show that, under conditions of excessive dietary lipids, the PolgD257A mutation contributes to increased excretion and reduced absorption of lipid. Furthermore, the elevated lipase levels suggest that the components required for lipid absorption are available for processing dietary fat.

PolgD257A mice on HFW diet have a reduced lipid absorption rate. Liver secretion of triglycerides was determined by injection of tyloxapol into both WT and Polg mice given either a NC or HFW diet. At 7 months of age, liver secretion was similar in Polg and WT on both diets (Fig. 4.4A). In NC mice, TG secretion from WT livers (5.5 ± 0.2 mg/dL/min) was slightly higher than TG secretion from the Polg livers (4.1 ± 0.5 mg/dL/min), diet significantly reduced TG secretion from the liver ($P < 0.001$), but TG secretion was similar in livers from WT (4.2 ± 0.2 mg/dL/min) and Polg (3.9 ± 0.7 mg/dL/min) (Fig. 4.4B). Analyzing together by ANOVA, Polg mice secrete less TG than WT mice (genotype effect, $P < 0.001$).

To determine the acute absorption capacity of the small intestine, WT and Polg mice were administered an oral gavage of olive oil to represent a bolus of dietary triglycerides. In mice fed NC for 3 months, both Polg and WT mice absorbed exogenously administered triglycerides at a similar rate (Fig. 4.4C). TG absorption by the small intestine of WT (24.4 ± 1.6 mg/dL/min) mice was slightly higher than Polg (21.8 ± 1.6 mg/dL/min) TG absorption by the small intestines, but the difference was not significant. In contrast, TG absorption was reduced in both WT and Polg mice conditioned on HFW for 3 months (diet effect, $P < 0.001$ by ANOVA). WT HFW mice experience a 51.2% reduction in the amount of triglycerides absorbed compared to WT NC mice whereas Polg HFW mice experience a 70.8% reduction in

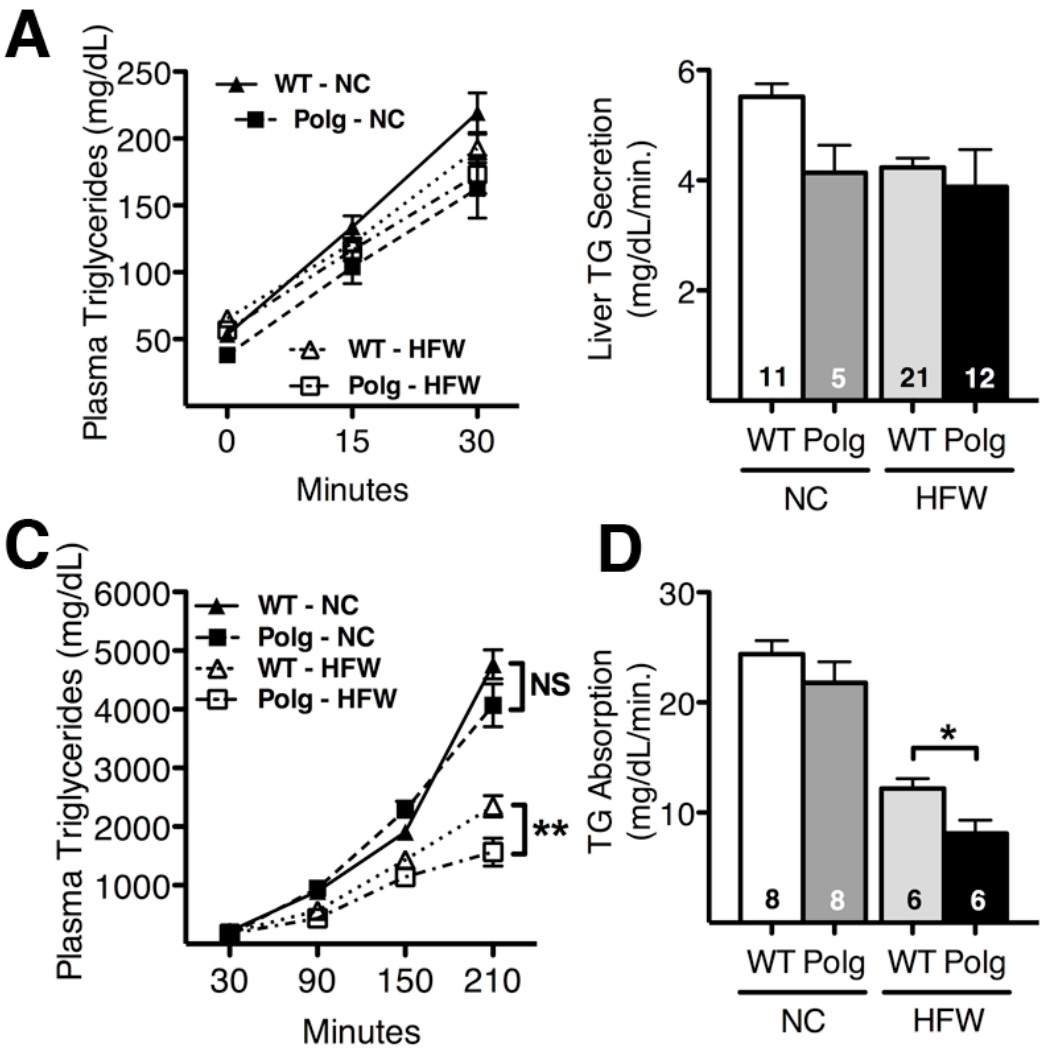

Figure 4.4: Triglyceride secretion and absorption. Animals were injected with tyloxapol and triglyceride secretion form the liver determined by plasma collections at 0, 15, and 30 minutes post tyloxapol injection. Plasma TG (A) and TG secretion (B) was the same in WT NC, Polg NC, WT HFW, and Polg HFW. At 30 minutes post tyloxapol, animals were administered a bolus of olive oil and plasma collected at 60, 120, and 180 minutes post olive oil gavage. Plasma TG (C) and TG absorption (D) were similar in normal diet fed mice. High fat diet decreased TG absorption in both mice with Polg HFW being significantly lower than WT HFW. All data are represented as Mean ± SEM. * $P < 0.05$ by Tukey-Kramer HSD.

the amount of triglycerides absorbed by the small intestine compared to Polg NC mice. A comparison of animals in the HFW group shows that the Polg mice have a reduced triglyceride absorption (8.1 ± 0.7 mg/dL/min) that is 40.3% lower than the WT mice (12.2 ± 0.9 mg/dL/min, $P < 0.05$). This data confirms that Polg mice have an impaired ability to absorb dietary lipids through the small intestine.

Pancreatic gene expression of digestive enzymes. Gene expression in the pancreas was determined to test whether the Polg mice have impaired production of the essential enzymes required during digestion. In mice given HFW for 3 months, gene expression of insulin is dramatically increased only in WT mice confirming an increase in insulin production seen in these mice (Table 4.2). Expression of genes related to digestion of fat and proteins, *Pnlip*, *Clps*, *Prss1*, and *Ctrb1*, in the pancreas was not affected by genotype and diet (Table 4.2). Pancreatic gene expression of *Amy2* was higher in WT mice than in Polg mice (genotype effect, $P < 0.05$ by ANOVA). These results confirm the pancreas is producing normal levels of the digestion enzymes: lipase, co-lipase, trypsinogen, and chymotrypsinogen. However, the PolgD257A mutation has a negative effect on the production of Amylase, for carbohydrate digestion.

Enterokinase activity. Enterokinase, also known as enteropeptidase, is responsible for the cleavage and activation of trypsinogen to trypsin, and this activation step occurs in the duodenum in the small intestine (39). Relative enterokinase activity as determined by the conversion of trypsinogen to trypsin was the same in both Polg and WT mice given HFW diet for 3 months (Fig. 4.5). This result shows that the PolgD257A mutation does not disrupt the activity of enterokinase.

Table 4.2: Summary of pancreatic gene expression

Gene	Normal Chow (NC)		High Fat Western (HFW)		Two-Way ANOVA			Function
	WT (n=11)	Polg (n=11)	WT (n=8)	Polg (n=8)	Diet	Genotype	Interaction	
Ins2	1.00 ± 0.20	1.04 ± 0.26	2.26 ± 0.63	0.71 ± 0.29[A]	NS	<0.05	<0.05	Production of Insulin
Amy2	1.00 ± 0.23	0.46 ± 0.13	0.86 ± 0.32	0.40 ± 0.19	NS	<0.05	NS	Breaks down starch to sugar (Amylase)
Prss1	1.00 ± 0.20	0.71 ± 0.13	0.86 ± 0.23	1.31 ± 0.32	NS	NS	NS	Activates digestive enzymes (Trypsinogen)
Ctrb1	1.00 ± 0.29	0.55 ± 0.14	0.68 ± 0.29	1.81 ± 0.57[B]	NS	NS	NS	Proteins to amino acids (Chymotrypsinogen)
Pnlip	1.00 ± 0.29	0.59 ± 0.13	0.65 ± 0.24	1.33 ± 0.45	NS	NS	NS	Breaks down dietary fat (Pancreatic lipase)
Clps	1.00 ± 0.19	0.82 ± 0.28	1.03 ± 0.34	1.55 ± 0.49	NS	NS	NS	Required by *Pnlip* (Pancreatic co-lipase)

Data are given as mean±SEM. All statistics performed using Tukey-Kramer HSD.

[A] $P < 0.05$ vs. WT HFW

[B] $P < 0.05$ vs. Polg NC

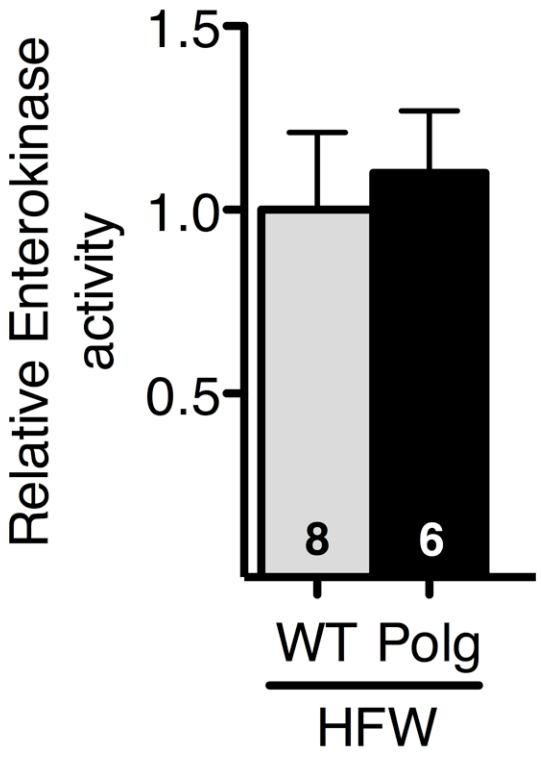

Figure 4.5: Enterokinase. Relative activity of enterokinase in small intestine isolated from 7-month-old wild type and Polg mice administered high fat diet. All data are represented as Mean ± SEM. WT (n = 8) and Polg (n = 6)

Small intestine morphology. As described in Chapter 3, villi length is similar in WT (372 ± 10 μm) and Polg (382 ± 11 μm) mice fed NC diet for 3 months. However, villi width increased in Polg NC diet (65 ± 1 μm) compared to WT NC diet (57 ± 1 μm, $P < 0.001$). In NC diet, Polg crypt length (97 ± 3 μm) and width (52 ± 1 μm) are markedly larger ($P < 0.001$) compared to WT crypt length (71 ± 1 μm) and width (41 ± 1 μm). In NC diet, smooth muscle thickness decreases in Polg mice (39 ± 2 μm) compared to WT mice (47 ± 2 μm, $P < 0.01$). HFW diet increases villi length ($P < 0.001$ by ANOVA) in both WT (434 ± 14 μm) and Polg (532 ± 12 μm) while Polg HFW diet mice have longer villi compared to WT HFW diet mice ($P < 0.001$). HFW diet increases villi width ($P < 0.001$ by ANOVA) in WT (62 ± 1 μm) and Polg (65 ± 2 μm) mice. HFW diet decreases crypt length ($P < 0.001$ by ANOVA) and width ($P < 0.001$ by ANOVA) in both WT and Polg mice. In Polg HFW diet mice, crypt length (76 ± 2 μm) and width (42 ± 1 μm) are markedly larger than WT HFW diet crypt length (59 ± 1 μm, $P < 0.001$) and width (34 ± 1 μm, $P < 0.001$). HFW diet increases smooth muscle thickness ($P < 0.001$ by ANOVA) in WT (50 ± 1 μm) and Polg (43 ± 2 μm) mice. The thickness of the smooth muscle is markedly reduced in Polg HFW mice compared to WT HFW mice ($P < 0.01$). Table 4.3 summarizes the differences found in intestinal morphology measurements. Overall, the Polg mutation contributes to morphology changes in the small intestine, but the changes are not exacerbated by the administration of HFW diet.

The small intestine lacteals are important for delivering fat into the blood (40). Morphological changes such as dilation due to lacteal obstruction in the small intestine can impact the transport of fats into the body (41, 42). Intestinal lacteals, as assessed by Lyve-1 staining, were not different in WT (Fig. 4.6A) and Polg (Fig. 4.6B) mice. Furthermore when mice were fed a HFW diet, intestinal lacteals did not change in size nor shape in WT (Fig.

Table 4.3: Intestinal morphology measurements

	Normal Chow		Western Diet		Two-Way ANOVA		
	WT (n=100)	Polg (n=100)	WT (n=100)	Polg (n=100)	Diet	Genotype	Interaction
Villi Length (μm)	372 ± 10	382 ± 11	434 ± 14[E,F]	532 ± 12[A,B,C]	<0.001	<0.001	<0.001
Villi Width (μm)	57 ± 1	65 ± 1[A]	62 ± 1	65 ± 2[A]	<0.001	NS	NS
Crypt Length (μm)	71 ± 1	97 ± 3[A,C,D]	59 ± 1[A]	76 ± 2[C]	<0.001	<0.001	0.02
Crypt Width (μm)	41 ± 1	52 ± 1[A,C,D]	34 ± 1[A]	42 ± 1[C]	<0.001	<0.001	NS
Smooth Muscle Width (μm)	47 ± 2	39 ± 2[E]	50 ± 1[B]	43 ± 2[G]	<0.001	0.02	NS

Data are given as mean±SEM. All statistics performed using Tukey-Kramer HSD.

[A] $P < 0.001$ vs. WT NC

[B] $P < 0.001$ vs. Polg NC

[C] $P < 0.001$ vs. WT WD

[D] $P < 0.001$ vs. Polg WD

[E] $P < 0.01$ vs. WT NC

[F] $P < 0.01$ vs. Polg NC

[G] $P < 0.01$ vs. WT WD

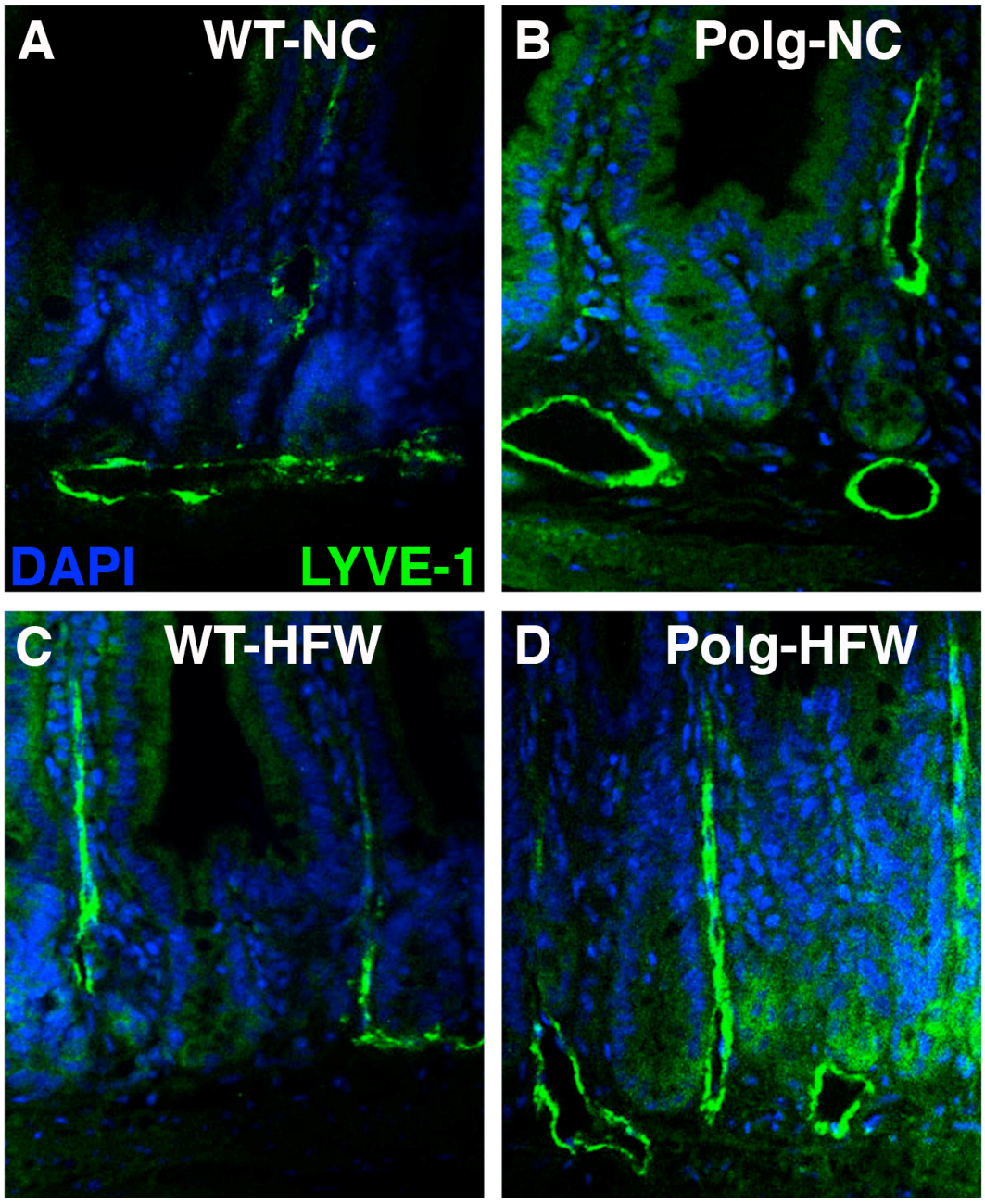

Figure 4.6: Small intestine lacteals. Immunostaining of small intestines with Lyve-1 in (A) WT NC, (B) Polg NC, (C) WT HFW, and (D) Polg HFW shows no discernible differences in lymphatic structure regardless of diet and genotype.

4.6C) and Polg (Fig. 4.6D) mice. When combined, these data suggest that the small intestine undergoes age related changes in morphology caused by the PolgD257A mutation; however the morphology of the intestinal lacteals is not disturbed.

Small intestine apoptosis and S-phase proliferation. As described in Chapter 3, WT mice have apoptosis that is confined to the tips of the villi (Fig. 4.7A, yellow arrows). The PolgD257A mutation increases apoptosis in the villi of the small intestines (Fig. 4.7B, small yellow arrows). HFW diet increases apoptosis (diet effect $P < 0.001$ by ANOVA) mainly at the tips of the villi in both WT (Fig. 4.7C) and Polg mice (Fig. 4.7D). In both diets, the PolgD257A mutation increases apoptosis in the villi as compared to WT mice (Fig. 4.7E, genotype effect $P < 0.001$ by ANOVA). The elevated levels of apoptosis in the villi caused by both PolgD257A mutation and HFW diet contribute to a diet-genotype interaction ($P < 0.05$ by ANOVA).

HFW diet does not increase apoptosis in the crypt region in WT mice (Fig. 4.8C) compared to NC diet WT mice (Fig. 4.8A). As I have previously described in chapter 3, the PolgD257A mutation increases apoptosis in the crypts. Polg mice in both diets have increased apoptosis in the crypt compartment (Fig. 4.8B, D) compared to WT mice. There is a strong PolgD257A effect in the crypt region ($P < 0.001$ by ANOVA) as evident by the increase in apoptosis seen in both diets of Polg mice compared to WT mice (Fig. 4.8E). No diet effect and no interaction between diet and genotype in apoptosis of the crypt compartment were observed by ANOVA.

As previously described in Chapter 3, the PolgD257A mutation decreases S-phase proliferation in the crypts. In both diets, the PolgD257A mutation decreases S-phase cell proliferation in Polg mice (Fig. 4.9B, D) compared to WT mice (Fig. 4.9A, C). HFW diet

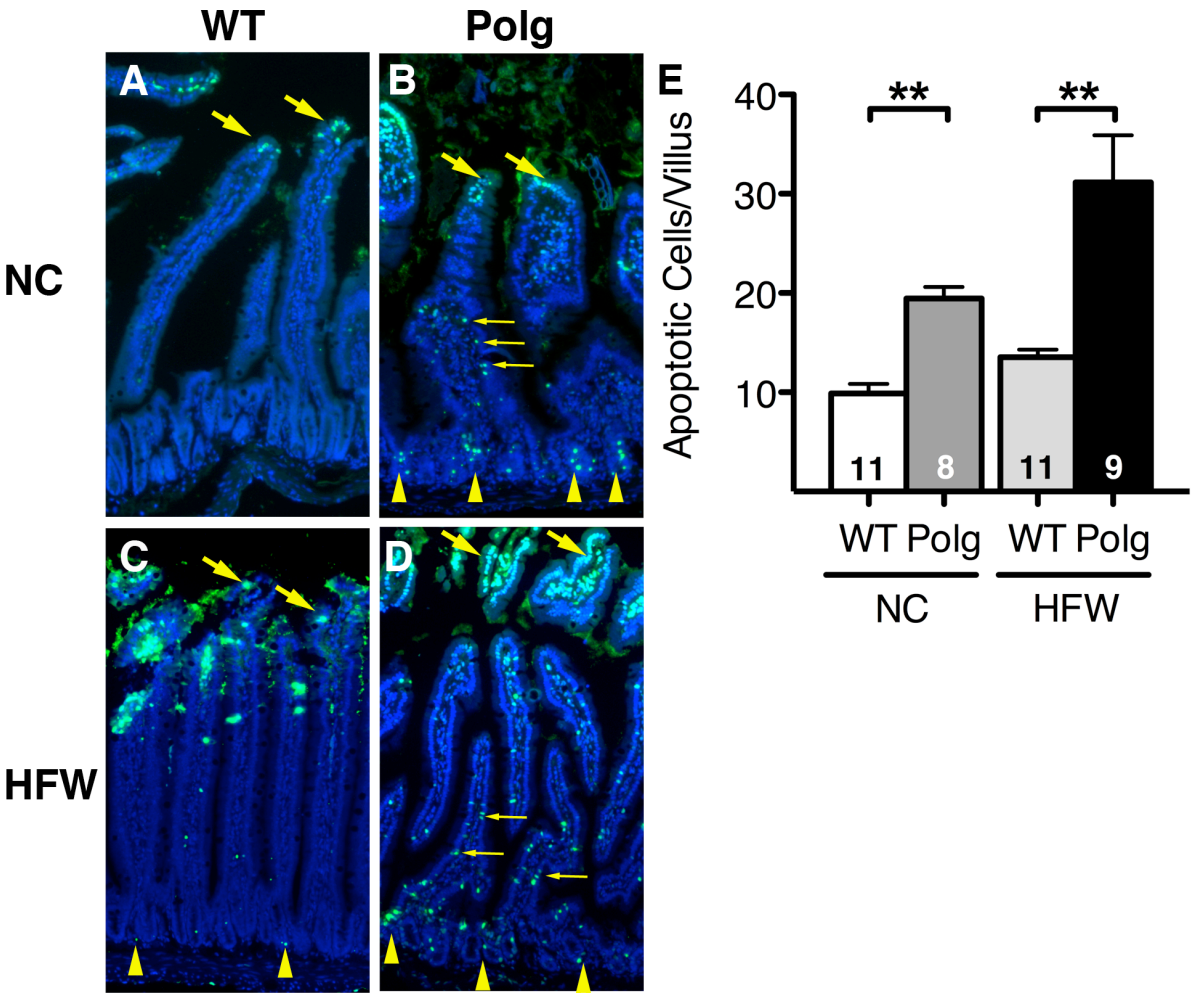

Figure 4.7: Apoptosis in wild type and PolgD257A small intestines. (A) wild type small intestine with apoptosis located at tip of each villus with large yellow arrows indicating apoptotic cells. (B) Polg small intestines have similar levels of apoptosis at the tip of each villus indicated with large yellow arrows. Small yellow arrows indicate an increase in apoptotic cells in the columnar epithelial cells along the length of the villi. Apoptosis increases slightly with high fat diet in both (C) wild type small intestines and (D) Polg small intestines. (E) Quantification of apoptosis found in the villi. All data are represented as Mean ± SEM. ** $P < 0.01$ between WT (n = 11) and Polg (n ≥ 8) by Tukey-Kramer HSD. Nuclei staining – blue and Apoptosis – green

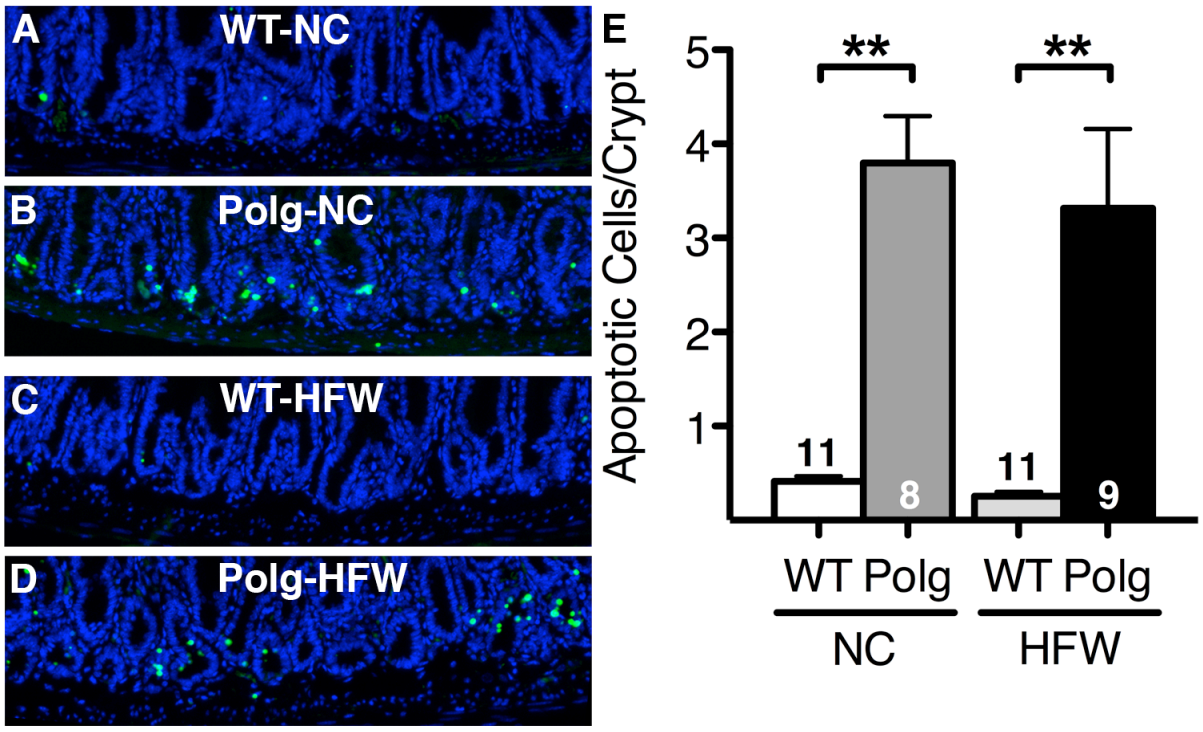

Figure 4.8: Apoptosis of small intestine in the crypts of Lieberkuhn. (A) Apoptosis and S-phase proliferation in Wild type and PolgD257A crypts of Lieberkuhn. Apoptosis is located in the region of the transit amplifying cells of wild type (A) and Polg (B) crypts in normal diet administered mice. Wild type crypts have few apoptotic cells in this region while Polg mice have numerous apoptotic cells. High fat diet does not change apoptosis in this region, however apoptosis in wild type (C) remains lower than Polg (D) mice administered high fat diet. Quantification of apoptotic cells per crypt (E) comparing wild type and Polg mice administered either normal or high fat diet. All data are represented as Mean ± SEM. *** $P < 0.001$ between WT ($n \geq 8$) and Polg ($n \geq 8$) by Tukey-Kramer HSD. Nuclei staining – blue and Apoptosis – green

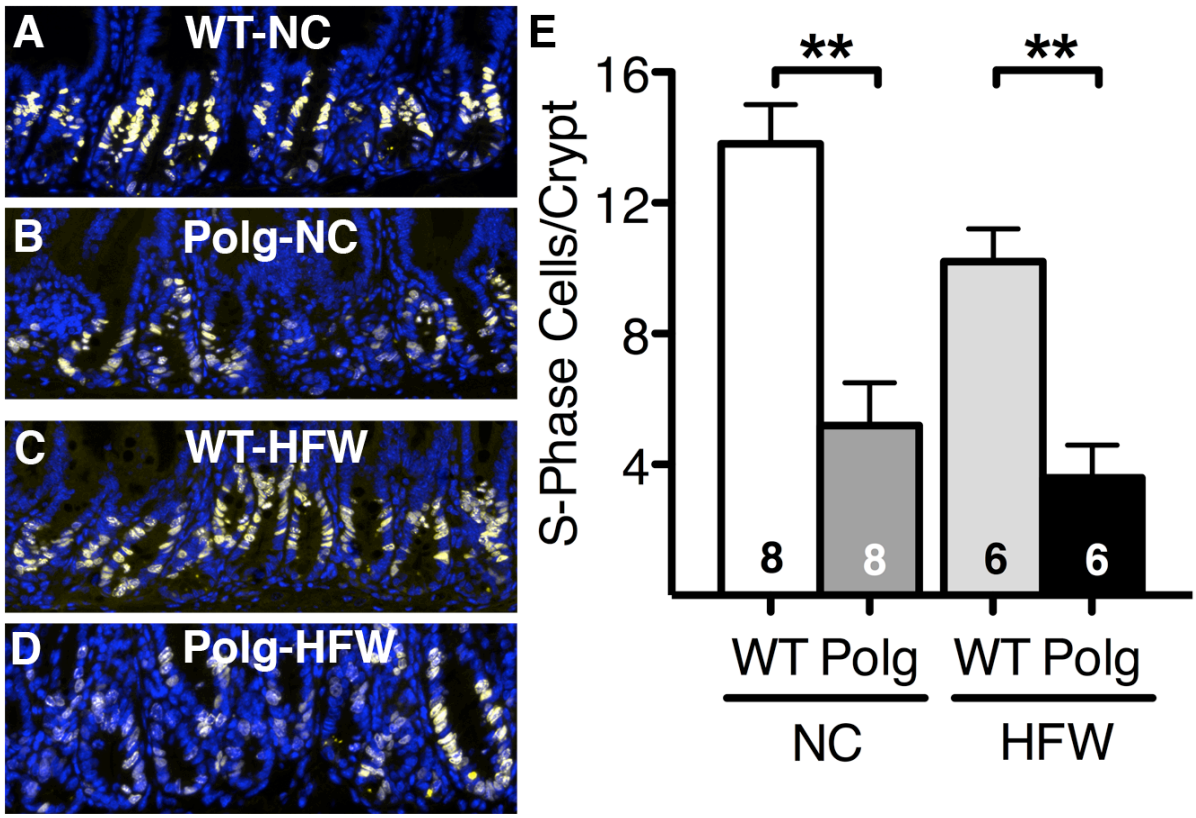

Figure 4.9: S-phase cell proliferation in the crypts of Lieberkuhn. EdU incorporation in S-phase cells in the transit amplifying region is found in the crypts of wild type (A) and Polg (B) mice administered normal diet. Wild type mice have numerous and robust staining of S-phase cells in this region while Polg mice have fewer and less intense staining of S-phase cells in this region. High fat diet reduces the intensity of s-phase labeled cells in wild type (C) and Polg (D) compared to normal diet mice. Polg staining is reduced compared to wild type mice regardless of diet. Quantification of S-phase proliferating cells per crypt (E) comparing wild type and Polg mice administered either normal or high fat diet. All data are represented as Mean ± SEM. *** $P < 0.001$ between WT ($n \geq 6$) and Polg ($n \geq 6$) by Tukey-Kramer HSD. Nuclei staining – blue and S-phase cells – yellow

significantly decreases S-phase cell proliferation in the crypt region as compared to NC diet (diet effect $P < 0.05$ by ANOVA). There is a strong PolgD257A effect in the crypt region as evident by the decrease in S-phase cell proliferation (Fig. 4.9E, $P < 0.001$ by ANOVA) compared to WT mice. No interaction between diet and genotype were observed by ANOVA. Together, these data suggest that the PolgD257A mutation markedly affects the small intestine by increasing apoptosis and decreasing S-phase cell proliferation; however, HFW diet does not affect these changes in PolgD257A mice.

Small intestine gene expression. Intestinal gene expression of transporters and co-transporters were evaluated to determine if the PolgD257A mutation decreases mRNA levels thereby reducing the transport of compounds across the epithelial cell membranes. There were no differences seen in WT and Polg mice on either diet in the following transporter genes: *SGLT* (Solute carrier family 2 – sodium/glucose), *Octn2* (Solute carrier family 22 – organic cation), *Mct1* (Solute carrier family 16 – monocarboxylic acid), *Nbc3* (Solute carrier family 4 – sodium bicarbonate), *Hpt1* (Cadherin 17), *Fabp1* (fatty acid binding protein 1), *Fabp2* (fatty acid binding protein 2), *Svct1* (Solute carrier family 23 member 1 – nucleobase), and *NaDC-1* (Solute carrier family 13 member 2 – sodium-dependent dicarboxylate). *Glut2* (Solute carrier family 2 – facilitated glucose) and *Sfxn1* (Sideroflexin 1 – iron) were significantly lower in Polg mice compared to WT mice ($P < 0.01$ by ANOVA), but not affected by diet. *Pept1* (Solute carrier family 15 – oligopeptide) was significantly lower in HFW diet mice compared to NC diet mice ($P < 0.05$ by ANOVA), but not affected by genotype. No differences were found in Na/K ATPase $\alpha 1$ and $\beta 1$, both of which are required for the establishment of the Na+/K gradient used during co-transport of molecules. Table 4.4 summarizes the gene expression of the various small intestine transporters tested. These data demonstrate that gene

Table 4.4: Summary of Gene Expression Data of Intestinal Transporters

	Normal Chow		Western Diet		Two-Way ANOVA			
	WT (n=5)	Polg (n=4)	WT (n=7)	Polg (n=4)	Diet	Genotype	Interaction	Function
Glut2	1.00 ± 0.23	0.26 ± 0.11	1.13 ± 0.22	0.40 ± 0.09	NS	<0.01	NS	facilitated glucose transport
Sglt	1.00 ± 0.29	0.86 ± 0.19	1.18 ± 0.41	0.47 ± 0.09	NS	NS	NS	sodium/glucose co-transporter
Octn2	1.00 ± 0.26	1.00 ± 0.14	1.51 ± 0.32	1.83 ± 0.55	NS	NS	NS	organic cation transport
Sfxn1	1.00 ± 0.19	0.36 ± 0.07	0.77 ± 0.16	0.40 ± 0.12	NS	<0.01	NS	iron transport
Mct1	1.00 ± 0.24	0.73 ± 0.09	1.20 ± .23	1.38 ± 0.26	NS	NS	NS	monocarboxylic acid transport
Nbc3	1.00 ± 0.60	0.21 ± 0.06	0.75 ± 0.17	0.88 ± 0.30	NS	NS	NS	sodium bicarbonate co-transporter
Hpt1	1.00 ± 0.29	0.84 ± 0.19	1.01 ± 0.20	1.02 ± 0.21	NS	NS	NS	proton-dependent peptide transporter
Pept1	1.00 ± 0.39	0.66 ± 0.15	0.25 ± 0.12	0.36 ± 0.22	<0.05	NS	NS	proton-dependent peptide co-transporter
Fabp1	1.00 ± 0.44	0.74 ± 0.32	1.62 ± 0.37	2.70 ± 1.44	NS	NS	NS	fatty acid transport
Fabp2	1.00 ± 0.29	1.36 ± 0.38	1.08 ± 0.23	0.88 ± 0.29	NS	NS	NS	fatty acid transport
Svct1	1.00 ± 0.44	0.65 ± 0.10	0.89 ± 0.53	0.12 ± 0.08	NS	NS	NS	Vitamin C transport
NaDC-1	1.00 ± 0.35	0.56 ± 0.15	1.10 ± 0.48	0.09 ± 0.03	NS	NS	NS	sodium dicarboxylate co-transporter
Na/K ATPase α1	1.00 ± 0.30	0.85 ± 0.09	1.74 ± 0.40	1.38 ± 0.52	NS	NS	NS	Sets sodium gradient for transport
Na/K ATPase β1	1.00 ± 0.37	0.73 ± 0.17	1.01 ± 0.28	0.82 ± 0.12	NS	NS	NS	Sets sodium gradient for transport

Data are given as mean±SEM. All statistics performed using Tukey-Kramer HSD.

expression of most intestinal transporters remains unchanged in the presence of the PolgD257A mutation regardless of the diet administered.

Assessment of mitochondria. Total DNA was isolated from tissues and real-time PCR amplification for the Cytochrome b gene was performed to assay mitochondrial DNA content using amplification of the Na-K-Cl cotransporter 2 gene (*NKCC2)* as an indicator of the content of nuclear DNA. No differences in mitochondria DNA content (Fig. 4.10A-D) were observed in the intestine, pancreas, kidney, or liver. A diet effect was seen in the content of mtDNA only in the liver where HFW diet significantly reduced the mtDNA content compared to NC diet ($P < 0.05$ by ANOVA). The D-17 deletion, a deletion of ~3.8kb in relation to the D-loop, in the mtDNA genome was determined relative to the presence of the mitochondrial cytochrome b gene. No differences were found in the D17 deletions (Fig. 4.10E-H) within the small intestine, pancreas, or kidney. The deletion was increased in WT HFW livers but not in Polg HFW, confirming that HFW feeding stressed the WT livers but not so in the Polg livers.

In homogenized tissue, oxygen consumption occurs by both mitochondrial and non-mitochondrial origins with the majority of respiration occurring via mitochondria. Oxygen consumption in crude small intestine homogenates showed no difference between the two genotypes (Fig 4.11). Oxygen consumption by the crude small intestine homogenate was dramatically increased in mice fed a HFW diet compared to those fed NC diet, yet there were no differences between Polg and WT mice in either diet group.

Due to the heterogeneous population of cells found in the small intestines and the multiple sources of respiration found in cells, isolated mitochondria from the liver was used to determine the functional characteristics of the mitochondria from WT and Polg mice. Mitochondria isolated from WT and Polg mice fed NC diet had a similar bioenergetics profile

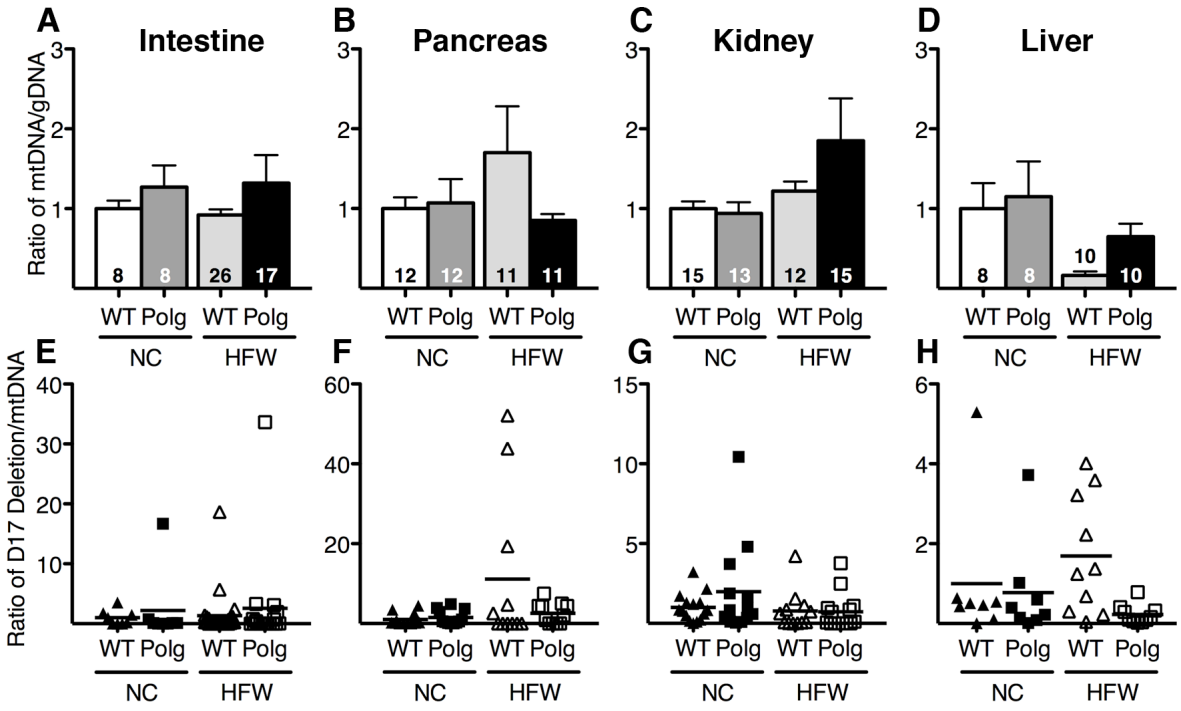

Figure 4.10: Mitochondrial DNA in the small intestine (A, E), pancreas (B, F), kidney (C, G), and liver (D, H). DNA was isolated from tissues and Real-time PCR amplification for the Cytochrome b gene was performed to assay mitochondrial DNA content using amplification of the Na-K-Cl cotransporter 2 gene (*NKCC2)* as an indicator of the content of nuclear DNA. A deletion of ~3.8kb in relation to the D-loop of mtDNA was assayed using a primer probe set that recognizes the loss of the D-17 region in the mtDNA genome (A, B, C, D) Mitochondrial DNA content relative to genomic DNA and (E, F, G, H) D17 deletions in the pancreas, kidney, and small intestine, respectively, of 7 month old wild type NC, Polg NC, wild type HFW, and Polg HFW. The extent of D-17 deletions was expressed relative to the mtDNA gene coding for Cytochrome b in each animal. All data are represented as Mean ± SEM. ($n \geq 8$) Numbers in the bars indicate the number of animals.

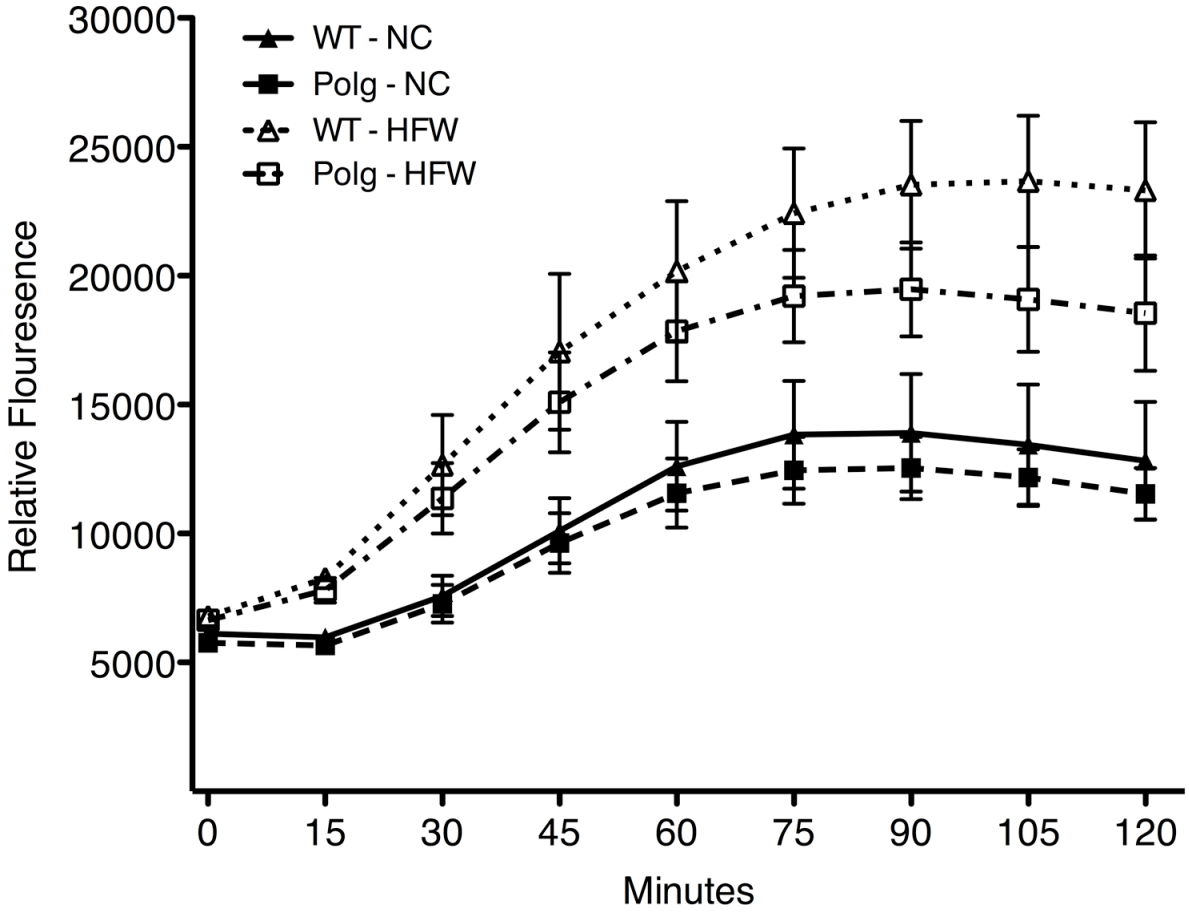

Figure 4.11: Oxygen consumption by small intestine homogenates. High fat diet increases oxygen consumption in both wild type and PolgD257A small intestine homogenates compared to normal diet administered wild type and PolgD257A small intestine homogenates. No difference was observed between genotypes. All data are represented as Mean ± SEM in 7-month-old WT NC (n = 6), Polg NC (n = 6), WT HFW (n = 4), and Polg HFW (n = 4).

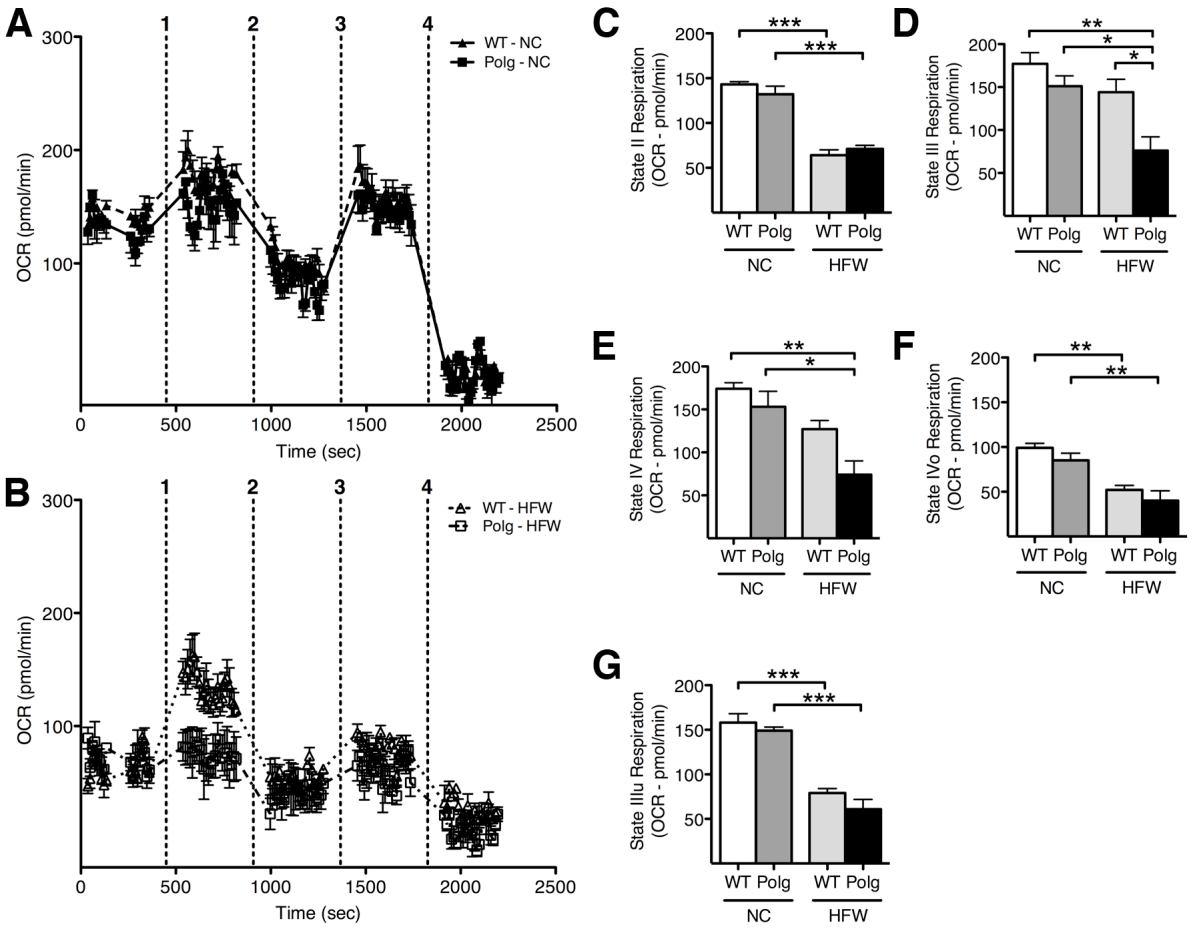

Figure 4.12: Bioenergetics of isolated liver mitochondria. Bioenergetic profiles of isolated mitochondria from wild type and PolgD257A mice when administered normal diet (A) and high fat diet (B) measuring oxygen consumption during sequential injections of ADP (1), Oligomycin (2), FCCP (3), and Anti-mycin A (4). State II "basal" respiration (C), State III "ADP stimulated" respiration (D), State IV "ADP exhausted" respiration (E), State IVo "ATP inhibited" respiration (F), and State IIIu "uncoupled" respiration (G) in 7-month-old WT NC, Polg NC, WT HFW, and Polg HFW. All data are represented as Mean ± SEM. *** $P < 0.001$, ** $P < 0.01$, and * $P < 0.05$ by Tukey-Kramer HSD.

(Fig. 4.12A). HFW diet decreased the bioenergetics profile in both WT and Polg isolated mitochondria (Fig. 4.12B). Both WT and Polg mice fed HFW diet for three months had reduced respiration at State II (basal respiration), IVo (ATP synthesis blocked), and IIIu (coupling abolished) compared to NC diet mice (Fig. 4.12C, F, G). Isolated mitochondria from Polg mice fed a HFW diet have a lower State III respiration, reduced ability to convert ADP to ATP, after administering ADP than WT mice fed a HFW diet (Fig. 4.12D). Respiration at State IV was reduced in only Polg mice on HFW diet compared to Polg mice on NC diet (Fig. 4.13E). Multifactorial ANOVA revealed dietary effects in State II, IV, IVo, and IIIu where NC diet values are significantly higher than HFW diet values. Multifactorial ANOVA also revealed a genotype effect in State III, IV, IVo, and IIIu where WT values are significantly higher than Polg values. No diet-genotype interaction was found by ANOVA in this study. Taken together, these data show that while mitochondria copy number and damage via DNA deletions are not increased in Polg mice, mitochondria function of Polg mice fed HFW diet is impaired at complex V, the mitochondrial encoded portion of ATP synthase that converts ADP to ATP.

Oxygen consumption and basal metabolic rate. Both young (3-months) and old (7-months) WT and Polg mice were placed into Oxymax cages to determine metabolic activity while on NC and HFW diet. At 3 months of age, Respiratory Exchange Ratio (RER) in WT and Polg mice are similar when administered NC, but replacement with HFW causes RER in WT mice to dramatically increase to >1.0 while Polg mice show a blunted response compared to mice on NC diet (Fig. 4.13A). Similarly, at 7 months of age, RER in WT and Polg mice are similar when administered NC diet, but replacement with HFW causes RER in WT mice to dramatically increase to >1.0 while Polg mice show a blunted response compared to mice on NC diet (Fig. 4.13B). In both 3-month and 7-month mice, basal metabolic rate (Fig. 4.13C, F),

activity (Fig. 4.13D, G), and heat generation (Fig. 4.13E, H) were not different between WT and Polg mice administered either diet. In 3-month-olds, food consumption in WT mice after switch to HFW diet (4.8 ± 0.2 g/Day) was significantly higher than Polg mice after switching to HFW diet (3.6 ± 0.2 g/Day). In 7-month-olds, food consumption in WT mice after switch to HFW diet (5.2 ± 0.2 g/Day) was also significantly higher than Polg mice after switching to HFW diet (3.1 ± 0.2 g/Day). The increase in food consumption in both 3 and 7 month old WT mice is likely responsible for the increased RER since more calories are entering the body. These data show that WT mice develop an acute response in metabolism to HFW diet while Polg mice do not respond when changed to HFW diet. In the acute response experiment, changes in RER, activity, basal metabolic rate, and energy expenditure (heat) were minimal.

To determine the long-term effects of diet on these parameters, PolgD257A mice were given either NC or HFW diet for 3 months and placed into Oxymax changes to assess global metabolism. Wild type mice on both diets did not eat during the experiment and have been excluded for the comparison. During the light cycle, RER was similar in Polg-NC and Polg-HFW mice. During the dark cycle when animals are most active, RER was higher in Polg NC mice compared to Polg HFW mice, but the difference was not significant (Fig. 4.14A). Basal metabolic rate, activity, and energy expenditure were all similar in Polg NC and Polg HFW mice (Fig. 4.14B-D). When combined, the acute response and prolonged response experimental data demonstrates that the PolgD257A mutation does not alter the global metabolism by increasing the global metabolic rate of the animal on either NC or HFW diet.

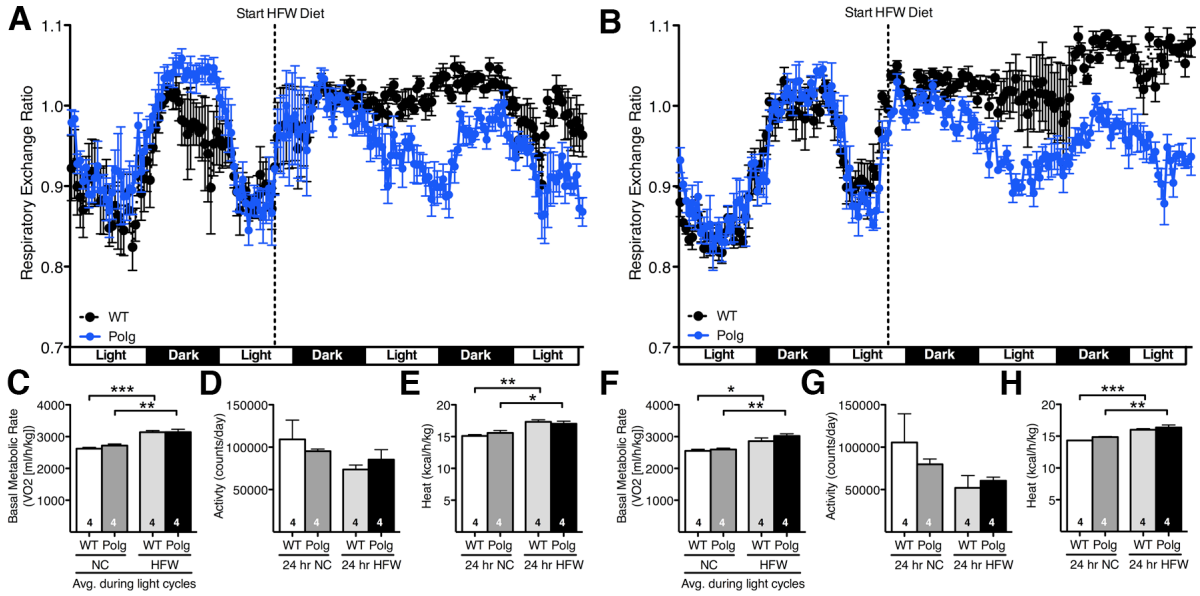

Figure 4.13: Calorimetry in 3-month-old and 7-month-old PolgD257A mice. Respiratory exchange ratio in 3-month-old (A) and 7-month-old (B) wild type and PolgD257A mice given a normal diet for 48 hrs followed by high fat diet for 48 hrs. Basal metabolic rate in 3-month-old (C) and 7-month-old (F) wild type and PolgD257A mice given a normal diet for 48 hrs followed by high fat diet for 48 hrs. Activity in 3-month-old (D) and 7-month-old (G) wild type and PolgD257A mice given a normal diet for 48 hrs followed by high fat diet for 48 hrs. Energy expenditure in 3-month-old (E) and 7-month-old (H) wild type and PolgD257A mice given a normal diet for 48 hrs followed by high fat diet for 48 hrs. All data are represented as Mean ± SEM. *** $P < 0.001$, ** $P < 0.01$, and * $P < 0.05$ by Tukey-Kramer HSD.

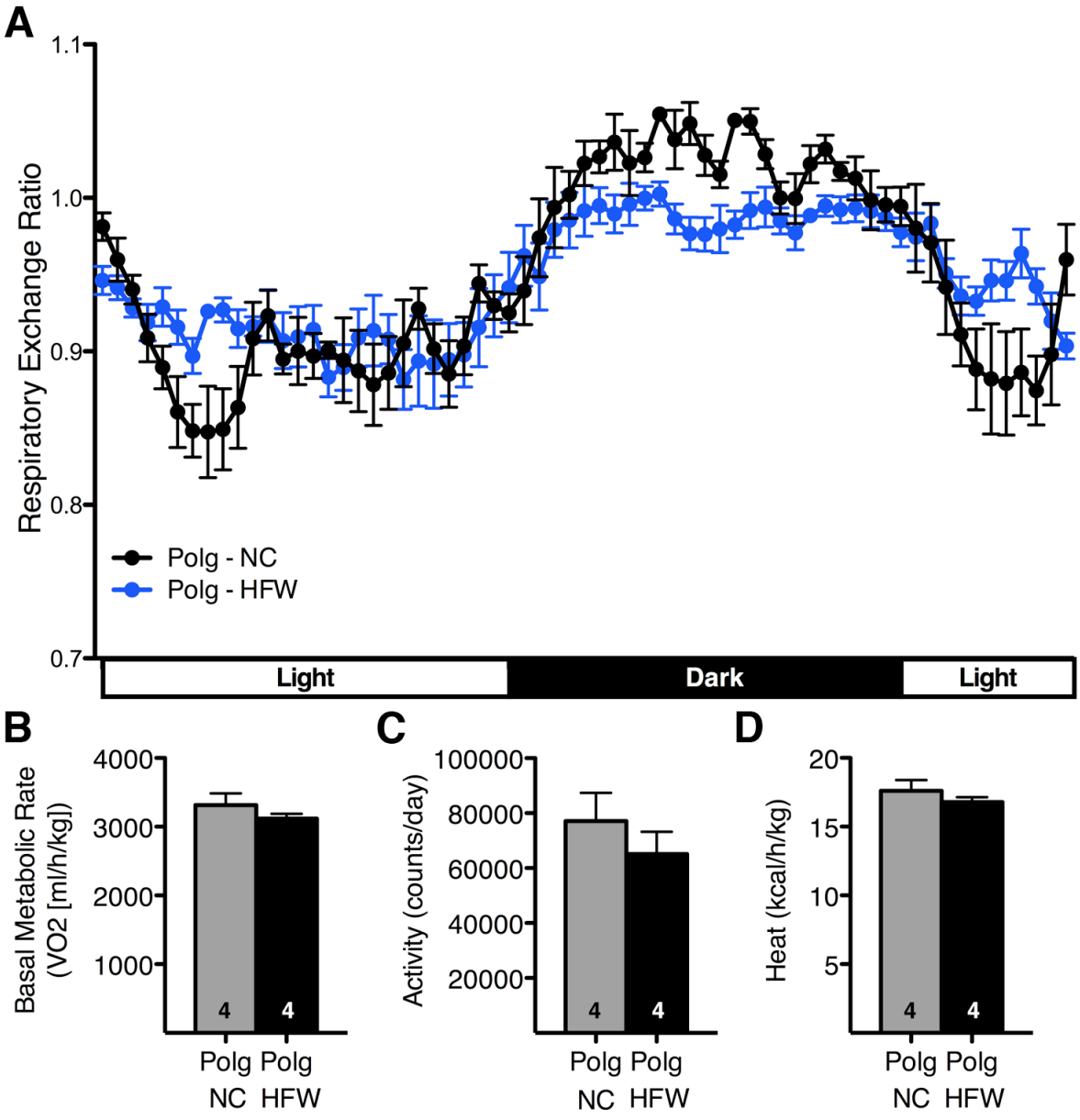

Figure 4.14: Calorimetry in 7-month-old PolgD257A mice fed either NC or HFW diet for 3 months. (A) Respiratory exchange ratio in 7-month-old PolgD257A mice given a NC (black) of HFW (blue) diet. (B) Basal metabolic rate, (C) Activity, and (D) Energy expenditure 7-month-old PolgD257A mice given a NC or HFW diet for 3 months. All data are represented as Mean ± SEM.

4.5 Discussion

Considering the importance of mitochondria in aging, I expected that the PolgD257A mutation, which increases mitochondrial DNA mutations, would develop mal-absorption. Accumulations of mitochondrial DNA mutations play a role in the development of an accelerated aging phenotype (25, 26), and increases in mitochondrial DNA mutations have been found in the elderly (10). In addition, mitochondrial DNA mutations have been shown to be the underlying genetic factor in several metabolic diseases (43, 44), and have their greatest effect in cells that are metabolically active or highly proliferative (17-21). The intestinal phenotypes of PolgD257A mice: increased apoptosis and decreased proliferation in the crypt and increased enterocyte half-life in the villi, could account for the mal-absorption in aging. In this chapter, I tested this hypothesis using mice on NC and on HFW. I found that the PolgD257A mice on NC diet were indistinguishable from wild type mice on NC diet. In contrast, PolgD257A mice administered HFW diet did not gain weight compared to wild type mice administered HFW diet. Insulin sensitivity was impaired in wild type mice but not PolgD257A mice on HFW diet. This protection from diet induced obesity and insulin resistance was due at least in part because PolgD257A mice on HFW diet had increased excretion of fat in the feces. However, fat absorption in PolgD257A mice on HFW diet was similar to wild type mice on HFW diet. In the villi, HFW diet increased apoptotic cells to 30%, but did not alter apoptosis and proliferation in the crypt compartment in PolgD257A mice. All of the metabolic measurements taken during the administration of HFW diet, basal plasma glucose, triglycerides, and cholesterol, were significantly lower in mutant mice compared to wild type controls suggesting limited dietary absorption in the PolgD257A mice.

To rule out a digestive problem, pancreatic gene expression of the digestive enzymes

revealed that all are produced at normal. These results confirm that enzymes necessary for processing the diet as it enters the small intestine are present, although they do not address whether the enzymes are active. The digestive enzymes chymotrypsinogen, lipase, co-lipase, and amylase all require activation within the small intestine by trypsin, and trypsin requires activation from its inactive state, trypsinogen. Enterokinase, also known as enteropeptidase, is responsible for converting trypsinogen to trypsin (45). Analysis of enterokinase activity was comparable in wild type and PolgD257A mice on HFW diet. These data rule out digestive components as a cause for reduced absorption of dietary fats.

A global increase in metabolism does not account for the differences in fat storage in PolgD257A and wild type mice on HFW diet. By measuring global oxygen consumption and carbon dioxide respiration, metabolism of various sources of energy were evaluated. Respiratory exchange ratio is a calculation based on the amount of CO_2 produced/ amount of O_2 consumed. When RER approaches 1.0, carbohydrates are the primary source of energy. When RER approaches 0.7, fat is the primary source of energy. When the PolgD257A mice were fed a high fat, high carbohydrate diet, I expected to see an increase utilization of fat and an RER approaching 0.7. However, the PolgD257A mice did not alter their pattern of utilization of carbohydrates and fats. This is based on the RER not changing dramatically when the mice were switched from NC diet to HFW diet. On the other hand, the wild type animals responded to the change in diet by consuming primarily carbohydrates. Since the diet is high in carbohydrates, this result is not surprising. The reason wild type mice fed HFW diet gain significant amounts of weight is likely due to an acute increase in caloric intake (21.47 kcal/day) compared to PolgD257A (12.7 kcal/day). Furthermore, wild type mice fed HFW diet overwhelming use carbohydrates, convert unused carbohydrates to fat for storage, and store

excess fat in the adipose tissue while PolgD257A mice fed HFW diet use more fat than carbohydrates. In support of this, inguinal and gonadal fat weights were significantly larger in WT HFW mice compared to Polg HFW mice. While these results do not show an increase in metabolism in PolgD257A mice fed a HFW diet, they do confirm that the PolgD257A mutation plays a pivot role in intestinal absorption and adipose storage of fat.

On a cellular level, I have shown in Chapter 3 that an increase in cell apoptosis and a decrease in cell proliferation occurs specifically in the transit amplifying cells located in the crypts of Lieberkuhn in the small intestine of PolgD257A mice. In normal small intestines, there are low levels of apoptosis observed in the intestinal crypts used primarily as a maintenance system to eliminate extra or damaged stem cells within in the intestinal crypt (46, 47). In aging mice and humans, there is no evidence of increased apoptosis in the crypt region. Increased apoptosis has been reported in rats when given a dose of radiation causing apoptosis in the proliferating cells of the small intestine (46). Yet the question remained as to whether these collective changes are sufficient to cause a functional change in the small intestine. Intestinal gene expression did not reveal any specific changes. The evidence presented in chapter 3 suggests that villous epithelial cell replacement of the intestinal epithelial cells has been reduced. Cell replacement is a common occurrence in the epithelial cells of the small intestine with complete cell replenishment estimated to take approximately 3.3 days (48). However, cell migration in intestinal epithelial cells of PolgD257A mice is greater than 4 days. It is possible that increasing the time for cell renewal of the intestinal epithelial cells would allow dysfunctional cells with reduced absorptive capacity to remain for a longer period of time. This would explain the defect in absorption as enterocytes are the primary absorptive cell in the intestine. Although generally assumed that aging leads to reduced absorptive capacity,

whether the retained epithelial cells are dysfunctional enterocytes remains an important question, and is currently a hot topic in the gastrointestinal field.

While the exact mechanism for the reduced lipid absorption in PolgD257A mutants has yet to be elucidated, lipid absorption is limited by the PolgD257A mutation prompting a concern that administering HFW diet to PolgD257A mice causes malnourishment. However, they are absorbing more total fat from diet than NC fed mice, and similar amounts as WT HFW mice, and the plasma levels of lipid soluble vitamins D and E were not affected by the PolgD257A mutation even under the high dietary lipid load. Although PolgD257A mutation caused reduced expression of *Glut2* gene in the small intestine and amylase gene in the pancreas, monosaccharide carbohydrate absorption (glucose) was not affected in PolgD257A mice regardless of diet since administering an oral gavage of glucose produced a normal spike in plasma glucose. However, I cannot exclude a possibility that the PolgD257A mutation causes a defect in carbohydrate digestion and/or disaccharide conversion to monosaccharide since the main source of carbohydrates in the HFW diet is sucrose, which requires conversion to glucose before absorption can proceed. It does not appear the PolgD257A mice administered HFW diet lack essential nutrients for survival. Overall, the limited caloric intake appears to be beneficial to the PolgD257A mice.

In conclusion, I have demonstrated that the PolgD257A mutation limits lipid absorption when a diet high in fat and carbohydrates is administered. However, PolgD257A mice do not exhibit any overt signs of intestinal mal-absorption. The most striking evidence for intestinal dysfunction in PolgD257A mice is the increase in fecal fat excretion as a consequence of a limited fat absorption. This prevents the excess accumulation of body fat and protects from the

development of insulin resistance. Establishing a clear mechanism as to why the PolgD257A mutation causes the absorption problems remains elusive.

REFERENCES

1. Thomson AB (2009) Small intestinal disorders in the elderly. *Best Pract Res Clin Gastroenterol* 23(6):861-874.

2. Drozdowski L & Thomson AB (2006) Aging and the intestine. *World J Gastroenterol* 12(47):7578-7584.

3. Corazza GR*, et al.* (1998) Proliferating cell nuclear antigen expression is increased in small bowel epithelium in the elderly. *Mech Ageing Dev* 104(1):1-9.

4. Webster SG & Leeming JT (1975) The appearance of the small bowel mucosa in old age. *Age Ageing* 4(3):168-174.

5. Ciccocioppo R*, et al.* (2002) Small bowel enterocyte apoptosis and proliferation are increased in the elderly. *Gerontology* 48(4):204-208.

6. Holt PR, Pascal RR, & Kotler DP (1984) Effect of aging upon small intestinal structure in the Fischer rat. *J Gerontol* 39(6):642-647.

7. Martin K, Kirkwood TB, & Potten CS (1998) Age changes in stem cells of murine small intestinal crypts. *Exp Cell Res* 241(2):316-323.

8. Mandir N, FitzGerald AJ, & Goodlad RA (2005) Differences in the effects of age on intestinal proliferation, crypt fission and apoptosis on the small intestine and the colon of the rat. *Int J Exp Pathol* 86(2):125-130.

9. Xiao ZQ*, et al.* (2001) Aging is associated with increased proliferation and decreased apoptosis in the colonic mucosa. *Mech Ageing Dev* 122(15):1849-1864.

10. Chomyn A & Attardi G (2003) MtDNA mutations in aging and apoptosis. *Biochem Biophys Res Commun* 304(3):519-529.

11. Kujoth GC, Leeuwenburgh C, & Prolla TA (2006) Mitochondrial DNA mutations and apoptosis in mammalian aging. *Cancer Res* 66(15):7386-7389.

12. Lee CM, Weindruch R, & Aiken JM (1997) Age-associated alterations of the mitochondrial genome. *Free Radic Biol Med* 22(7):1259-1269.

13. Greaves LC & Turnbull DM (2009) Mitochondrial DNA mutations and ageing. *Biochim Biophys Acta* 1790(10):1015-1020.

14. Larsson NG (2010) Somatic mitochondrial DNA mutations in mammalian aging. *Annu Rev Biochem* 79:683-706.

15. Chen H & Chan DC (2005) Emerging functions of mammalian mitochondrial fusion and fission. *Hum Mol Genet* 14 Spec No. 2:R283-289.

16. Chan DC (2006) Mitochondrial fusion and fission in mammals. *Annu Rev Cell Dev Biol* 22:79-99.

17. Simmons RA, Suponitsky-Kroyter I, & Selak MA (2005) Progressive accumulation of mitochondrial DNA mutations and decline in mitochondrial function lead to beta-cell failure. *J Biol Chem* 280(31):28785-28791.

18. Someya S*, et al.* (2008) The role of mtDNA mutations in the pathogenesis of age-related hearing loss in mice carrying a mutator DNA polymerase gamma. *Neurobiol Aging* 29(7):1080-1092.

19. Trifunovic A & Larsson NG (2008) Mitochondrial dysfunction as a cause of ageing. *J Intern Med* 263(2):167-178.

20. Wang J, Markesbery WR, & Lovell MA (2006) Increased oxidative damage in nuclear and mitochondrial DNA in mild cognitive impairment. *J Neurochem* 96(3):825-832.

21. Zhang D*, et al.* (2003) Mitochondrial DNA mutations activate the mitochondrial apoptotic pathway and cause dilated cardiomyopathy. *Cardiovasc Res* 57(1):147-157.

22. DiMauro S & Tanji K (1997) Mitochondrial disorders. *Jpn J Hum Genet* 42(4):473-487.

23. Wallace DC (1994) Mitochondrial DNA mutations in diseases of energy metabolism. *J Bioenerg Biomembr* 26(3):241-250.

24. Hance N, Ekstrand MI, & Trifunovic A (2005) Mitochondrial DNA polymerase gamma is essential for mammalian embryogenesis. *Hum Mol Genet* 14(13):1775-1783.

25. Kujoth GC, *et al.* (2005) Mitochondrial DNA mutations, oxidative stress, and apoptosis in mammalian aging. *Science* 309(5733):481-484.

26. Trifunovic A, *et al.* (2004) Premature ageing in mice expressing defective mitochondrial DNA polymerase. *Nature* 429(6990):417-423.

27. Traber MG, Kayden HJ, Green JB, & Green MH (1986) Absorption of water-miscible forms of vitamin E in a patient with cholestasis and in thoracic duct-cannulated rats. *Am J Clin Nutr* 44(6):914-923.

28. Kuperman Y, *et al.* (2010) Perifornical Urocortin-3 mediates the link between stress-induced anxiety and energy homeostasis. *Proc Natl Acad Sci U S A* 107(18):8393-8398.

29. Schoiswohl G, *et al.* (2010) Adipose triglyceride lipase plays a key role in the supply of the working muscle with fatty acids. *J Lipid Res* 51(3):490-499.

30. Tran M, *et al.* (1994) The acid steatocrit: a much improved method. *J Pediatr Gastroenterol Nutr* 19(3):299-303.

31. Takahashi N, *et al.* (2007) Increased energy expenditure, dietary fat wasting, and resistance to diet-induced obesity in mice lacking renin. *Cell Metab* 6(6):506-512.

32. Kalivianakis M, *et al.* (2000) Detection of impaired intestinal absorption of long-chain fatty acids: validation studies of a novel test in a rat model of fat malabsorption. *Am J Clin Nutr* 72(1):174-180.

33. Salic A & Mitchison TJ (2008) A chemical method for fast and sensitive detection of DNA synthesis in vivo. *Proc Natl Acad Sci U S A* 105(7):2415-2420.

34. Chomczynski P & Sacchi N (1987) Single-step method of RNA isolation by acid guanidinium thiocyanate-phenol-chloroform extraction. *Anal Biochem* 162(1):156-159.

35. Yuan X, *et al.* (1998) Structure of murine enterokinase (enteropeptidase) and expression in small intestine during development. *Am J Physiol* 274(2 Pt 1):G342-349.

36. Johnson LA, Altenburg MK, Walzem RL, Scanga LT, & Maeda N (2008) Absence of hyperlipidemia in LDL receptor-deficient mice having apolipoprotein B100 without the putative receptor-binding sequences. *Arterioscler Thromb Vasc Biol* 28(10):1745-1752.

37. Leonard SW, Terasawa Y, Farese RV, Jr., & Traber MG (2002) Incorporation of deuterated RRR- or all-rac-alpha-tocopherol in plasma and tissues of alpha-tocopherol transfer protein--null mice. *Am J Clin Nutr* 75(3):555-560.

38. Frezza C, Cipolat S, & Scorrano L (2007) Organelle isolation: functional mitochondria from mouse liver, muscle and cultured fibroblasts. *Nat Protoc* 2(2):287-295.

39. Zamolodchikova TS, Sokolova EA, Lu D, & Sadler JE (2000) Activation of recombinant proenteropeptidase by duodenase. *FEBS Lett* 466(2-3):295-299.

40. Palay SL & Karlin LJ (1959) An electron microscopic study of the intestinal villus. II. The pathway of fat absorption. *J Biophys Biochem Cytol* 5(3):373-384.

41. Freeman HJ & Nimmo M (2011) Intestinal lymphangiectasia in adults. *World J Gastrointest Oncol* 3(2):19-23.

42. Vignes S & Bellanger J (2008) Primary intestinal lymphangiectasia (Waldmann's disease). *Orphanet J Rare Dis* 3:5.

43. Taylor RW & Turnbull DM (2005) Mitochondrial DNA mutations in human disease. *Nat Rev Genet* 6(5):389-402.

44. Wallace DC (2010) Mitochondrial DNA mutations in disease and aging. *Environ Mol Mutagen* 51(5):440-450.

45. Kunitz M (1939) Formation of Trypsin from Crystalline Trypsinogen by Means of Enterokinase. *J Gen Physiol* 22(4):429-446.

46. Merritt AJ*, et al.* (1994) The role of p53 in spontaneous and radiation-induced apoptosis in the gastrointestinal tract of normal and p53-deficient mice. *Cancer Res* 54(3):614-617.

47. Potten CS (1992) The significance of spontaneous and induced apoptosis in the gastrointestinal tract of mice. *Cancer Metastasis Rev* 11(2):179-195.

48. Cheng H & Leblond CP (1974) Origin, differentiation and renewal of the four main epithelial cell types in the mouse small intestine. I. Columnar cell. *Am J Anat* 141(4):461-479.

Chapter 5

CONCLUSIONS

This dissertation describes the use of animal models to investigate the role of mitochondrial DNA mutations in diabetes, obesity, and diabetic complications. While mitochondrial DNA mutations are expected to enhance disease especially metabolic disease, the results presented here describe the many unexpected findings associated with mitochondrial DNA mutations and metabolic diseases in animal models. The significant findings and conclusions for each chapter are discussed below.

Chapter 2

Significant points

1. Diabetes improves in diabetic Akita male mice homozygous for the Polg D257A mutation.
2. The improvement in diabetes is due to appetite suppression caused by a premature decline in testosterone production associated with increased damage to Leydig cells.
3. Testosterone replacement in double mutant mice increases hyperglycemia back to levels seen in simply diabetic Akita male mice.
4. Mitochondrial debris is increased in euglycemic double mutant mice and significantly increases with testosterone administration suggesting a role of mitochondrial DNA mutations in kidney pathology.

Discussion and Future directions

In this chapter, I describe an unforeseen improvement in Akita diabetic male mice homozygous for the PolgD257A mutation. As previously described, the "Akita" mutation has a more potent affect on male mice as opposed to female mice (1). In my study, diabetes in the double mutant male mice improved to levels that were similar to female Akita mice. A recent study illustrated a similar finding when diabetic Akita male mice were gonadectomized effectively reducing hyperglycemia (2). The underlining mechanism causing the reduced diabetic phenotype in my study was traced to testis dysfunction directly caused by the PolgD257A mutation. The dysfunction in the testis causes a change in appetite in the double mutant mice that effectively improves diabetes. I also demonstrated that testosterone replacement therapy in these double mutant mice returns hyperglycemia back to levels seen in simply diabetic mice. While this finding was unexpected, the results of this study uncovered the hyperphagic mechanism of diabetes in Akita mice and emphasized the importance of hyperphagia in this mouse model of type 1 diabetes. This mechanism is not equivalent to what occurs in type 1 diabetes in humans. Type 1 diabetes in humans is characterized by an autoimmune response triggering destruction of pancreatic beta cells (3-6). While the mechanism described here does not apply to human diabetic patients, it provided convincing evidence for the role of testosterone in the hyperglycemia of male mice.

Although my initial question of the role of mitochondrial DNA mutations in diabetic nephropathy was not answered, this study showed that mitochondrial DNA mutations may be a contributing factor to kidney pathology. A previous study has suggested that mitochondrial DNA mutations may be involved with enhancing nephropathy (7). It still remains a possibility that mitochondrial DNA mutations can affect the kidney, which is a metabolically active organ.

However, it is unclear whether the mtDNA mutations act causally with respect to diabetic complications, or are just consequences of the condition.

Alternative *in vivo* approaches can be utilized to answer whether mitochondrial DNA mutations play a causal role in diabetic nephropathy. The limitation of the current model is that global increases in mitochondrial DNA mutations affect multiple organs that contribute to improved diabetes. To investigate diabetic nephropathy, a conditional mouse model of PolgD257A would prove useful in answering this question. The conditional PolgD257A mouse model will be discussed later. Alternatively, kidney transplants could be utilized with PolgD257A kidneys as a donor and Akita mice as the recipient. This technique is technically challenging even in healthy mice, and would require a larger pool of animals to produce an effective experiment. Nevertheless, both of these options could potentially address our question.

Chapter 3

Significant points

1. Apoptosis is increased in the intestinal stem and progenitor cells found in the crypts of Lieberkuhn.
2. S-phase cell proliferation is also disrupted in the crypt compartment.
3. The PolgD257A mutation disrupts the cell cycle of the intestinal stem and progenitor cells causing a decrease in cell migration through the small intestine villi.

Discussion and Future directions

In this chapter, I describe the novel finding that the PolgD257A mutation increases cell apoptosis and decreases S-phase cell proliferation. Previously, the PolgD257A mutation was described as having increased apoptosis of columnar epithelial cells in the villi of the small intestine (8). In my study, the cell cycle is disrupted in these highly proliferative cells of the small intestine, and suggests that mitochondrial function plays a central role in the regulation of the cell cycle. As previously described in Chapter 3 on page 91, mitochondria are important in generating ATP required during the cell cycle and allowing procession through the cell cycle. Due to the heterogeneous nature of the PolgD257A crypts, determining an exact mechanism proved challenging. It wasn't until recently that the stem cells of the crypts could be cultured *in vitro* (9). The results of culturing the isolated stem cells reveals a defect in proliferation caused by the PolgD257A mutation supporting the *in vivo* results of the disrupted cell cycle and slower cell migration in the small intestine. The intestinal stem cell is adversely affected by the PolgD257A mutation that lead to defect in the cell cycle and cell proliferation. Essentially, the cells in the crypts of PolgD257A are behaving as though they are experiencing a damage response that triggers the higher apoptosis. This event has been described under conditions of damage induced by radiation where exposed cells become apoptotic (10). These results, while not surprising, underline the importance of the mitochondria in the natural process of cell self-renewal. This study did not cover the functional aspect of the increase in apoptosis and the decrease in cell proliferation. One would assume that mitochondrial dysfunction of the small intestine in the PolgD257A mouse would lead to issues with nutrient absorption, however no overt phenotype has been described. This prompted the question: Does the increase in

apoptosis and decrease in cell proliferation have a functional impact on the small intestine? I addressed this question in Chapter 4 of this dissertation.

Several reports (including the results described in Chapter 2) demonstrated that the PolgD257A mutation affects the testis, hair, skin, small intestine, and bone marrow (8, 11-13). The trend here is that all of these affected tissues are highly regenerative organ systems. In fact, the PolgD257A mouse is described as a mouse model of premature aging. This may be the case in that the PolgD257A mouse exhibits many aspects of human aging. However, the PolgD257A mutation seems to cause more problems with basic processes involving cell division. It is possible that the PolgD257A mouse model is more representative of a model for defects in cell proliferation rather than a model of premature aging. Information relating to the basic properties of the human aging small intestine is sparse and not well studied. The PolgD257A mutation clearly causes significantly more damage in the stem and progenitor cells located in the crypts. Whether this increase in damage is found in aging humans or aging rodents remains to be determined.

With the results present so far, the PolgD257A mouse could allow for expansion into other fields such as cancer. Since it appears that the PolgD257A mouse model has a global defect in cell proliferation, it would be interesting to cross this mouse with well-established models of cancer. Such a strategy would allow us to determine the contribution of mitochondrial dysfunction to cancer considering cancer is based on a disruption of the cell cycle leading to uncontrolled cell growth. Other groups may be pursuing this idea, but the results have yet to be reported.

Chapter 4

Significant points

1. The PolgD257A mutation does not affect nutrient absorption in mice maintained on NC diet.
2. The PolgD257A mutation protects against diet induced obesity and insulin resistance.
3. The increases in apoptosis and decreases in cell proliferation in the small intestine are likely triggering the mal-absorption of lipids when mice are administered HFW diet.
4. The failure to gain weight on the HFW diet is not the result of increased metabolism or increased energy expenditure.

Discussion and Future directions

Aging is thought to be the main contributing factor leading to the apparent mal-absorption yet the exact mechanism behind the dysfunction of the aging small intestine is not known. The goal of the experiments described in this chapter is to elucidate the effect of increasing mtDNA mutations in the small intestine on nutritional absorption, and on obesity and type 2 diabetes. I used the prematurely aging PolgD257A mutant mouse as a genetic tool to answer this question, and determine the role of mitochondrial DNA mutations in the functionality of the small intestine. In this chapter, I demonstrate that the PolgD257A mutation can prevent HFW diet induced obesity. I was not surprised to find that the PolgD257A mutant mice on NC diet are not affected by the changes in cell cycle and apoptosis in the small intestine since the mice used in both Chapters 2 and 3 were fed a NC diet and no overt phenotype was present. However, PolgD257A mice on HFW diet were protected against diet-

induced obesity and insulin resistance. Both digestion and metabolism did not change in the presence of the PolgD257A mutation suggesting another mechanism. It is likely that the changes in apoptosis and cell cycle in the small intestine of the PolgD257A mice impairs their ability to absorb dietary lipids preventing the accumulation of fat without disturbing nutritional balance. The results of the acid steatocrit determined that fat is not being absorbed efficiently in the PolgD257A mice, and this result may be the only evidence for the failure of PolgD257A mice to accumulate fat.

Alternatively, one possible mechanism for the reduced obesity phenotype of PolgD257A mice on HFW diet could be the reduced ability to breakdown carbohydrates. It is likely that both carbohydrates and lipids are required for fat storage and obesity. A high dietary intake of carbohydrates along with high consumption of lipids could work in unison. In this situation, both excess carbohydrates and lipids would be stored together in the fat depots allowing a rapid accumulation of fat. If PolgD257A mice cannot process carbohydrates as efficiently during digestion as wild type mice then the PolgD257A mice would not develop the obesity phenotype. This could easily explain the rapid accumulation of fat in wild type mice in the acute experiments and the inability of PolgD257A mice to store any fat during the experiment. One finding during this study was that PolgD257A mice produce less pancreatic amylase. Amylase is essential for the breakdown of carbohydrates during the initial stages of digestion (14). While amylase was low in PolgD257A mice regardless of diet, it is not the only enzyme responsible for the breakdown of carbohydrates. The HFW diet contains sucrose as its main source of carbohydrates. Sucrose is broken down into glucose and fructose by the enzyme sucrase (15). In obese mice, sucrase increases with age and signifies the start of obesity (16). For instance, if sucrase activity is low in the PolgD257A mice, this would lead to a reduction in

the break down of complex disaccharides to the easily absorbed monosaccharides. Carbohydrate metabolism has been linked to a decrease sucrase leading to mal-absorption by the small intestine (17). Monosaccharides such as glucose can be absorbed by active transport (*Sglt*), passive transport (*Glut2*), or by alternative diffusion pathways in the small intestine (15). Whether this mechanism is plausible remains to be determined, and should be a focus for further study.

Creation of a Conditional Mouse Model of PolgD257A

The use of a conditional mouse models has its advantages over typical knock in or knock out mouse models. In the case of mitochondrial DNA polymerase gamma, deletion of the gene proves to be embryonic lethal (18). Engineering a mutation into *Polg* (D257A) leads to a global expression of the mutant allele (8, 12). In order to ask more intricate questions involving mitochondrial DNA mutations and diabetic related complications, I set out to create a conditional knock-in of the PolgD257A mutation. This model will allow the tissue specific expression of PolgD257A, and bypass the complications associated with global expression of PolgD257A as I have described in Chapter 2, 3, and 4. The targeting vector was successfully engineered, and introduced into multiple embryonic stem (ES) cell lines. Multiple positive ES clones were created and microinjected into blastocysts. The chimeras generated were of exceptional quality. Chimeras were bred to wild type mice to generate a germ line transmitted mouse with the targeting of the conditional PolgD257A mutation. However, multiple attempts to generate a germ line animal failed.

Based on my previous work with the PolgD257A mouse model, it has become apparent that a conditional allele of PolgD257A would provide an exceptional tool to determine the

effect of accumulating mitochondrial DNA mutations in individual tissues while maintaining diabetes. As I have shown in Chapter 2, the PolgD257A mutation causes a disruption of the testis that ultimately affects appetite in the diabetic mice leading to an improvement in hyperglycemia. Due to this improvement in diabetes, diabetic induced complications did not develop. In this case, a conditional allele could bypass the testis dysfunction and target the kidney allowing us to evaluate the role of accumulating mitochondrial DNA mutations in nephropathy. In Chapters 3 and 4, intestinal related problems were observed in PolgD257A mice leading to mal-absorption on HFW diet. The intestinal changes and subsequent mal absorption would have a detrimental effect on any metabolic studies in the PolgD257A mouse. In this case, a conditional allele could bypass the small intestine dysfunction and target individual tissue for long term studies on the effects of accumulating mitochondrial DNA mutations (aging) on individual organs.

The PolgD257A conditional targeting vector was created as follows: 1) the cDNA (exons 3-26) for *Polg* was fused to the endogenous exon 3 in the genome sequence of *Polg*; 2) the mutated exon 3 with the D257A mutation was created by PCR and sequenced for accuracy; and 3) the cDNA from exon 3 to exon 26 was flanked by LoxP sites to allow Cre mediated deletion. Figure 5.1 illustrates the genomic structure of Polg (Fig. 5.1A), the conditional targeting vector (Fig. 5.1B), and the targeted allele after homologous recombination (Fig. 5.1C). Once germ line transmission of the conditional allele was achieved, the mutant mouse would express wild type Polg until exposure of the Cre recombinase (Fig. 5.2A). In the presence of Cre recombinase, the wild type *Polg* sequence is excised and the PolgD257A mutant is expressed (Fig. 5.2B). The completed targeting vector was electroporated into B6 (C57BL/6) embryonic stem cells. PCR screening of the targeted B6 ES clones yielded 4

positives out of 194 clones screened. Southern blot analysis of the PCR positive clones confirmed that 3 out of 4 ES clones were correctly targeted for the conditional PolgD257A allele (Fig. 5.3A). All 3 clones were used for microinjection yielding 46 potential chimeras. Using B6 cells requires PCR screening of all mice to determine chimeras since coat color cannot be used in this approach. Eleven male chimeras and two female chimeras were confirmed by PCR. All 13 chimeras were bred to wild type C57BL/6 mice. Offspring of chimeras crossed to wild type mice were screened for both Neomycin and the PolgD257A mutation. Breeding of these animals proceeded for 18 months with no positive germ line transmission.

A second targeting experiment was performed using E14 (Ola/129) embryonic stem cells. This approach would allow for determination of chimeras by coat color, which is the standard approach for generating gene targeted mice. PCR screening of the targeted E14 ES clones yielded 20 positives out of 242 clones screened. Southern blot analysis of the PCR positive clones confirmed that 18 out of 20 ES clones were correctly targeted for the conditional PolgD257A allele (Fig. 5.3B). Six individual clones (1F3, 1F10, 3A3, 3D10, 3F1, and 3H3) were microinjected. However, no chimeras were produced. The remaining clones were pooled and microinjected over a 5-day period. Over 20 excellent chimeras (based on cost color >70% agouti) were generated by microinjection of these pooled ES clones. All chimeras were bred to wild type C57BL/6 mice. Offspring of this breeding between chimeras and wild type mice produced either black or agouti pups with agouti pups indicating a transmission event. One chimera consistently produced both black and agouti litters. However, screening of the agouti pups revealed no positive germ line transmission of conditional PolgD257A mutation. Breeding of these animals proceeded for >12 months with no positive germ line

transmission. The breeding of these chimeras continued for 16 months at which point the chimeras were no longer producing pups. Thus, I discontinued the generation of this mouse model.

In conclusion, this targeting plan produced no viable germ line animals, while this approach was discontinued. The targeting vector was sequenced for errors introduced during PCR and cloning, and no errors were found through out the targeting vector. PCR on the positive ES clones showed that every component engineered into the targeting vector was found robustly in the positive ES clones. The PolgD257A mutation introduces a new restriction site, XhoI, in exon 3. I confirmed by PCR and digest with XhoI that the PolgD257A mutation was present in the ES clones. It is unclear why germ line transmission was not achieved for this experiment. It could be possible that the cDNA or other components such as the selection markers still being present creates a toxicity that prevents germ line transmission. Other targeting approaches such as the unidirectional Cre-LoxP system (19) could be utilized in order to generate this conditional allele.

Overall Conclusion

The goal of this dissertation was to explore the role of mitochondrial DNA mutations in the development of diabetes, obesity, and diabetic complications. The reversal of diabetes was surprising since mitochondrial dysfunction is widely accepted to cause metabolic disorders. Nevertheless, the first study determined the role of testosterone in the reduction of appetite and improvement in diabetes underlying the importance of hyperphagia in the Akita type 1 diabetic model. This study also provided further support for the reason behind the severity of diabetes in Akita males versus the mild diabetes found in Akita females. While diabetic complications

could not be assessed using the PolgD257A mice, the mitochondrial debris seen in double mutant mice provides a glimpse into the role of mitochondrial DNA mutations play in the development of kidney pathology. The second study shows the importance of functional mitochondria in the maintenance of intestinal stem and progenitors cells. The PolgD257A mutation causes increased apoptosis and decreased cell proliferation in the stem and progenitor cells in the crypts of Lieberkuhn that has not been reported in these mice as well as in aging humans and rodents. I demonstrated that mitochondrial dysfunction is pivotal in disrupting the cell cycle and reducing intestinal epithelial cell migration. The final study explored the functional aspects of these changes in the small intestine when placed under the dietary stress of HFW diet. HFW diet causes obesity in wild type mice, but not in PolgD257A mice. This protective effect is likely the result of the increase in apoptosis and the decrease in cell proliferation that causes the lipid mal-absorption.

These studies have provided insight into the role of mitochondrial DNA mutations in the regulation of diabetes in Akita male mice, the regulation of cell cycle in intestinal stem and progenitor cells, and the regulation of small intestine function during high dietary lipid loads. These unexpected results have provided a precautionary light on the use of PolgD257A mice in metabolic studies and the importance of a PolgD257A conditional mouse model in any further metabolic study.

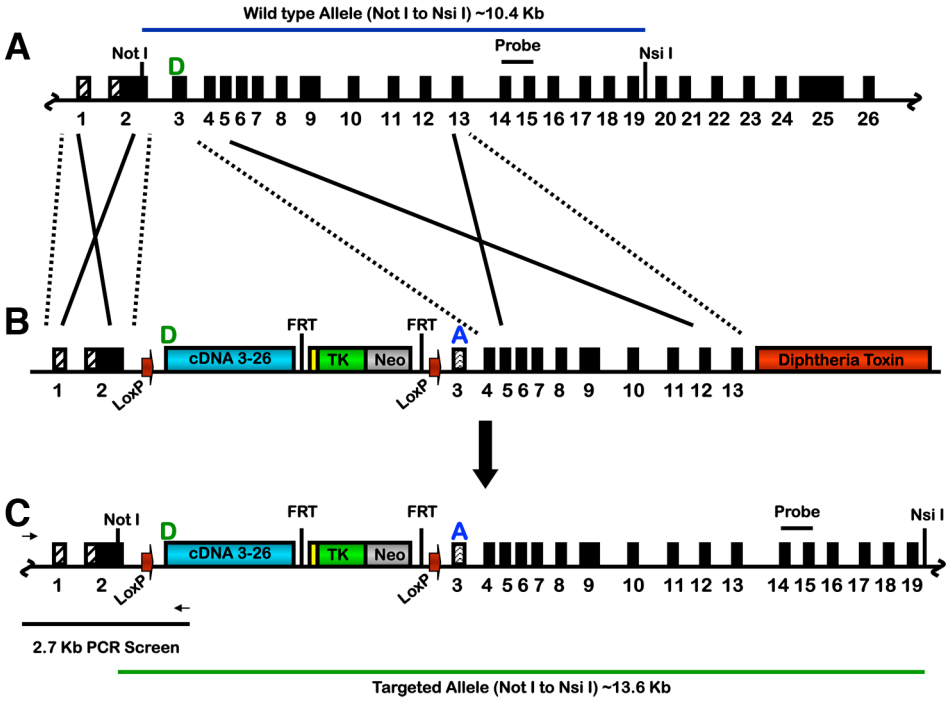

Figure 5.1: Illustration of *Polg* genomic sequence and targeting of conditional targeting vector by homologous recombination. (A) Genomic structure of *Polg* consisting of 26 exons. Green D represents the wild type exon 3 with Aspartic Acid in amino acid position 257. (B) Structure of the PolgD257A conditional targeting vector. Blue A represents the mutant exon 3 with Alanine in amino acid position 257. Diphtheria toxin was used as a marker for negative selection of non-homologous recombination. Neomycin (Neo) was used for positive selection of homologous recombination. Thymidine kinase (TK) was used as a negative selection for non-Flp mediated recombination. (C) Targeted *Polg* allele with wild type PolgD257 surrounded by LoxP sites followed by the PolgD257A mutation. Not I to Nsi I was used for genomic screening to differentiate wild type (10.4 Kb) and the targeted allele (13.6 Kb).

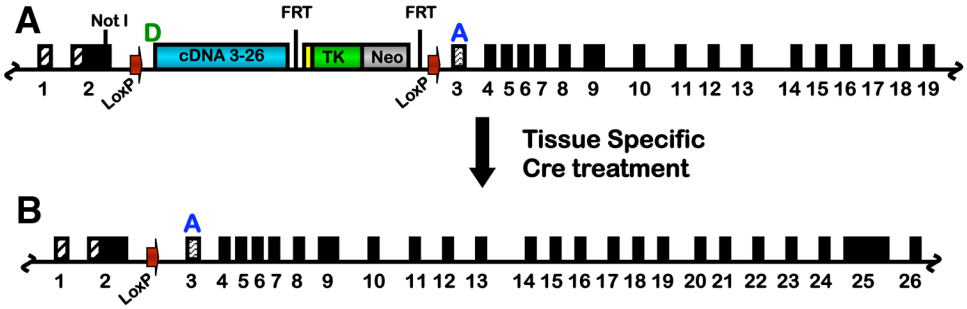

Figure 5.2: Illustration of Cre-mediated excision of the PolgD257 resulting in PolgD257A. (A) Targeted Polg conditional allele prior to Cre recombinase. (B) Mutant PolgD257A allele after Cre recombinase deletion of PolgD257.

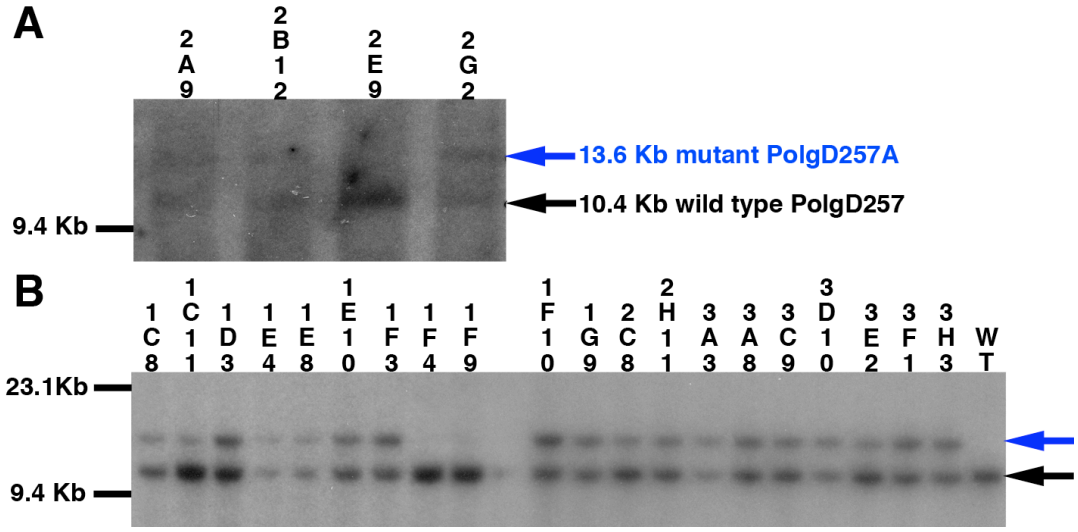

Figure 5.3: Southern blots of conditional PolgD257A targeting. (A) Targeting in B6 ES cells yielded 3 of 4 positively target ES clones. (B) Targeting in E14 ES cells yielded 18 of 20 positively targeted ES clones. Black arrows represents the size of the wild type PolgD257 allele while blue arrows represents the size of the PolgD257A conditional allele.

REFERENCES

1. Yoshioka M, Kayo T, Ikeda T, & Koizumi A (1997) A novel locus, Mody4, distal to D7Mit189 on chromosome 7 determines early-onset NIDDM in nonobese C57BL/6 (Akita) mutant mice. *Diabetes* 46(5):887-894.

2. Toyoshima M*, et al.* (2007) Dimorphic gene expression patterns of anorexigenic and orexigenic peptides in hypothalamus account male and female hyperphagia in Akita type 1 diabetic mice. *Biochemical and biophysical research communications* 352(3):703-708.

3. Yoon JW (1990) The role of viruses and environmental factors in the induction of diabetes. *Curr Top Microbiol Immunol* 164:95-123.

4. Yoon JW (1991) Role of viruses in the pathogenesis of IDDM. *Ann Med* 23(4):437-445.

5. Yoon JW, Jun HS, & Santamaria P (1998) Cellular and molecular mechanisms for the initiation and progression of beta cell destruction resulting from the collaboration between macrophages and T cells. *Autoimmunity* 27(2):109-122.

6. Yoon JW & Ray UR (1985) Perspectives on the role of viruses in insulin-dependent diabetes. *Diabetes Care* 8 Suppl 1:39-44.

7. Kakoki M, Takahashi N, Jennette JC, & Smithies O (2004) Diabetic nephropathy is markedly enhanced in mice lacking the bradykinin B2 receptor. *Proceedings of the National Academy of Sciences of the United States of America* 101(36):13302-13305.

8. Kujoth GC*, et al.* (2005) Mitochondrial DNA mutations, oxidative stress, and apoptosis in mammalian aging. *Science (New York, N.Y.)* 309(5733):481-484.

9. Sato T*, et al.* (2011) Paneth cells constitute the niche for Lgr5 stem cells in intestinal crypts. *Nature* 469(7330):415-418.

10. Merritt AJ*, et al.* (1994) The role of p53 in spontaneous and radiation-induced apoptosis in the gastrointestinal tract of normal and p53-deficient mice. *Cancer Res* 54(3):614-617.

11. Chen ML, *et al.* (2009) Erythroid dysplasia, megaloblastic anemia, and impaired lymphopoiesis arising from mitochondrial dysfunction. *Blood* 114(19):4045-4053.

12. Trifunovic A, *et al.* (2004) Premature ageing in mice expressing defective mitochondrial DNA polymerase. *Nature* 429(6990):417-423.

13. Fox R, *et al.* (2011) Mitochondrial DNA polymerase editing mutation, PolgD257A, reduces the diabetic phenotype of Akita male mice by suppressing appetite. *Proc Natl Acad Sci U S A* 108(21):8779-8784.

14. Caspary WF (1992) Physiology and pathophysiology of intestinal absorption. *Am J Clin Nutr* 55(1 Suppl):299S-308S.

15. Drozdowski LA & Thomson AB (2006) Intestinal sugar transport. *World J Gastroenterol* 12(11):1657-1670.

16. Flores CA, *et al.* (1990) Age-related changes in sucrase and lactase activity in the small intestine of 3- and 10-week-old obese mice (C57BL/6Jobob). *J Am Coll Nutr* 9(3):255-260.

17. Sander P, *et al.* (2006) Novel mutations in the human sucrase-isomaltase gene (SI) that cause congenital carbohydrate malabsorption. *Hum Mutat* 27(1):119.

18. Hance N, Ekstrand MI, & Trifunovic A (2005) Mitochondrial DNA polymerase gamma is essential for mammalian embryogenesis. *Human molecular genetics* 14(13):1775-1783.

19. Oberdoerffer P, Otipoby KL, Maruyama M, & Rajewsky K (2003) Unidirectional Cre-mediated genetic inversion in mice using the mutant loxP pair lox66/lox71. *Nucleic Acids Res* 31(22):e140.